Åbo Akademi University

Diti Desai

Mesoporous Silica Nanoparticles as Versatile Intracellular Drug Delivery Platform

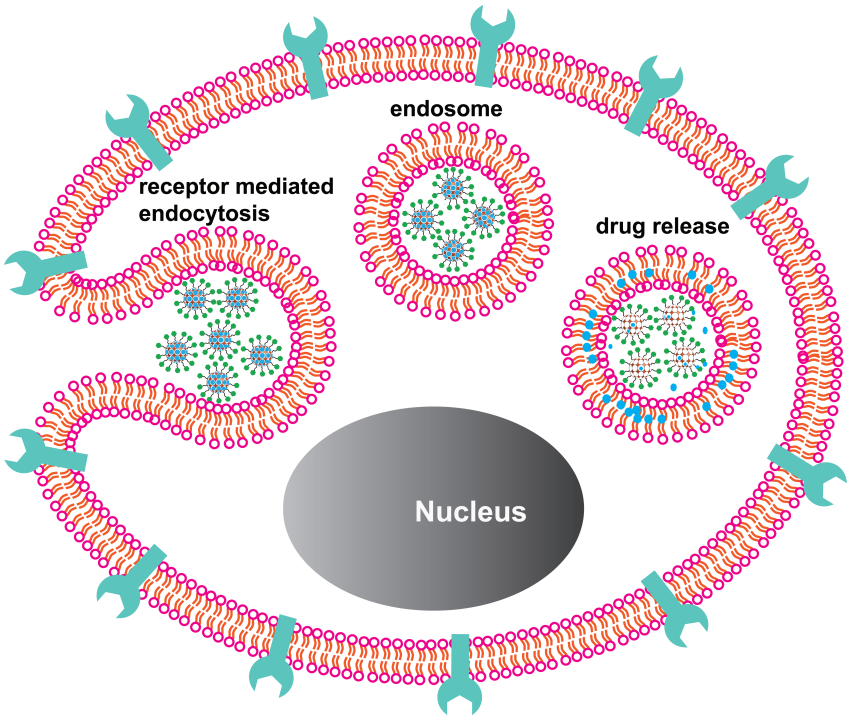

Diti Jayesh Desai

Born 1987 in Valsad, Gujarat, India

Obtained her M. Pharm degree at The M. S. University of Baroda (2010)

B. Pharm degree at Veer Narmad South Gujarat University (2008)

(Cover photo description: Page 21)

MESOPOROUS SILICA NANOPARTICLES AS VERSATILE INTRACELLULAR DRUG DELIVERY PLATFORM

DITI DESAI

Pharmaceutical Sciences Laboratory
Faculty of Science and Engineering
Åbo Akademi University
Åbo, Finland 2016

Supervised by

Prof. Jessica M. Rosenholm

Pharmaceutical Sciences Laboratory

Åbo Akademi University

Finland

Reviewed by

Prof. Jörg Huwyler

Department of Pharmaceutical Sciences

University of Basel

Switzerland

Prof. Vesa-Pekka Lehto

Department of Applied Physics

University of Eastern Finland

Finland

Opponent

Prof. Jörg Huwyler

Department of Pharmaceutical Sciences

University of Basel

Switzerland

ISBN 978-952-12-3469-9 (Print)

ISBN 978-952-12-3470-5 (PDF)

Painosalama Oy – Turku, Finland 2016

To my family

TABLE OF CONTENTS

ABSTRACT

SAMMANFATTNING

LIST OF ORIGINAL PUBLICATIONS

CONTRIBUTION OF THE AUTHOR

LIST OF SUPPORTING PUBLICATIONS

SYMBOLS AND ABBREVIATIONS

1. INTRODUCTION…….....1

2. REVIEW OF THE LITERATURE……...…….....3

2.1. Nanopharmaceuticals……...3

2.2. Fabrication of nanoparticles……4

2.2.1. Synthesis of mesoporous silica nanoparticles(MSNs)……..5

2.2.2. MSNs size, pore size and template removal……..8

2.3. Surface functionalization of MSNs……10

2.3.1. Direct functionalization by co-condensation……11

2.3.2. Functionalization by post-synthetic modification……12

2.3.3. Gate keeping mechanism for on-command drug delivery……14

2.3.4. Functionalization with targeting ligands……..19

2.4. Drug incorporation and release……...22

2.4.1. Drug incorporation…..……22

2.4.2. Drug release……23

2.5. Biomedical applications of MSNs……..24

2.5.1. Cellular interactions……25

2.5.1.1. Effect of MSNs' size…….……25

2.5.1.2. Effect of MSNs' surface charge……27

2.5.1.3. Effect of MSNs' hydrophobicity and surface properties……28

2.5.2. Biocompatability and bio-distribution……..29

2.5.3. Barriers for drug delivery……30

2.5.4. Endosomal escape……31

2.5.5. Drug delivery……...31

2.5.5.1. Oral route……..31

2.5.5.2. Intravenous route……33

3. AIM OF THE STUDY……...35
4. CHARACTERIZATION TECHNIQUES……....36
4.1. Electron microscopy……...36
4.1.1. Transmission electron microscopy (TEM)……..36
4.1.2. Scanning electron microscopy (SEM)…….37
4.2. Nitrogen sorption analysis……..38
4.3. Small angle x-ray diffraction (SAXD)……...41
4.4. Thermogravimetric analysis (TGA)……42
4.5. Dynamic light scattering (DLS)……..43
4.6. Electrokinetic zeta potential measurement…….45
4.7. Fluorescence spectroscopy……..47
4.8. Ultraviolet -Visible spectroscopy (UV)……..48
4.9. High performance liquid chromatography (HPLC)……50
4.10. Confocal laser scanning microscopy (CLSM)……...…..51
4.11. Flow cytometry…….52
5. SUMMARY OF THE RESULTS……..55
5.1. Mesoporous nanocarriers for delivery of hydrophobic cargoes…….55
5.1.1. Design and characterization of the mesoporous nanoparticles……...…56
5.1.1.1. Functionalization of MSNs……...56
5.1.1.2. Physicochemical characterization of the synthesized MSNs…….….58
5.1.1.3. Effect of surface coating on serum protein adsorption…….60
5.1.2. Drug loading and release……..62
5.1.2.1. Loading of furosemide in different surface functionalized MSNs…...62
5.1.2.2. Loading of celastrol and release in buffer…….63
5.1.2.3. Loading of curcumin and measurement of effect on particles' fluorescence…….…..64
5.1.3. Cellular interactions……..66
5.1.3.1. Cytotoxicity assay……66
5.1.3.2. Influence of PEI coating on cell viability……..……..67
5.1.3.3. Cellular uptake of differently functionalized MSNs……...68
5.1.3.4. Exocytosis of nanoparticles…….……72
5.1.3.5. Influence of surface charge on route of uptake……....72
5.1.3.6. Influence of loading of hydrophobic cargo on intracellular pathway..73

5.1.3.7. Effect on permeability of furosemide through Caco-2 monolayers….74
5.1.3.8. Apoptotic effect of celastrol loaded MSNs on cancer cells……75
5.1.4. In vivo bio-distribution and pharmacodynamics studies……..…77
5.1.4.1. *In vivo* bio-distribution of fluorescent MSNs in the gastrointestinal tract……..77
5.1.4.2. Stability of drug loaded MSNs in simulated gastric fluid……...79
5.1.4.3. *In vivo* oral drug delivery efficiency……...80
5.2. Mesoporous nanocarriers for delivery of hydrophilic cargoes……...83
5.2.1. Design and characterization of the mesoporous nanoparticles……...83
5.2.1.1. Surface functionalization and coating of MSNs with lipid bilayer….84
5.2.1.2. Physicochemical characterization of the synthesized MSNs…….....85
5.2.2. Drug loading and release……..87
5.2.1.1. Loading of calcein and zoledronic acid……...87
5.2.1.2. Stability of lipid bilayer after drug loading and change in zeta potential as function of pH……..88
5.2.3. Cellular interactions……..91
5.2.3.1. Cytotoxicity assay……...91
5.2.3.2. Cellular uptake and effect of outer leaflet of lipid bilayer on cargo release……..91
5.2.3.3. Influence of outer leaflet of lipid coating on the route of uptake…..94
5.2.3.4. Evaluation of *in vitro* efficacy of the drug loaded lipid bilayer coated MSNs in breast cancer cells……..95
5.2.4. In vivo delivery and safety studies……96
5.2.4.1. *In vivo* delivery of the drug loaded lipid bilayer coated MSNs ……...……..96
5.2.4.2. Safety evaluation of lipid bilayer coated MSNs after *in vivo* administration……97
6. CONCLUSIONS AND FUTURE OUTLOOK……..……..…..98
7. ACKNOWLEDGEMENTS……101
8. REFERENCES……102

Abstract

Mesoporous silica nanoparticles (MSNs) have attracted substantial attention for their application in drug delivery and biomedicine. MSNs have been established as a promising and novel drug delivery vehicle due to their unique structural properties, such as high surface area, large pore volume, tunable pore diameter, and narrow pore size distribution. Furthermore, they provide the possibility to include various surface functions and are biocompatible.

For efficient drug delivery using mesoporous silica nanocarriers, their physicochemical characteristics should be controlled to predict their behavior under physiological conditions. The surface function on the particles determines their fate in the physiological environment. Further, the surface functionalization needs to be tailored according to the cargo molecule to be delivered. In this thesis, various surface functionalization strategies of MSNs employing different polymers and lipids were utilized to fabricate novel drug delivery nanocarriers for hydrophobic and hydrophilic drugs, in order to improve the efficacy of poorly aqueous soluble drugs and to achieve sustained or triggered drug release. Adequate surface functionalizations provide colloidal stability and reduce protein adsorption on the particle surface. By the application of zwitterionic coating on the MSN surface, protein adsorption on the particle surface can be diminished.

For intravenous delivery, first passive targeting (extravasation) of nanoparticles at the tumor site is required and then active targeting to cancer cells using small molecular targeting ligands can be achieved, which provides the advantage of lowering the dose and reducing the side effects imparted on healthy cells. In this thesis, MSNs were designed for active cellular targeting using glucose and folic acid as targeting ligands, and further loaded with anticancer drug molecules. Therapeutic efficacy of the drug molecules were significantly improved using MSNs compared to free drug *in vitro* and *in vivo*.

For oral drug delivery, the drug molecule should be protected from degradation in the gastrointestinal (GI) tract and permeability through the mucus layer needed to be improved. In this thesis, MSNs were functionalized by polymeric surface grafts, which has facilitated drug transport through the mucosal barrier and enhanced intestinal cellular internalization. Drug targeting in different parts of the intestine could be tuned by surface modifications, and polyethylene glycosylation (PEGylation) of nanoparticles in combination with polyethylene imine (PEI) as particle surface coating enhanced the internalization of MSNs into intestinal epithelial cells.

For the delivery of hydrophilic anticancer molecules after intravenous administration requires protection from non-specific uptake in healthy cells. In this thesis, hydrophilic molecules were loaded in MSNs, which were further coated with lipid bilayer for intracellular drug delivery. MSNs provided delivery to cancer cells without any observed toxicity to normal cells *in vivo*.

The thesis reports the importance of a) surface modification needed with respect to the properties of the cargo molecules, and b) appropriate evaluation of biophysicochemical interactions of nanocarriers for their future drug delivery applications. This knowledge can facilitate the development of nanomedicines with desired properties for cancer therapy with reduced side effects.

Sammanfattning

Mesoporösa kiseldioxid nanopartiklar (MSN) har etablerat sig som lovande läkemedelsbärare på grund av sina unika strukturella egenskaper, såsom stor ytarea och porvolym, justerbar pordiameter och snäv porstorleksfördelning. Dessutom är de biokompatibla, bionedbrytbara och kan flexibelt ytfunktionaliseras.

För effektiv användning av MSN partiklar som läkemedelsbärare måste deras fysikalisk-kemiska egenskaper vara välkontrollerade, för att kunna förutspå deras beteende under fysiologiska förhållanden. Partikelns ytfunktionalitet bestämmer dess öde i den fysiologiska miljön. Dessutom skall funktionaliseringen av partikelytan anpassas till den läkemedelsmolekyl som skall transporteras. I denna avhandling har olika ytfunktionaliseringsstrategier, som utnyttjar polymerer och lipider, använts för att tillverka nya nanoformuleringar för både hydrofoba och hydrofila läkemedelsmolekyler. Detta har gjorts i syfte att förbättra effektiviteten hos svårlösliga molekyler, och för att uppnå en jämn och kontrollerbar läkemedelsfrisättning. För vattenlösliga molekyler måste MSN partiklarna ytterligare beläggas med ett lipiddubbelskikt, vilken fungerar som en ogenomsläpplig barriär för molekylerna under transporten, för att möjliggöra intracellulär läkemedelstillförsel. Lämplig ytfunktionalisering ger därutöver kolloidal stabilitet och minskar proteinadsorptionen på partikelytan. Genom att funktionalisera en zwitterjonisk beläggning på MSN partikelns yta kan proteinadsorptionen på partikelytan minskas.

Vid intravenös tillförsel måste nanopartiklarna föst passivt föras till tumörområdet varefter det går att aktivt styra partiklarna till cancercellerna med hjälp av småmolekylära målsökande ligander. Detta ger fördelen att dosen kan minskas, och samtidigt minskar biverkningarna på de friska cellerna. I denna avhandling har MSN partiklar designats för aktiv cellulär styrning med hjälp av glukos och folsyra som målsökande ligander. Partiklarna fylldes därefter med anticancerläkemedel. Jämfört med fritt läkemedel, förbättrades den terapeutiska effekten av läkemedelsmolekylerna genom användning av MSN som bärarmaterial.

För oral medicinering bör läkemedelsmolekylen skyddas från nedbrytning i mag-tarmkanalen. Samtidigt måste permeabiliteten genom slemhinnan förbättras. I denna avhandling har MSN partiklar funktionaliserats med hjälp av polymera ytbeläggningar, vilket har möjliggjort transport av läkemedlet genom slemhinnan och förbättrat upptaget i tarmcellerna. Läkemedlet kunde målstyras till olika delar av tarmen genom att modifiera partikelytan. Ytfunktionalisering med polyetylenglykol (PEGylering) av nanopartiklarna i kombination

med användning av polyetylenimin (PEI) som ytbeläggning på partiklarna förbättrade upptaget av MSN i epitelcellerna i tarmen.

Avhandlingen poängterar vikten av a) ytmodifieringen som måste anpassas till egenskaperna hos den läkemedelsmolekyl som skall transporteras och b) en noggrann undersökning av nanobärarnas fysikalisk-kemiska egenskaper och hur dessa växelverkar med biologiska system vid evaluering av deras användningspotential som läkemedelsbärare. Denna kunskap kan underlätta utvecklingen av nanoläkemedel, som har önskade egenskaper för cancerterapi och därmed även leder till mindre biverkningar.

List of original publications

1. Design considerations for mesoporous silica nanoparticulate systems in facilitating biomedical applications

Diti Desai, Didem Şen Karaman, Neeraj Prabhakar, Sina Tadayon, Alain Duchanoy, Diana M. Toivola, Sadhana Rajput, Tuomas Näreoja, Jessica M. Rosenholm. *Mesoporous Biomaterials* 04/**2014**; 1:16-43

2. Sugar-decorated mesoporous silica nanoparticles as delivery vehicles for the poorly soluble drug celastrol enables targeted induction of apoptosis in cancer cells

Erik Niemelä*, Diti Desai*, Yves Nkizinkiko, John Eriksson, Jessica M. Rosenholm. *European Journal of Pharmaceutics and Biopharmaceutics* **2015**; 96: 11-21

3. Targeted modulation of cell differentiation in distinct regions of the gastrointestinal tract via oral administration of differently PEG-PEI functionalized mesoporous silica nanoparticles

Diti Desai, Neeraj Prabhakar, Veronika Mamaeva, Didem Şen Karaman, Iris A.K. Lähdeniemi, Cecilia Sahlgren, Jessica M. Rosenholm, Diana Toivola. *International Journal of Nanomedicine* **2016**; 11: 299-313

4. Tethered lipid bilayer gates: Toward extended retention of hydrophilic cargo in porous nanocarriers

Jixi Zhang, Diti Desai, Jessica Rosenholm. *Advanced Functional Materials* **2014**; 24(16): 2352-60

5. Lipid bilayer-gated mesoporous silica nanocarriers for tumor targeted delivery of zoledronic acid *in vivo* (manuscript)

Diti Desai, Jixi Zhang, Jouko Sandholm, Jaakko Lehtimäki, Tove Grönroos, Johanna Tuomela,* Jessica M. Rosenholm*

Contribution of the author

In PAPER I, the author was responsible for some of the sample preparations (MSN2 series) and surface modifications (PEI-, PEG-PEI-, Succ-, and Succ-PEI-MSN2, Stöber-PEI, PS-PEI) and their characterizations. The analysis of the characterization data was performed by the author. The author has also performed *in vitro* experiments and analysis of these data. Author has contributed writing the first draft. D. Sen Karaman has prepared and characterized rest of the samples. N. Prabhakar has performed two photon *in vivo* imaging and life-time measurement of the fluorophores.

In PAPER II, the author was responsible for all the sample preparations, surface modifications, and their characterizations and writing of the first draft. Author has performed the measurement of glucose consumption by the different cells. E. Niemelä and Y. Nkizinkiko have performed the *in vitro* experiments. Author has contributed for analysis of *in vitro* data.

In PAPER III, the author was responsible for all the sample preparations, surface modifications, and their characterizations and writing of the first draft. Author has performed *in vitro* and *in vivo* experiments, and analysis of the data. N. Prabhakar and V. Mamaeva have contributed for *in vivo* biodistribution experiment. D. Şen Karaman helped in the PEG modification. I.A.K. Lähdeniemi has performed RT-PCR experiment.

In PAPER IV, the particle synthesis was carried out in collaboration with J. Zhang. Author has performed all the *in vitro* experiments. Author has contributed writing the first draft. J. Zhang has performed characterization and analysis of the data.

In PAPER V, the author was responsible for the sample preparations, surface modifications, and their characterizations and writing of the first draft. Author has performed some *in vitro* experiments and analysis of data. J. Zhang has contributed in drug loading experiment. J. Lehtimäki, J. Sandholm, T. Grönroos and J. Tuomela have performed *Incucyte* imaging, *in vivo* experiments and analysis of data.

List of supporting publications

1. Shape engineering vs organic modification of inorganic nanoparticles as a tool for enhancing cellular internalization

Didem Şen Karaman, **Diti Desai**, Rajendran Senthilkumar, Emma Johansson, Natalie Råtts, Magnus Odén, John Eriksson, Cecilia Sahlgren, Diana Toivola, Jessica Rosenholm. *Nanoscale Research Letters* **2012**; 7(1): 358

2. Inhibiting Notch activity in breast cancer stem cells by glucose functionalized nanoparticles carrying γ-secretase inhibitors

Veronika Mamaeva, Rasmus Niemi, Michaela Beck, Ezgi Özliseli, **Diti Desai**, Sebastian Landor, Tove Grönroos, Pauliina Kronqvist, Ina Pettersen, Jessica Rosenholm, Mika Linden, Cecilia Sahlgren. *Molecular Therapy* **2016**; 24 (5): 926–936

3. Preparation of curcumin loaded mesoporous silica nanoparticles: Determining polarizability inside the mesopores

Digambara Patra, Didem Şen Karaman, **Diti Desai**, Elsy El Khoury, Jessica Rosenholm. *Materials Research Bulletin* **2016**; 84: 267-272

4. Prolonged dye release from mesoporous silica-based imaging probes facilitates long-term optical tracking of cell populations *in vivo*

Jessica M. Rosenholm, Tina Gulin-Sarfraz, Veronika Mamaeva, Rasmus Niemi, Ezgi Özliseli, **Diti Desai**, Daniel Antfolk, Eva von Haartman, Desiré Lindberg, Neeraj Prabhakar, Tuomas Näreoja, Cecilia Sahlgren. *Small* **2016**; 12(12): 1578-1592

Symbols and abbreviations

ζ	Zeta potential
θ	Scattering angle
Φ	Quantum yield
λ	Wavelength
ACA	Acetic acid
AFM	Atomic force microscopy
APTES	(3-Aminopropyl)triethoxysilane
APTMS	(3-Aminopropyl)trimethoxysilane
BCS	Biopharmaceutical classification system
BET	Brunauer-Emmett-Teller theory for surface area determination
BJH	Barrett-Joyner-Halenda for pore size determination
Chol	Cholesterol
CLSM	Confocal laser scanning microscopy
CMC	Critical micelle concentration
CPP	Critical packing parameter (of surfactants)
CTAB	Cetyltrimethylammonium bromide
CTAC	Cetyltrimethylammonium chloride
DAPT	γ-secretase inhibitor compound, N-[N-(3,5-Difluorophenacetyl)-L-alanyl]-S-phenylglycine t-butyl ester
DLS	Dynamic Light Scattering
DMAP	N,N-Dimethylpyridin-4-amine
DMHA	N,N- dimethyl-hexadecylamine
DOPE	1,2-dioleoyl-sn-glycero-3-phosphoethanolamine
DOPC	1,2-dioleoyl-sn- glycero-3-phosphocholine
DOPS	1,2-dioleoyl-sn-glycero-3-phospho-L-serine
DOTAP	1,2-dioleoyl-3-trimethylammoniumpropane
DSC	N, N'-disuccinimidyl carbonate
DPPS	1,2-dipalmitoyl-sn-glycero-3- phosphocholine
DSPE	1,2-Distearoyl-sn-glycero-3-phosphoethanolamine
EDC	1-Ethyl-3-(3-(dimethylamino)propyl)-carbodiimide
EGFR	Epidermal growth factor receptor
EPR	Enhanced permeability and retention
FA	Folic acid
FCS	Fecal calf serum
FDA	Food and drug administration
FITC	Fluorescein isothiocyanate
FSC	Forward scatter
GA_{aq}	Glucuronic acid functionalization in aqeous condition
GA_{org}	Glucuronic acid functionalization in organic condition
Gluc	Glucose
GLUT	Glucose transporter
GIT	Gastrointestinal tract
GSI	Gamma Secretase Inhibitor
HPLC	High Performance Liquid Chromatography
HEPES	2-[4-(2-hydroxyethyl) piperazin-1-yl] ethanesulfonic acid buffer
hMSC	Human mesenchymal stem cell
ICP-MS	Inductively coupled plasma-mass spectrometry
ICP-OES	Inductively coupled plasma-optical emission spectrometry

IEP	Isoelectric point
in vitro	from Latin: “in living”, *i.e.* under physiological conditions intravenous
in vivo	from Latin: “in glass”, *i.e.* under simulated physiological conditions
i.p.	Intraperitoneal
i.v.	Intravenous
IUPAC	International union of pure and applied chemistry
LB	Lipid bilayer
LCST	Lower critical solution temperature
mal	Maleimide
MCM	Mobil composition of matter
MES	Morpholinoethanesulfonic acid buffer
MPS	Mononuclear phagocyte system
MRI	Magnetic resonance imaging
MSN	Mesoporous silica nanoparticles
NHS	N-hydroxysuccinimide
NIR	Near infrared
NLDFT	Non local density functional theory
PAS	Periodic Acid-Schiff
PBS	Phosphate Buffer Saline
PEG	Polyethyleneglycol
PEI	Poly(ethyleneimine)
PMT	Photomultiplier tube
POPC	1-palmitoyl-2-oleoyl-sn-glycero-3-phosphocholine
POPG	1-palmitoyl-2-oleoyl-sn-glycero-3-phosphoglycerol
pQCT	Peripheral quantitative computed tomography
RES	Reticuloendothelial system
RGD	Arginine-glycine-aspartic acid
RT-PCR	Reverse transcription polymerase chain reaction
SAXD	Small angle X-ray diffraction
SEM	Scanning electron microscopy
SGF	Simulated gastric fluid
SIF	Simulated intestinal fluid
SSC	Side scatter
Succ	Succinic acid
TEM	Transmission electron microscopy
TEOS	Tetraethyl orthosilicate
TGA	Thermogravimetric analysis
TLR9	Toll like receptor 9
TMB	Trimethylbelzene
TMOS	Tetramethyl orthosilicate
TPOS	Tetrapropyl orthosilicate
TRITC	Tetramethylrhodamine-5-isothiocyanate
UV	Ultraviolet-Visible
WHO	World health organization

1. Introduction

Drug delivery systems have been designed to improve the pharmacological properties of drug molecules by modifying their pharmacokinetic profile and bio-distribution.[1] The unfavorable physicochemical properties of many drug compounds affect their bioavailability and consequently the efficacy of the treatment. For example, for oral administration of poorly water- soluble drugs, the dissolution rate may be slower than the GI transit time, which results in therapeutically unacceptable bioavailability. Intravenous administration of poorly water-soluble drugs is more complex, requiring the application of organic solvents to dissolve them prior to their administration. Delivery of peptides, proteins or other macromolecules suffers due to their degradation in the biological fluids, losing their therapeutic activity. Delivery of the chemotherapeutic agents faces additional challenge due to non-specificity, leading to deleterious off-target side effects and low therapeutic efficacy. For these reasons, drug delivery systems have been extensively used as tools for nanomedicine in the treatment of various ailments.[2]

Nanomedicine is the application of nanotechnology to medicine for the prevention, diagnosis and treatment of diseases, for better understanding the complex underlying pathophysiology of diseases, and for improving the quality of life of patients. It is the most dynamic research area of nanotechnology.[3] The nanoscale material's physicochemical properties such as melting point, magnetic property, electrical conductivity, chemical reactivity change significantly from those at a larger scale due to their small size, which provides a larger surface area to interact with surrounding biological environments and hold pledge in the clinical field. The possibilities of various modifications in structure, surface properties and affinity ligand choices for nanoparticle systems provides useful advantages for drug delivery, imaging, and targeting in biological systems.

There are a few nanomedicines that have been approved by the US Food and Drug Administration (FDA) for clinical applications, such as Doxil®, Abraxane®, Lipoplatin, and Marqibo®. However, there are several key barriers blocking the clinical translation of laboratory-developed nanomedicines,[4] which include encapsulation of sufficient therapeutic agents with an activated release, delivery of the nanocarriers efficiently to the desired location in the framework of multiple *in vivo* physiological barriers, toxicity of the engineered nanomaterials, and scalable and cost-effective fabrication of well-dispersed nanocarriers. Great efforts are directed towards the development of new biocompatible and biodegradable

inorganic nanomaterials, which in turn, offer great versatility for the development of advanced drug delivery systems.

Among inorganic nanomaterials, amorphous silica nanoparticles have unique adsorption capacity, low density, and biocompatibility, which make them potential candidates for various biomedical applications.[5] Fumed silica (Aerosil®) has been widely employed in pharmaceutical formulations, cosmetics, and food products as an excipient and it is 'generally recognized as safe' by the US Food and Drug Administration (US FDA).[6] Further, silica nanoparticles 'Cornell Dots' have received FDA safety approval for human clinical Phase I trials for targeted molecular imaging of cancer, and therefore, have become most promising inorganic nanomaterials for biomedical application.[7]

Amongst silica materials, mesoporous silica nanoparticles (MSNs) offer numerous unique and expedient structural properties, such as high surface area (> 700 m^2/g), large pore volume (>1cm^3/g), tunable pore diameter (2 - 10 nm), stable mesostructure, modular morphology (sizes and shape) and three different functional domains (silica framework, exterior particle surface, and interior pore surfaces). The high surface area and pore volume are mostly beneficial for high drug loading. The loaded therapeutic agents, such as small molecules, enzymes, peptides, and oligonucleotides, can be efficiently protected in the mesopores from undesired degradation in harsh environments, such as stomach and intestine, before reaching the designated target.[8,9] Further, the release of drug molecules from the highly ordered mesoporous structure can be fine-tuned to provide therapeutic local concentration at the targeted area, thus reducing the overall dose required for the treatment. The loading of guest molecules to MSNs can be done without adsorption of organic solvent molecules in mesopores that are often toxic to normal cells. Additionally, the external surface of MSNs can be functionalized with gated molecules for on-command drug delivery.[10]

Mesoporous silica nanoparticles have increased application in the field of nanomedicine including drug delivery, targeting and diagnosis, due to their modular design characteristics. In this thesis, physicochemical characteristics of mesoporous silica nanoparticles have been modulated, evaluated and subsequently its potential in drug delivery application has been validated.

2. Review of the literature

2.1. Nanopharmaceuticals

Nanotechnology is an emerging multidisciplinary field based on the engineering of functional systems at the molecular scale. The convergence of nanotechnology and medicine has led to the interdisciplinary field of nanomedicine.[11] Nanomedicine is the application of science and technology for diagnosing, treating and preventing disease and traumatic injury, for relieving pain, and for preserving and improving human health, using molecular tools and molecular knowledge of the human body.[3] Nanopharmaceuticals include nanomaterials for delivery of drug molecules. Nanopharmaceuticals have been described as pharmaceuticals engineered on the nanoscale, i.e., pharmaceuticals where the nanomaterial plays the pivotal therapeutic role or adds additional functionality to the previous compound.[12]

The highest causes of mortality in Europe are cardiovascular disease and cancer.[13] According to the World Health Organization (WHO), there will be 15 million new cases of cancer worldwide in 2020. The main reason for an increase in the number of cancer deaths is the lack of selective delivery of anticancer compounds to cancer tissue, and further high systemic exposure of anticancer agents leads to dose-related toxicity and resistance to therapeutic agents. Hence, delivery of anticancer agents at the target site is required in order to overcome current limitations in cancer therapy. Nanomedicine is expected to contribute significantly to overcoming these limitations in cancer therapy and improving drug delivery, and thereby increasing efficacy while decreasing the side effects of anticancer drugs.[14] A number of liposomal, polymeric, and inorganic nanomaterials based nanopharmaceuticals are currently undergoing clinical trials or have been clinically approved (Table 1). These therapeutic agents have reduced the adverse side effects associated with non-specific organ uptake of chemotherapeutic agents.

For the cancer therapy, ideal features of nanopharmaceuticals include: (a) enhanced drug accumulation at the target site, (b) offering a high drug loading capacity and ability to efficiently carry poorly soluble drugs, (c) extended circulation or residence time, (d) controlled drug release profiles, (e) providing protection of drugs against enzymatic or hydrolytic degradation in the body, (f) minimum non-specific cellular and blood-protein binding properties, (g) biocompatibility and biodegradability, (h) long-term physical and chemical stability, and (i) ease of consistent, reproducible synthesis.[15] To attain those properties, the fabrication design of nanoparticles should be chosen properly, and their

physicochemical properties must be thoroughly evaluated.

Table. 1 Summary of cancer nanomedicines approved and undergoing clinical trial[16]

Nanoparticle	Name	Cancer Target	Status	Reference
Liposome	Doxil	Sarcoma	Approved	
Liposome	Lerafaon	General	Phase I	NCT00024648
Liposome	Marqibo	Leukemia	Approved	
Liposome	Lipoplatin	Pacreatic/Head and Neck/breast Malignant pleural effusion	Approved Phase I	NCT02702700
Liposome	Onivyde	Pancreatic	Approved	
Liposome	Myocet	Breast	Approved	
Albumin	Abraxane	General	Approved	
Polymeric micelle	NC-6004	Pancreatic	Phase III	NCT02043288
Polymeric micelle	Genexol-PM	Metastatic Breast	Approved	
Polymeric micelle	Paclical	Ovarian	Phase III	NCT00989131
Carbon nanoparticle	CH40	Gastric	Phase III	NCT02123407
Silica nanoparticle	Cornell dots	Cancer Probe	Phase I	NCT02106598
Gold nanoshell	Aurolase	Head & Neck	Phase I	NCT00848042
Cyclodextrin	CRLX101	General	Phase II	NCT00333502
Polymeric micelle	BIND-014	Prostate	Phase II	NCT01812746
Gold nanoparticle	Aurimmune	Head & Neck	Phase I	NCT00356980

2.2. Fabrication of nanoparticles

Techniques used for the generation of nanoscale structures can be divided roughly into two groups: top-down and bottom-up approaches.[17] The top-down approach initiates with large objects at least in one or two dimensions and reduces their lateral dimensions in order to achieve fine feature and nanoscale materials, whereas the bottom-up approach produces nanoscale structures as small building blocks and then assembles them into larger nanostructures via hierarchical synthesis. The bottom-up approach utilizes processes based on transformations in solution, e.g. sol-gel processing, co-precipitation, template synthesis, supercritical fluid synthesis, and ionic liquid synthesis. Common materials used in bottom-up approaches are block-copolymers, colloids, amphiphiles, and liquid crystals. The top-down approach introduces internal stress and surface defects (i.e. imperfections), and it is not cost-effective. It has been stated that the bottom-up approach is more advantageous as it has a better chance of producing nanostructures with fewer defects, more homogenous chemical composition, and better short- or long- range ordering.[18] However, scaling up remains a major challenge for the bottom-up approach.

Among the different bottom-up approaches, sol-gel process is expedient in terms of high chemical homogeneity, possibility of controlling size and morphology, and low processing temperatures. [19] The sol-gel process can be defined as the hydrolysis and condensation of a liquid precursor to a solid. The whole process can be characterized by several distinct steps: formation of stable solutions of precursors (the sol); further reaction of the sol with a bridged, rigid, porous network (the gel) enclosing a continuous liquid phase by gelation, drying (the removal of liquids from the gel network) and densification; and decomposition of the gels at high temperature. (Figure 1a) A suitable precursor and a solvent is the key to the synthesis of monodispersed nanoparticles by sol-gel processes.[20] Molecular self-assembly is an intrinsic property of certain molecules such as surfactants, lipids, co-polymers, to spontaneously assemble without guidance from an outside source to various kinds of ordered structures. These amphiphilic systems are classified into single-phase (homogenous) and heterogeneous systems. The homogenous systems are further divided into isotropic solutions, solid phases, and liquid crystalline phases.[21] Depending on the solution composition, spherical, cylindrical or rod-like micelles, hexagonally ordered or cubic crystals, lamellar phases, and inverse micellar liquid crystals can be formed. (Figure 1b) The liquid crystalline phases have the short-range (molecular) disorder but some distinct order over larger distances.

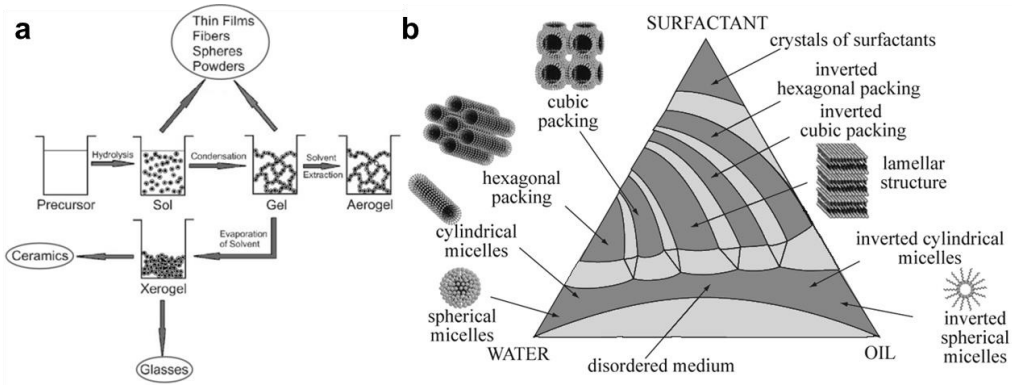

Figure 1. (a) Typical steps in the sol-gel process (b) Schematic phase diagram of surfactant-oil-water systems showing a variety of self-assembled structures that can be used as templates for nanostructured materials synthesis (Adapted from references 20,22)

2.2.1. Synthesis of mesoporous silica nanoparticles (MSNs)

Ordered mesoporous materials are unique materials and they are defined by ordered, repetitive mesostructures of pores and disordered arrangement at the atomic level. They can be synthesized with various different pore sizes, structures and framework compositions. The

family of mesoporous silica materials was first discovered by Kresge *et al*.[23,24] at the Mobil Oil Company in the early 1990s by employing surfactants as structure directing agents around which inorganic material can deposit through hydrolysis and condensation via sol-gel approach, and creating a mesoscopically ordered hybrid inorganic material. The ordered pore structure of inorganic silica materials is obtained after removal of surfactants by thermal calcination or chemical extraction.

The formation of the mesoporous materials is governed by two phenomena- (a) the dynamics of surfactant molecules to form molecular assemblies, which lead to micelle formation and eventually formation of a liquid crystal, and (b) the ability of the inorganic oxide to undergo condensation reactions to form extended, thermally stable structures. The synthesis of mesoporous materials closely resembles the self-assembly process in biological systems. The four main components for the synthesis are a source of silica, structure-directing agent (surfactants), solvent, and a catalyst. In detail, the synthesis process is based on the dissolution of surfactant molecules into polar solvents to obtain liquid crystals. When the concentration of surfactant is above critical micelle concentration (cmc), the surfactant molecules aggregate to form micelles. The shape and size of the micelles depend on the type of surfactant, surfactant concentration, pH, temperature, and the presence of co-surfactants, etc.[25,26] Depending on the experiment condition, the micelles aggregate forms supramicellar structures with hexagonal, cubic or laminar geometry, based on that geometry, the mesoporous framework is constructed. The porosity of ordered mesoporous materials also relies on the type of surfactant used during the liquid crystal templating mechanism.[27] Then, the silica source is added which condenses around the supramicellar structures. The second mechanism is the cooperative liquid-crystal template, which suggests that it is also possible that the lyotropic liquid-crystalline phase is formed even at concentrations of surfactant molecules below the cmc, prevailing as a cooperative assembly of the surfactant and the silica precursor. (Figure 2)

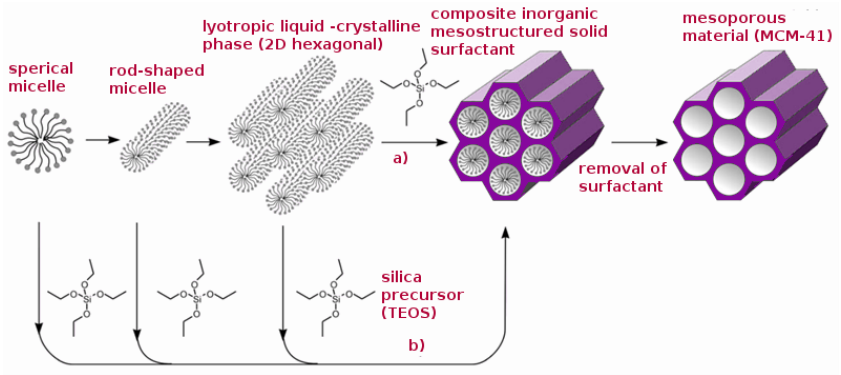

Figure 2. Formation of mesoporous materials by structure-directing agents: (a) true liquid-crystal template mechanism, (b) cooperative liquid-crystal template mechanism (Adapted from reference 25)

The MCM-type silica materials are synthesized by using cationic quaternary ammonium surfactant under basic conditions. The most well-known representatives of this class include MCM-41 with a 2D-hexagonal *p6mm* structure, MCM-50 with a lamellar *p2* structure, and MCM-48 with a 3D-bicontinuous cubic *Ia3d* structure.[23,28] (Figure 3) Depending on the predominant pore sizes, the porous solid materials are classified by IUPAC; pores with a diameter ranging from 2 to 50 nm are termed mesoporous material. The mesoporous MCM-41 class of materials has well-defined pore size distribution with a pore diameter ranging from 1.5 to 10 nm and with high surface areas (≥700 m^2/g). In this thesis work, MCM-41-type hexagonally ordered nanoparticles were synthesized and studied.

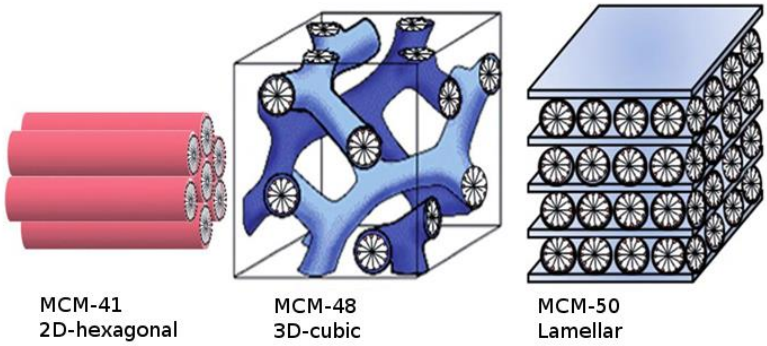

Figure 3. Schematic presentation of different mesoporous structures, including their pore symmetries (Adapted from reference 29)

2.2.2. MSNs size, pore size, and template removal

The silica source and nature of the surfactant decide the nature of the interaction.[30] For the mesoporous silica synthesis, the fundamental condition is an attractive interaction between the head group of surfactant and the silica precursor to ensure inclusion of the structure-directing agent without phase separation taking place. Different interaction can take place between the inorganic precursor and the head group of structure directing agent which can be either electrostatic, counter-ion mediated or hydrogen-bonding interactions. Most common silica precursors used for mesoporous silica synthesis are alkoxysilanes, e.g. tetramethyl orthosilicate (TMOS), tetraethyl orthosilicate (TEOS), tetrapropyl orthosilicate (TPOS) and tetrabutyl orthosilicate (TBOS). The rate of hydrolysis decreases with increasing size of the alkoxy group of the silane, which is caused by steric hindrance (spatial effects) and observed particularly in branched, bulkier precursors.[20] Alkaline and diluted conditions are generally utilized to synthesize negatively charged particles to avoid inter-particle aggregation. Monodisperse particles are obtained by template-directed alkaline synthesis and by using very dilute silane concentrations. The particle size of the MSNs can be modulated by controlling the pH of the reaction solution; decrease in pH leads to decrease in particle size[31] and by varying the initial silicate and surfactant concentrations under dilute condition.[32] For the synthesis of MSNs in alkaline conditions various approaches have been employed, such as use of water and EtOH as co-solvent in dilute condition, pH adjustment or dilution together with pH quenching, etc.[33] Mann and co-workers have prepared MSNs by employing a pH-quenching method. At higher pH, silica condensation is faster and electrostatic interactions between silica and cationic surfactants are stronger, which induces the fast simultaneous assembling and growth of the silica-surfactant nuclei and by rapidly lowering the pH, silica condensation rate becomes slower, which enables the synthesis of small (~15-23 nm) size particles.[34] It has also been reported that organosilanes together with TEOS in the reaction mixture led to a smaller particle size compared to using only TEOS as a source of silica, which indicates that functional silanes also act as size quenchers. The addition of organosilane increases the number of nuclei formation during the nucleation process and smaller particle size is obtained.[33]

The most commonly used structure-directing agent/template for the synthesis of MCM-41 is cetyltrimethylammonium bromide (or chloride). It is a template with an alkyl chain containing sixteen -CH_2 moieties. The *in situ* assembly of CTAB/CTAC micellar structures in the reaction medium can allow for the synthesis of silica structures containing interconnected

open pores. This template yields MCM-41 with a uniform pore size of approximately 2.7 nm. By using templates with longer or shorter alkyl chains, the pore size can be controlled. Nevertheless, due to the limited range of alkylammonium ions suitable for the preparation of MCM-41, the pore size can be adjusted to a small extent only. Some auxiliary organics like 1,3,5-trimethylbenzene,[35] hexane[36,37] or N,N- dimethyl-hexadecylamine (DMHA)[38] can be introduced to adjust the pore size of the material to a remarkable extent. Being apolar, these organics cannot be dissolved in water but they can be absorbed in the hydrophobic core of the template micelles. Due to this absorption, the micelles swell, thus increasing the average size of the mesopores in the MCM-41 up to values of approximately 8-10 nm in diameter. Mixtures of two surfactants can also be used to fine-tune the pore size of MCM-41 material.[39]

The template can be removed after the silica network has obtained a sufficient degree of condensation to create the porous structure. The conventional method of surfactant removal is by calcination, in which the as-synthetized dried materials are subjected to heat in air at heating rates of 1 °C /min up to at least 550 °C, followed by isothermal heating for 4-8 hours.[40] The calcination of the as-synthesized MCM-type material affects the surface area, pore size, and pore volume of the material. The heat treatment leads to contraction of the silica structure compared to the as-synthetized material, which is due to an increased degree of condensation of the silica network. The calcination procedure may also influence particle aggregation/agglomeration in aqueous media, as calcination results in a more hydrophobic surface. The alternative template extraction methods include acid treatment, liquid extraction, and supercritical fluid extraction depending on the synthesis employed. [41,42] For the MCM-41 type of materials prepared under basic conditions, strong electrostatic interactions occur between the negatively charged silica network and the cationic surfactant head groups. An ion exchange process by using acids or cationic proton donors is required to remove the template. Extraction procedures employed for this kind of materials involve extraction using ethanolic solution of ammonium nitrate or acidic ethanol. The extraction process can be enhanced by heating up of the particle dispersion up to 60-70 °C or simultaneous sonication treatment during the template removal. For the materials synthesized by co-condensation procedure, the calcination can cause decomposition of the organic functions of the material, and therefore, template removal by ion exchange or extraction method is preferred.

2.3. Surface functionalization of MSNs

Surface functionalization of inorganic mesoporous materials with organic moieties provides organic-inorganic hybrids, where the inorganic and organic components are linked via different interactions. MSNs prepared by surfactant-templated sol-gel techniques are highly versatile substrates for the formation of functional materials. The advantage of MSNs is the possibility to obtain three functional domains - the silica framework, external particle surface, and interior pore surfaces.[43,44] Functional groups which are on the exterior surface of the particles are more accessible and therefore they can be easily functionalized as compared to internal pore surface. Surface silanol (both free Si-OH and geminal $Si(OH)_2$) groups act as expedient anchoring points for organic functionalization. For the high coverage of silica surface with functional groups, a large number of surface silanols needs to be present after surfactant removal.

Organic functionalization of mesoporous silica permits tuning of the surface properties (hydrophilicity, hydrophobicity, binding with guest molecules), modulation of surface reactivity, protection of the surface, and alteration of the optical (e.g. fluorophores)[45] and the electrical properties (e.g. conducting polymers)[46]. The surface modification of the particles should be decided according to aimed application as surface characteristics play a key role in determining its interaction with the surrounding media, dispersion stability in the physiological environment, and it also provides access to introduce additional functions (such as 'smart gatekeeper' polymers) for a specific application. Additionally, particle surface can be engineered with targeting moieties such as small molecules, peptides or antibodies to achieve specific interactions with cells/tissue. The overall composition of the MSN surface has a high impact on the pharmacokinetics of the particles in a physiological environment.

Generally, the functionalization of MSNs can be accomplished by co-condensation or by post-synthetic modification (i.e., grafting or surface polymerization).[25,43,47] (Figure 4)

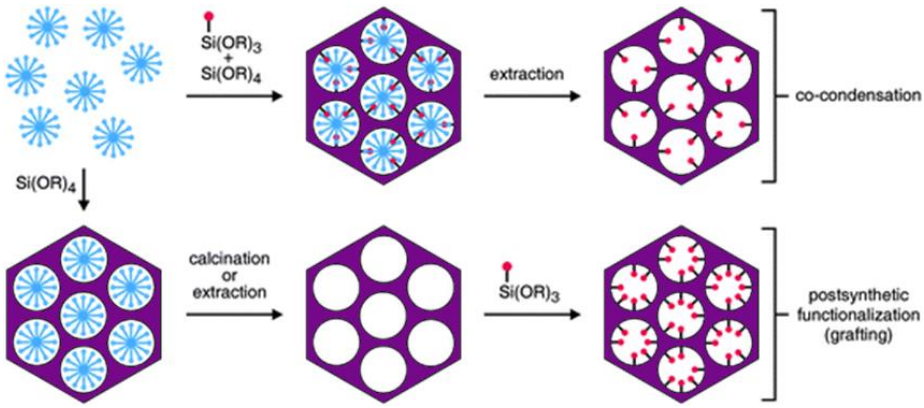

Figure 4. Schematic representation showing functionalization of mesoporous silica particles by co-condensation and by post-grafting methods (Adapted from reference 48)

2.3.1. Direct functionalization by co-condensation [25, 43, 49]

In co-condensation approach, a condensable precursor having the desired functional group is added to the mixture containing components for the formation of the mesoporous silica, which leads to materials with organic residues anchored covalently to the pore walls. In most cases, organoalkoxysilanes of type R–Si(OR′)$_3$ are used as precursors. The reason for that is co-condensation of tetraalkoxysilanes ((RO)$_4$Si) with terminal trialkoxyorganosilanes of the type R–Si(OR′)$_3$ forms Si–C bonds facilitating incorporation of a variety of organic groups into the material. The co-condensation method has the advantages of homogeneous surface coverage in one pot synthesis, better control over the amount of organoalkoxysilanes groups incorporated in the MSNs compared to post-grafting method, and the opportunity of using a wide variety of organofunctional groups. Further, organic functionalities are usually introduced during the synthesis stage; hence, the problem of pore blocking does not occur. However, this approach has a limitation for amount of organoalkoxysilanes groups that can be incorporated in the materials, as they can have a pronounced effect on the pore structure and morphology of the mesoporous material. High functionalization degrees often lead to a decrease in mesoscopic order and a reduction in the pore diameter, pore volume, and specific surface areas. Further, the structure-directing agent must be removed by extraction procedures, as template removal by calcination would destroy the organic moieties. Co-condensation approach provides an opportunity to prepare inherently fluorescent particles during the synthesis in one-step. Usually, this is conducted by pre-reacting a fluorophore-containing reactive group (e.g. isothiocyanate group; fluorescein isothiocyanate or tetramethylrhodamine isothiocyanate) with an organosilane that is subsequently used in the

co-condensation synthesis, yielding inherently fluorescent silica nanoparticles. In this thesis work, fluorophores have been introduced via co-condensation approach.

2.3.2. Functionalization by post-synthetic modification [25,43,50]

Post-synthesis modification of a pre-fabricated mesoporous material by attachment of functional molecules on the surface of the mesopores is usually carried out after surfactant removal, by chemical conjugation (grafting), surface polymerization or by adsorption of the functional groups. The original structure of the mesoporous support is maintained after the grafting procedure. In the grafting process, surface silanol (both free Si-OH and geminal $Si(OH)_2$) groups act as expedient anchoring points for organic functionalization via elimination reactions. For the high coverage of silica surface with functional groups, a large number of surface silanols needs to be present after surfactant removal. In the case of high-density organosilanes grafting, reactions at the pore opening might result in the inhomogeneous distribution of functional groups, and cause blocking of the pores.[51] The reaction conditions such as polarity and dielectric constants of the solvents strongly affect the concentration of grafted organic groups.[52] Anhydrous functionalization conditions are crucial to prevent reaction of the organosilanes with water and for hierarchical polymerization of the organosilanes inside the pores.

Post-synthesis modification by surface polymerization is another technique to increase the number of outer functional groups. Covalently anchored polymer brushes were usually prepared using the '*grafting to'* and '*grafting from'* techniques.[53,54] In the '*grafting to'* approach, only end-functionalized polymer chains tethers to the SiO_2 surface under appropriate conditions. The polymer layer obtained by the '*grafting to'* approach is thinner compared to '*grafting from'* approach and has low grafting density. In the '*grafting from'* approach, first an initiator molecule is assembled directly onto the SiO_2 surface, which is then used to initiate the free radical or living polymerization. High grafting densities polymer brushes is attained by '*grafting from'* approach and it also allows the creation of polymer chains of a dendritic nature, which increases the number of outmost functional groups available for further modification.[55] (Figure 5) This approach allows higher control of functionality, density, and thickness of the polymer layers. For instance, the hyperbranching ring opening polymerization of aziridine initiated on silica surface produces hyperbranched polyethylene imine (PEI) functionalized particle surfaces resulting in highly positively charged particles with increased electrostatic stability in physiological conditions.[47,55] PEI surface coating on mesoporous silica surface facilitates binding with negatively charged cell

surfaces, leading to increased cellular internalization. Pure PEI has been shown to result in toxic side effects directly related to the molecular weight of branched PEI[56] but charge capping or derivatization of PEI with other functional groups can restrain the drawbacks of pure PEI.[57,58]

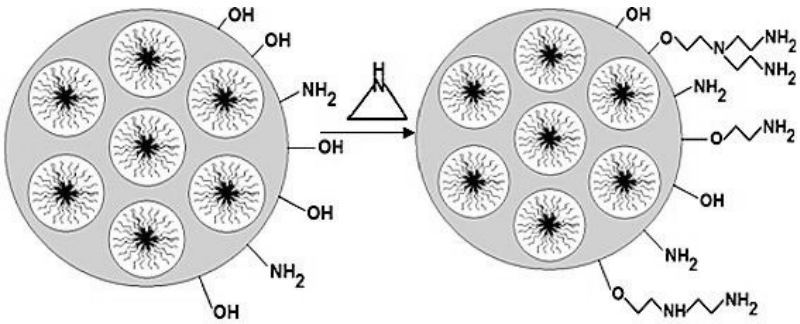

Figure 5. Schematic representation of surface functionalization by hyper branching polymerization of aziridine (Adapted from reference 59)

In this work, PEI functionalization has been carried out by employing the '*grafting from'* approach. For functionalization with Polyethylene glycol (PEG), the '*grafting to'* approach has been employed. The methoxy form of PEG, generally used for conjugation applications, has a single hydroxyl group that can be coupled with different entities such as MSN surface, small drugs, proteins, polymers, etc.[60] PEG, a hydrophilic and inert polymer, imparts a steric barrier to the surface of nanoparticles and reduces their protein binding which is the principal mechanism for the reticuloendothelial system (RES) to recognize the nanoparticles.[61] PEG has been widely used in biomedical drug delivery applications because it provides stealth effect by avoiding uptake of nanoparticles into the mononuclear phagocyte system (MPS), offers good particle dispersion in aqueous solvents. PEG has been reported as mucoadhesive agent, which aids to avoid binding with intestinal mucin networks and enhances penetration of nanoparticles through the mucin barrier.[62] In this work, PEGylation was achieved by attaching PEG either directly to the particle surface or via a grafted PEI layer.

Another technique that has also been used for the post-synthesis functionalization of particles is the adsorption method. Different surface modifiers such as small molecules, natural polymers and synthetic copolymers can be used for surface functionalization by adsorption method. The prerequisite for this technique is sufficient interaction between the particle surface and adsorbent compounds. However, in many cases, the formation of covalent bonds with the surface atoms is crucial for efficient functionalization, and hence the adsorption

method is less beneficial. Nonetheless, polymer adsorption onto surfaces is a widely used approach of surface functionalization. In this study, covalent surface grafting and surface polymerization were employed for the post-synthetic modification of MSNs.

2.3.3. Gate keeping mechanism for on-command drug delivery [10,63,64]

On-command stimuli-responsive drug delivery systems provide a convenient approach to deliver drugs in spatial-, temporal-, and dosage-controlled fashions. Compared with the sustained release system, the stimuli-responsive system can achieve drug release in a site-selective and controlled-release pattern, which can improve the therapeutic efficacy of the drug delivery system. Mesoporous silica supports provide possibility of including gate-like ensembles on the external surface for the design of nanosystems for on-command delivery applications. Implementation of such systems requires two subunits: First, a porous inorganic support, which is chemically inert material under a wide range of conditions, in which cargo is loaded, and second, certain molecular or supramolecular entities, attached to the external surface, which can control mass transport from the pores. The grafted entities on the outer layer should be biocompatible materials, which are susceptible to a specific physical incitement such as temperature,[65] light,[66] magnetic field and ultrasound,[67] or, in response to a specific stimulus such as pH,[68] redox potential,[69] enzymatic activities,[70] undergo a protonation, a hydrolytic cleavage, the rupture/formation of covalent bonds or a supramolecular conformational change. (Figure 6) Therefore, upon stimulation by an external stimulus, the release of drug molecules is thereby achieved. For the diagnosis and therapy, in combination referred as ‘theranostic’ applications, nanometer sized porous inorganic materials can be loaded with a therapeutic agent, together with an indicator molecule or a diagnostic marker.

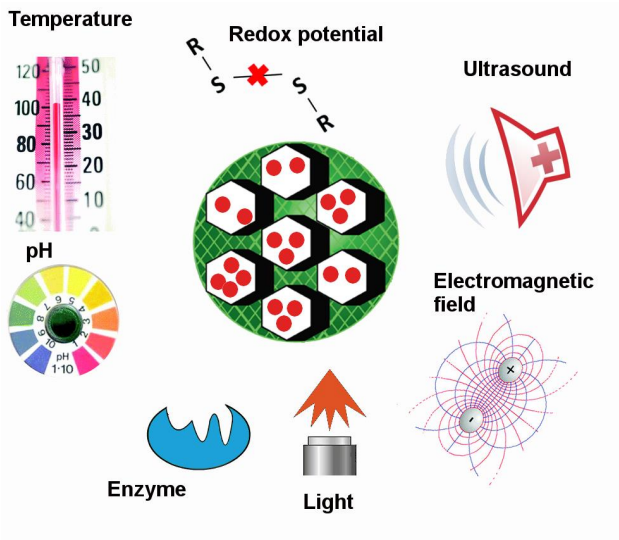

Figure 6. Schematic representation showing various gate keeping mechanisms on mesoporous silica nanocarrier

For temperature-gated delivery systems, porous materials have been capped with thermosensitive polymers which were able to deliver cargo after temperature dependent phase transition.[65] Existence of different temperatures are the characteristic in inflammatory diseases or in the tumoral tissues, which can be used to specifically deliver selected cargos. Thermosensitive polymer poly(N-isopropylacrylamide (PNIPAAm) and its derivative which shows lower critical solution temperature (LCST) around body temperature are usually employed.[71] Lopez and co-workers have used PNIPAAm as temperature-responsive cap grown on the inner pores of the mesoporous support. At a low temperature (below the LCST, ~32 °C), the polymer was hydrated and extended, closes the pores, and inhibits cargo (fluorescein, Rh6G) release, whereas at high temperatures (above the LCST, ~50 °C), the polymer was in a hydrophobic collapsed form, allows delivery of cargo.[72]

In light-driven gated systems, cargo release can be controlled spatially and temporally by fine-tuning the time and the area of light stimulus. (Figure 7) Light has the advantage of being applicable from outside of the patient in a noninvasive manner (usually near infrared radiation NIR radiation). The cargo release is usually triggered by light due to photodimerizations, photo cleavage of a chemical bond or photo induced heating of gold nanoparticles.[66] Lin and coworkers have developed photo responsive gold nanoparticle (AuNP) capped MSNs (PR-AuNPs-MSNs) based intracellular delivery system, the surface of the AuNP has been functionalized with a photoresponsive linker (thioundecyl-tetraethyleneglycolester-o-

nitrobenzylethyldimethyl ammonium bromide). The developed system showed zero premature release and controlled drug release by the application of low-power photo-irradiation under physiological conditions. Cell viability studies resulted in enhanced cytotoxicity of paclitaxel delivered using PR-AuNP-MSNs in human fibroblast and liver cells after photo-irradiation.[73]

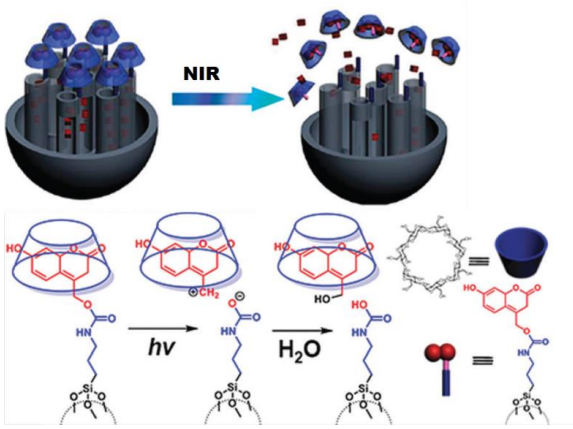

Figure 7. NIR light cleavable molecular switches on mesoporous silica nanocontainers (Adapted from reference 74)

Other physical stimuli such as magnetic fields and ultrasound can also be used for opening up molecular gates for controlled drug delivery by changing frequency, cycles, power, and time of application. It has been reported that magnetically activated systems have the advantage to provide extra control and to provide the guidance to the supported material with the use of external magnet, e.g. accumulation in selected tumor area.[75] Guo *et al*. have prepared core (a magnetic core of Fe_3O_4) - shell (mesoporous silica shell) nanoparticles by the Stöber method. The outer surface was decorated with diblock-thermosensitive copolymer poly((ethylene glycol)-co-(L-lactide)) and doxorubicin (DOX) was loaded as a model drug. The system was activated by heating or acidification, and the application of an alternating magnetic field (AMF) resulted in cargo delivery. Cell viability studies resulted in enhanced cell death when cells were treated with magnetic nanoparticles together with the application of AMF.[67] Wang *et al*. coated hollow MSNs with AuNPs, and loaded them with pyrene dye (as a model drug) and ultrasound-sensitive liquid perfluorohexane (PFH). The thiol-functional PEG was grafted onto the surface of the attached AuNPs. Application of ordinary ultrasound irradiation triggered the release of the loaded drug through the alteration of acoustic and thermal properties of the attached AuNPs. The authors have showed that MSNC@Au-PFH-PEG can

be used as a theranostic platform for contrast-intensified ultrasound imaging and combined chemotherapy.[76] Above reported approaches for triggered release are mostly based on temperature change.

Redox potential is another stimulus for controlled drug delivery since endogenous reducing agents found at the intracellular level can be used as triggers. (Figure 8) For some diseases, such as cancer, an increase in the concentration of redox-active species has been established. For example, disulfide bonds can be reduced by glutathione (GSH), the most abundant reducing agent *in vivo*. The GSH level in extracellular (2 μM) and intracellular (10 μM) environment is significantly different, furthermore, intracellular GSH levels in the tumor tissues are at least 4-fold higher than those in normal tissues. However, GSH is also present in healthy cells, so some amount of drug release will most likely also occur in healthy cells. The redox responsive systems employ disulfide bonds as a linker between porous support materials and capping agents (such as polymers, biomolecules or inorganic nanoparticles), which act as a stimulus to achieve 'on-demand' drug release. Wang and co-workers have modified MSN surface with PEG through biodegradable disulfide bonds. In their system, they have employed PEG chains as the gatekeepers that block the drug within mesopores and following the addition of glutathione, they have observed removal of gatekeepers and release of encapsulated drug (Rhodamine B).[77] However, some amount of drug release has also taken place without GSH, and GSH primarily accelerate the drug release.[77]

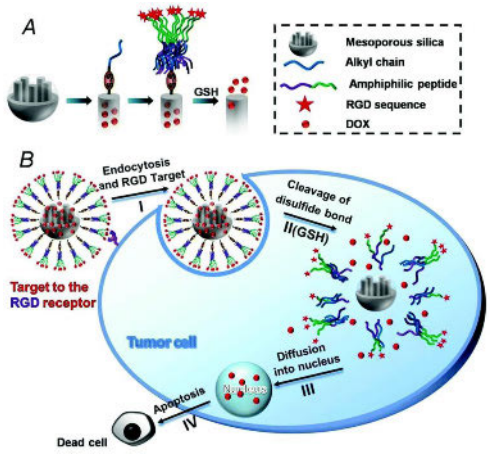

Figure 8. (A) Schematic representation showing structure of Redox responsive and RGD peptide targeted, DOX loaded mesoporous silica nanoparticles (B) Cell uptake through RGD mediated interaction, glutathione mediated drug release, drug diffusing in to cytoplasm and cancer cells apoptosis (Reference 78)

pH-responsive gates are a promising tool to develop delivery systems for nanomedicine. (Figure 9) The pH-responsive drug delivery can be achieved at the level of (a) organs (differential drug uptake along the gastrointestinal tract), (b) tissues (the pH gradients that exist in tumor microenvironments to achieve high local drug concentrations), and (c) intracellular level (to escape acidic endo-lysosomal compartments for cytoplasmic drug release). Wide varieties of imaginative ensembles including amines, different polymers, lipid bilayers, metallic complexes, and inorganic nanoparticles have been studied to control the release of selected cargos. Acrylic-based polymers such as poly(methacrylic acid) (PMAA) exhibit pH-dependent swelling, they retain a hydrophobic, collapsed state in the stomach due to the protonation of carboxyl groups whereas an increase in pH leads to their swelling due to carboxyl ionization and hydrogen bond breakage. N.Peppas has developed P(MAA-g-EG) hydrogels containing PEG grafts, which shows pH-dependent insulin release.[79]

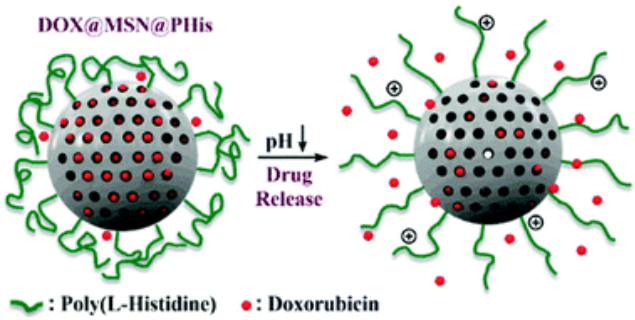

Figure 9. Schematic illustration showing DOX-loaded PHis-functionalized MSNs and pH-triggered controlled drug release (Adapted from reference 80)

Lipid bilayer (LB) deposition on the surface of MSNs acts as a diffusional barrier for the loaded drug and prevents premature drug leakage. Brinker and co-workers[81] have developed such 'protocells' by liposome fusion on MSNs, simultaneously with the loading of the cargo. They have prepared different materials by varying the liposome composition using 1,2-dioleoyl-sn-glycero-3-phosphocholine (DOPC), 1,2-dioleoyl-sn-glycero-3-phospho-L-serine (DOPS), and 1,2-dioleoyl-3-trimethylammoniumpropane (DOTAP) lipids. For the nanocarriers prepared with the DOTAP lipid, drug release was faster at pH 4 compared to that at pH 8. However, with their system loading capacity was quite low. In another study by the Brinker group[82], they have performed electrostatically mediated liposome fusion and lipid exchange with a nanoparticle supported bilayer after cargo loading using DOPS and DOTAP lipids to reduce premature drug release. This procedure involves tedious lipid exchange steps and produces electrostatically induced lipid bilayer defects. In another work, Ashley and

Brinker *et al*. have developed MSNs loaded with several cargos (DOX, 5-fluorouracil, or cisplatin, siRNA, diphtheria toxin, and quantum dots), and fused them with liposomes made of DOPC/ 1,2-dipalmitoyl-sn-glycero-3-phosphocholine (DPPC)/ 1,2-dioleoyl-sn-glycero-3-phosphoethanolamine (DOPE)/Cholesterol lipids. This supported lipid bilayer has been functionalized with a targeting peptide (SP94), with a fusogenic peptide (H5WYG) and with PEG moieties. These nanoparticles were internalized by human hepatocellular carcinoma cells (*in vitro),* and have released the entrapped cargo into the cytosol due to disruption of the lipid bilayer upon the protonation of imidazole subunits in the fusogenic peptide.[83] Bein and co-workers have prepared MSNs, coated with different lipid bilayers to release an entrapped cargo upon addition of small molecules. In this study, the pores of the MSNs were loaded with fluorescein or colchicine and capped by the formation of a lipid bilayer shell using DOPC, 1-palmitoyl-2-oleoyl-sn-glycero-3-phosphocholine (POPC), or a mixture of DOTAP/DOPC lipids.[84] However, low loading capacity of negatively charged guests observed for this system. The physically supported membrane is not thermodynamically and mechanically stable from the proximity of other lipophilic agents and defects in the supported lipid bilayer produced due to high surface porosity leading to premature drug leakage. Therefore, an intermediate lubricating layer between porous support and lipid bilayer, which provides opportunity for covalent conjugation of the inner leaflet of lipid bilayer with porous support would be beneficial for the site-specific delivery of hydrophilic molecules.

2.3.4. Functionalization with targeting ligands[85,86,87]

Targeting approaches can be broadly classified into two areas; passive and active targeting. Passive targeting exploits the normal bio-distribution that unadorned nanoparticles will take within the body. Upon intravenous delivery, plain nanoparticles are rapidly removed from circulation by opsonization, and they accumulate in the liver and spleen. Therefore, this clearance can be exploited to treat hepatic disorders such as liver fibrosis, hepatocellular carcinoma or liver cirrhosis. Tumor targeting requires circumvention of this clearance mechanism. Nanoparticles surface can be functionalized or coated with hydrophilic polymers to suppress opsonization and subsequent phagocytosis. Passive targeting at tumor sites is due to the enhanced permeability and retention (EPR) effect. The tumor vasculature has increased permeability due to disordered epithelial cell junctions; hence, tumor vessels are more permeable to nanoparticles than the well-defined vasculature found in normal tissue.[88] Moreover, tumors have poor lymphatic drainage, leading to further accumulation of the

nanoparticles at the diseased site.[89] A drawback of passive targeting is the extravasation of the delivery systems in off-targeting organs, such as liver, spleen, or bone marrow.

Active targeting involves the modification of the nanoparticle surface with a targeting ligands specific to cell surface components that are unique to, or upregulated in, dysplastic and pathologic tissues. Targeted delivery can potentially increase the efficacy and reduce the toxicity of therapeutic agents. Anchoring a biological targeting moiety onto an external surface allows homing, binding and internalization of the nanoparticles to the targeted sites such as cells and tissues, which contain overexpressed receptors.[90] (Figure 10) However, to achieve efficient *in vivo* active targeting, protein adsorption on the nanoparticles should be low and their blood circulation times should be high. As molecular targets are usually situated in the extravascular space of the tumor, nanoparticles rely on the EPR effect to reach their targets. Protein adsorption shields the targeting ligand and thus reduces the active targeting yield.[91] Targeting ligand does not increase tumor localization, but instead functions primarily in the uptake of the nanoparticle by the tumor cells.[92] The other advantage of actively (cancer cell-) targeted nanoformulations over passively targeted formulations is that they are taken up by cancer cells much more efficiently.[93] Targeting ligands fall into several classes: small molecules (vitamins, carbohydrate), peptides, monoclonal antibodies, and nucleic acids based aptamers.[94] For the conjugation of targeting ligands to nanoparticles, the surface of the nanoparticles is modified with an appropriate chemistry to introduce reactive moieties with functional groups. It is also important that the selected targeting ligand have a functional group that can be used for conjugation. Most of the conjugation chemistries involve covalent reactions that use amine reactive group, sulfhydryl reactive groups or carbonyl reactive groups. Non-covalent interaction between streptavidin and biotin is also commonly used.[95]

Small molecule folic acid (Vitamin B9) is a high affinity ligand of endogenous folate receptor, which is frequently up regulated in many types of human cancers.[96] Nanoparticles conjugated with folic acid can be actively internalized via receptor-mediated endocytosis and effectively directed to folate receptor-positive cancer cells.[97] Different research groups have prepared folic acid modified MSNs for cellular targeted drug delivery and observed enhanced uptake of folic acid modified nanoparticles in folate receptor positive cells.[98,99,100] Carbohydrates, which interact weakly with some cell surface receptors, can also serve as small molecule targeting ligands. Carbohydrates permit nanoparticle glycotargeting, which is based on endogenous lectin interactions with carbohydrates. Galactose modified nanoparticles can be internalized via asialoglycoprotein receptors,[101] mannose targeted nanoparticles

internalized via mannose receptors, which are highly expressed in the immune system for the treatment of diseases localized in macrophages,[102] and glucose conjugated nanoparticles internalized via glucose transporters (Gluts) overexpressed in tumor cells.[103] The major advantages of using small molecules as targeting ligand is their stability, ease of conjugation with nanoparticles, and the potential low cost.

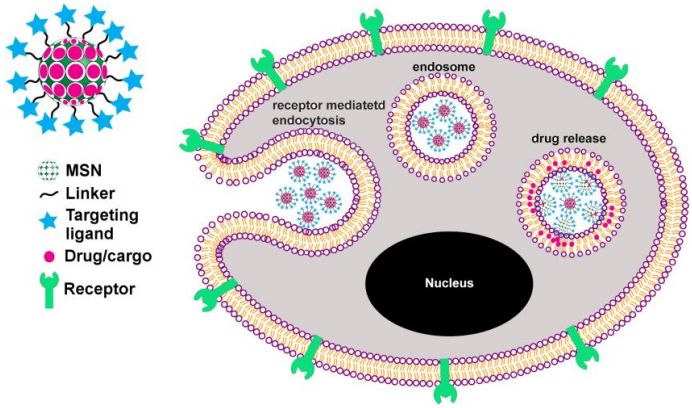

Figure 10. Schematic presentation showing design of MSNs functionalized with targeting ligand, their receptor mediated endocytosis and drug release (Adapted from Supp.Paper II)

Targeting peptides, discovered via phage display, binds to specific target protein typically expressed on the cell surface. For example, arginine-glycine-aspartic acid (RGD) peptide is used as a targeting ligand for αvβ3 integrin. Xiao and co-workers have employed RGD peptide functionalized dual responsive (pH and redox) tumor targeting MSNs for delivery of DOX.[104] As a targeting ligand, peptides provide smaller size compared to antibodies, as well as high specificity and affinity. Antibodies are used as targeting ligands due to their ability to target tumor-associated cell surface antigens. Tsai *et al*. have developed anti-HER2/neu mAb conjugated MSNs for selective targeting to breast cancer cells.[105] Wang *et al*. have prepared cetuximab (anti-EGFR monoclonal antibody) modified MSNs for efficient treatment of epidermal growth factor receptor (EGFR)-mutant lung cancer. Major issues of antibody targeting ligands include immunogenicity (production of unwanted immune response), stability, and difficulty for site-specific conjugation with nanoparticles.[106] Aptamers are short single-stranded nucleic acids (RNA or DNA) capable of displaying diverse structures, and they can bind with biochemical targets. Zhang *et al.* have developed aptamer-targeted drug nanocarriers, by capping mesoporous silica-coated quantum dots with a programmable DNA hybrid (an aptamer and antisense oligonucleotide of miR-2). The nanocarriers have been

delivered by aptamer-mediated recognition and endocytosis into HeLa cells, and controlled drug release was achieved, which led to a sustained lethality of the HeLa cells.[107]

2.4. Drug incorporation and release

2.4.1. Drug incorporation

MSNs have been established as a promising and novel drug delivery vehicles due to their unique structural properties, possibility to include various surface functionalities and biocompatibility, to ensure the controlled release and targeted drug delivery of a variety of drug molecules.[108,109,110] By loading drugs into the porous structures of these particles, it is possible to control drug release or deliver the appropriate concentrations of therapeutic molecules to the suitable locations.[111,112] The porous matrix may also protect biomolecules from enzymatic degradation. MSNs possess high specific surface area and large pore volumes, which allow incorporation of large quantities of drug molecules.[113]

In addition to the critical parameters associated with the carrier system, such as pore size, surface chemistry and hydrophilicity/hydrophobicity of MSNs, physicochemical properties of the drug molecule and loading methods can also affect the drug release profiles. The most common methods for loading drugs within the MSNs include physical adsorption into the inner pore walls by impregnation method (adsorption of drug in mesopores using highly saturated drug solution), and covalent bonding (conjugation of drug with nanoparticles).[114] The silica matrix remains intact in organic solvents; hence, different types of solvents can be employed in the drug loading steps. The solvent can be selected in terms of the drug's solubility in order to facilitate the drug adsorption to the pore walls over solvent-drug interactions. A hydrophobic solvent having low affinity for the drug molecule can be employed for high adsorption of the hydrophobic molecules. When the drug is hydrophilic/ water soluble, loading can be performed in aqueous solution employing different pH conditions and utilizing electrostatic interactions/ surface charge. The non-functionalized MSN particles are negatively charged, thus they can spontaneously adsorb positively charged molecules whereas amine functionalized MSNs have positively charged surface, which allows loading of negatively charged drug molecules. The adsorption of drug molecules to the silica matrix usually leads to monolayer formation, which can be demonstrated using a Langmuir isotherm.[115] Loading of drug compounds such as ibuprofen, vancomycin, alendronate,

gentamycin, camptothecin, paclitaxel, DNA, calcein, vitamin-B2, cyclic AMP into the mesopores have been reported using impregnation methods.[113,114]

Covalent bonding is another technique for loading of drug molecules into the porous structures; it provides e.g. enzyme responsive drug release. MSNs with surface functions such as thiol or amine groups can be directly employed for covalent based drug loading and be cleaved in the presence of an enzyme on tumor surfaces. Loading of cysteine, pro drug sulfasalazine, and paclitaxel have been reported using covalent bonding.[116,117,118] The main advantage of the covalent conjugation method is that it prevents undesired leaching of the cargo before it reaches the target site and payload release can occur after breakage of the covalent bonds. However, after covalent conjugation drug molecule may convert to inactive form; therefore, it is important to perform an appropriate assay to confirm the activity of the drugs following the release process.[118] Due to the following drawback, covalent bonding is not commonly employed for the drug loading in mesoporous silica nanocarriers.

2.4.2. Drug release

The drug loading inside the mesoporous nanocarrier can provide the opportunity for controlled drug release in order to maintain a drug concentration within the therapeutic window. The drug release can be either due to simple diffusion, pH driven release, photo-induced, temperature-driven or enzyme responsive release. In general, water-soluble drugs that are incorporated into a porous matrix are mainly released by diffusion, whereas for the poorly water-soluble drugs main release mechanism is through self-erosion of the matrix.[119] Additionally, the dissolution mechanism of carrier/matrix also depends on surface functionalization, type of drug and loading degree, thermal history, surfactant extraction method, particle size and pore size of mesoporous particles. One approach to obtaining on-demand release profile of drug molecule is to use gating materials attached to the pore entrances or inside the pores themselves, which can be triggered by an external stimulus.[10] (As explained in section 2.2.3) von Haartman *et al.* have studied the intracellular release mechanism of hydrophobic drug molecules from functionalized MSNs in relation to the biodegradation of the nanocarrier. They have observed that the cargo release was primarily dependent on the degradation of the nanocarrier in pure aqueous media, while in media mimicking intracellular conditions, the physicochemical properties of the cargo molecule and its interaction with the carrier and/or surrounding media were main release-governing factors.[120] Further, the physical state of the incorporated drugs: amorphous, crystalline or a combination of them, has an influence on the dissolution rate of drugs.[121]

2.5. Biomedical applications of MSNs

In the past few decades, various types of multifunctional nanomaterials for diagnosis and therapy referred as 'theranostics' have been developed. Numerous benefits in using these nanometer-sized delivery platforms include the ability to control the drug release rate, the accumulation at the targeted region of interest without damaging normal cells, and the possibility of achieving specific drug release upon activation by various external/internal stimuli, such as light, temperature, pH, and redox potential.[122]

Silicon is the second most abundant element on Earth's crust, where it is chiefly found in the form of silicon dioxide (silica). Silicic acid is profuse in bone, cartilage, and other supporting tissue, and is necessary for growth and health of the body's connective tissue.[123] Silica is widely used in pharmaceutical formulations, cosmetics, and food products as an excipient and it is 'generally recognized as safe by US FDA.[6] Many different amorphous silica materials have been proposed as drug delivery matrixes. Among them, the utility of mesoporous silica as a reservoir for drug delivery has been introduced for the first time by Vallet-Regi *et al.*[124] in 2001. The characteristic properties of MSNs include high surface area-to-volume ratio, easily modified surface properties, and high porosity, which allow high loading capacity (up to 100 wt%) without destabilization of the silica framework. Besides, surface of these nanocarriers can be functionalized with stimuli-responsive groups for the controlled drug release; all of this introduces them as a novel platform for various biomedical applications.

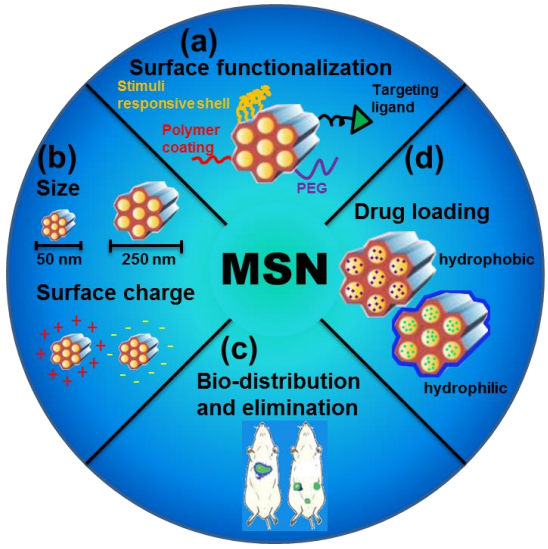

Figure 11. Mesoporous silica nanoparticle functionalization, morphology, drug loading and bio-distribution (A) Post-synthesis surface modification (e.g. targeting/tracking moiety

conjugation, PEGylation, stimuli responsive shell, or polymer coating), (B) Size and charge of MSNs can be precisely tailored to gratify application-specific needs (e.g. passive targeting); (C) Variation of synthesis and post-synthesis modifications result in unique, designer-specified bio-distribution and elimination profiles and (D) Cargo loading (e.g. siRNA, therapeutic drug and dye) (Adapted from reference 125)

After the discovery by Vallet-Regi *et al.*, mesoporous silica materials have been widely explored as drug delivery carrier in biomedical research. In 2003, Lai *et al*. have demonstrated modified MSNs to facilitate the stimuli-responsive controlled release of neurotransmitters and drugs.[126] However, the first report on the *in vivo* application of MSNs as diagnostic tools and therapeutic drug carrier was reported by Mou and coworkers in 2008.[127] Despite the existence of various *in vitro* and *in vivo* reports using MSNs as drug carriers available in the literature, there are many discrepancies in the obtained *in vivo* bio-distribution and toxicity results. These differences should be addressed by thorough physicochemical characterization of nanoparticles such as size, surface charge, pore structure, aggregation state, dispersibility, and biodegradability under biological conditions before administration, by careful evaluation of the relationship between physicochemical property and biological response of nanoparticles, and by the use of comparable testing platforms and model systems.

2.5.1. Cellular interactions

The cell membrane is a lipid-based membrane that envelops the cytoplasm and preserves the local chemical composition of a cell; it also plays an active role in the interaction with foreign macromolecules, including nanoparticles. To be internalized inside the cells, nanoparticles have to overcome the cell membrane barrier. The physicochemical properties of nanoparticles, such as size, shape, surface charge, hydrophobicity/hydrophilicity and surface chemistry or functionality, comprehensively determine the interactions of nanoparticles with biological systems.[128] Correlation of the surface physicochemical properties of nanoparticles with their interactions with biological systems provides key foundational data for nanomedicine. Depending on the property of the transported particle, different types of endocytosis pathways, which vary in the involved internalization machinery, cargo properties and the size of the transport vesicle, may mediate the cellular uptake.[129] Agglomeration of nanoparticles in physiological buffers or in plasma cause fast clearance of nanoparticles due to phagocytosis by macrophages of the MPS, which can be due to recognition of the plasmaproteins (opsonins) that bind on the surface of the nanoparticles. Thus, cellular internalization routes determine the fate and intracellular localization of nanoparticles, which

suggests that proper strategies to control the nanoparticle cellular internalization route can hugely augment their therapeutic outcome.[130] For example, it is currently approved that while large particles penetrate into the cells via phagocytosis, the cellular uptake of small particles occurs via different non-phagocytic mechanisms. Thus, it is important to evaluate physicochemical properties of MSNs properly to predict their behavior *in vitro* and *in vivo*.

2.5.1.1. Effect of MSNs' size

The particle size is an important parameter for designing suitable drug-carrier nanoparticle systems. One of the benefits of the nanoparticles is their ability to enter into the cells via endocytosis because of their similarity to many biomolecules or viruses in terms of size. This internalization can be energy dependent or via the engagement of caveolin or clathrin-coated pits, or other pathways independent of these proteins. (Figure 12)

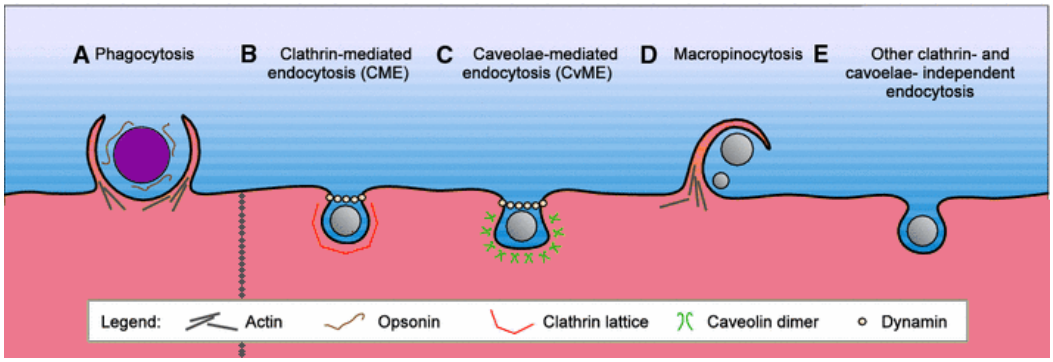

Figure 12. The cellular internalization pathways for the nanoparticles: (A) Larger nanoparticles are internalized via phagocytosis. Smaller particles can be internalized through several mechanisms, such as clathrin-mediated endocytosis (B), caveolae-mediated endocytosis (C), macropinocytosis (D), and clathrin-independent and caveolae-independent endocytosis (E). (Adapted from reference 131).

In the literature, different studies with MSNs have been carried out in order to determine the effect of size on cellular internalization. Rejman *et al.* have reported that internalization of nanoparticles smaller than 200 nm was mediated through active clathrin-coated pits, for nanoparticles with a size of 500 nm caveolae-mediated pathway became dominant.[132] Gao and coworkers have studied uptake mechanism of 60- 600 nm size negatively charged FITC-SiO_2 nanoparticles in HepG2 cells and observed that nanoparticles enter into the HepG2 via clathrin-mediated pathway and particle size showed no influence on the distribution and uptake mechanism of the silica nanoparticles.[133] However, Mou and coworkers have also

developed MSNs with different average sizes between 30-280 nm, and they have observed that cellular uptake is particle size dependent in the order of 50>30>110>250>170 nm and 50 nm is an optimal particle size to reach the maximum uptake of MSNs by HeLa cells.[31] However, authors have not explained the reason behind this finding. Nonetheless, Jiang et. al have reported that 40- and 50- nm particles demonstrate greatest effect to alter signaling processes essential for basic cell functions, which might be a reason for higher uptake of 50 nm particles.[134] Thus, the particle size is a crucial parameter for designing nanocarrier systems. In this study, we have used approx.70 nm and approx. 250 nm sized MSNs for delivery of different cargoes.

2.5.1.2. Effect of MSNs' surface charge

Various factors have been outlined to influence the kinetics and efficiency of intracellular endocytosis of MSN materials. One of the factors that can significantly affect nanoparticles' stability, cellular interactions, opsonization, phagocytosis, and bio-distribution is the surface charge of the nanoparticles.[135]

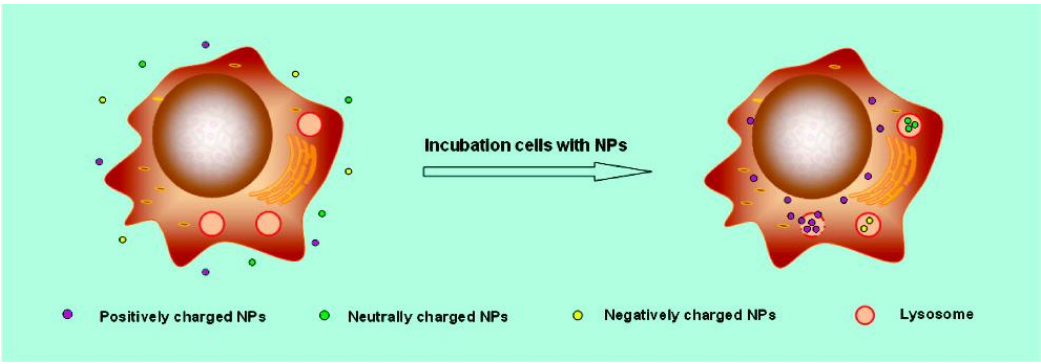

Figure 13. Cellular uptake and intracellular distribution of nanoparticles with different surface charges (Adapted from reference 136*)*

The cellular interaction of various nanoparticles is affected by the surface charge (positive, neutral or negative) of the nanoparticles.[136] (Figure 13) Usually, cellular internalization of positively charged nanoparticles is higher than the respective anionic nanoparticles; however, charge density and hydrophobicity of the particles are also important. Different studies have been performed to identify surface charge dependent uptake mechanisms, but still no general rule has been identified. Furthermore, the screening of the intracellular distribution of nanoparticles has indicated that some positively charged nanoparticles possess endosomal escape ability after being internalized into cells, whereas neutrally and negatively charged

nanoparticles prefer the lysosomal co-localization.[136] A plausible explanation for this phenomenon is that the abundant positive charge of the nanoparticles can cause additional pumping of protons into the endosome, with the influx of chloride ions to maintain the neutral charge, leading to increases ionic strength inside the endosome.[137] This then causes the physical rupture of the endosomal membrane because of the osmotic swelling, a phenomenon known as the 'proton-sponge' effect, resulting in the escape of the nanoparticles from the degradative lysosomal trafficking pathway. This behavior can increase the cytoplasmic localization of the positively charged nanoparticles and enhance the drug concentration around the nucleus. Slowing *et al.*, have reported that surface functionalities regulate the uptake of MSNs in HeLa cells, with positive zeta-potentials can be taken up more compared to their counterparts with negative zeta-potential, owing to a higher electrostatic affinity to the negatively charged cell membranes.[138] Chung *et al.*, have developed unmodified, weakly positive, moderately positive and strongly positively charged MSNs and studied their cellular internalization in 3T3-L1 cells and human mesenchymal stem cells (hMSC). They have observed a positive correlation between positive surface charge and the number of labeled cells for 3T3-L1 cells. Further, the charge effect on cellular uptake mechanism is cell type and surface charge (low, moderate or high) dependent. At a low surface charge, the normal clathrin- and actin-dependent mechanisms operate, above a certain threshold of surface charge unidentified charge-dependent mechanism starts to be effective for hMSC.[105] However, the above-mentioned studies were performed *in vitro* only, and for *in vivo* delivery, depending on the surface charge of the nanoparticles, formation of a protein corona occurs, which can change the fate of the nanoparticles.[139] Henceforth it is imperative to study the influence of surface charge together with charge density and a surface coating on MSNs' internalization pathway.

2.5.1.3. Effect of MSNs' hydrophobicity and surface properties

Another important aspect of nanoparticles for potential biomedical application is surface hydrophobicity. Nanoparticles require hydrophilicity for stable dispersion in water or aqueous environment. However, hydrophobicity is also required to enhance the interaction of nanoparticles with the cellular membrane to encourage uptake into cells. Since the nanoparticles' surface comes in direct contact with the cells during *in vitro* condition, and the cell membrane is rich in alkyl lipids and cholesterol, imparting a partially hydrophobic character to the cell surface. Hydrophobic nanoparticles have high affinity for the lipid bilayer of the cells and thus, the uptake of hydrophobic particles is more pronounced compared to the

hydrophilic particles. However, when hydrophobic nanoparticles within the cell membrane penetrate into the cytosol, the surface of the nanoparticle should become hydrophilic to allow facile permeation. The hydrophobic nanoparticles are more pronounced to opsonization after intravenous administration. The surface properties of nanoparticles are also important for further modification through electrostatic or hydrophilic/hydrophobic interactions. Shashtri and co-workers have shown that by balancing between lipophilicity and charge characteristics of lipid nanoparticles, they can be targeted to cholesterol-rich caveolae domains on the cell surface and thus exhibiting high specificity towards endothelial cells.[140] Thus, it is crucial to study internalization pathway and intracellular localization of MSNs in presence of different surface coatings such as polymeric or lipid bilayer coating.

2.5.2. Biocompatibility and bio-distribution

To evaluate the potential of MSNs as drug delivery carrier, properties such as bio-distribution, biocompatibility, and clearance from cellular systems are very important. For the nanocarrier system, a critical challenge is to have the capacity to deliver sufficient amount of drug to the desired location with less acute or chronic toxicity to the healthy cells than conventional therapies.[14] The other important concern for the nanocarrier is information concerning its *in vivo* bio-distribution.

Recent investigations on the *in vivo* bio-distribution and excretion of MSNs by different researchers have shown that MSNs accumulate mainly in the liver, kidney and urinary bladder after intravenous injection, and partially excrete through the renal route.[141,142] Further, bio-distribution of MSNs in tumor bearing mice is different than animal without any tumor, as passive accumulation of MSNs occurs in tumors due to their leaky nature and influence overall bio-distribution of MSNs. Hyeon and coworkers have applied dually active (fluorescent and magnetic) core-shell structured PEGylated MSNs of less than 100 nm and observed their accumulation in tumor 24 hours after intravenous administration, which is probably due to an EPR effect. No short-term toxicity effect of MSNs was observed in mice at a dosage below 200 mg kg^{-1}, which is significantly higher than the required dosage for drug delivery applications.[143] In another study, the same group have used PEGylated MSNs of 70 nm size, passively targeted to xenoimplanted MCF-7 tumors, and observed that MSNs also accumulate in the liver, spleen, and lungs, due to phagocytosis by macrophages.[144] Jie Lu *et al.* have studied biocompatibility and bio-distribution of 100-130 nm size MSNs using human cancer xenografts, and observed that MSNs are well tolerated up to 100 mg kg^{-1} dose and preferentially accumulate in tumors. Further, they have treated mice with camptothecin-

loaded MSNs, which showed suppression in tumor growth.[145] However, in this study the authors have employed fluorescence spectroscopy and ICP-MS techniques for the quantification of the amount of particles distributed in different organs. Nevertheless, they have not employed adequate controls (without nanoparticles) for background correction. For example, for the FITC particles (in green channel) background fluorescence in different tissues is very high, which is not taken into account, and different tissues have varying amount of endogenous silicon levels. The blood circulation time of the nanoparticles varies depending on their particle size, shape, surface charge and surface properties and functional groups[142,146] and therefore, detailed information on the bio-distribution, biocompatibility and drug delivery efficiency of MSNs with different surface functionalizations still needs further investigations.

2.5.3. Barriers for drug delivery

For any therapeutic agent to be effective, it must accumulate in target cells in optimal concentrations for a required duration of time. However, physiological and biochemical barriers prevent successful accumulation of nanopharmaceuticals at the disease sites. The physiological barriers for oral drug delivery include intestinal epithelium, which is highly absorptive and is composed of villi, covered with enterocytes, goblet cells, and mucus layer. Additionally, biochemical barriers such as low acidic pH in the stomach, metabolizing enzymes and efflux pump; makes drug delivery to GI tract more difficult.[147] Using intravenous administration route, these limitations of the oral route can be circumvented as the entire dose is distributed in the systemic circulation. Furthermore, even if a drug is in the bloodstream, treatment of certain diseases such as cancer or brain diseases requires overcoming other obstacles and crossing of other physiological barriers such as opsonization and subsequent sequestration by the MPS, nonspecific distribution, tumor microenvironment, cellular internalization, escape from endosomal and lysosomal compartments. After intravenous administration, nanoparticles undergo opsonization, involving the adsorption of plasma proteins, including serum albumin, apolipoproteins, complement components and immunoglobulins, onto the surface of circulating nanoparticles, and subsequent uptake by resident macrophages of the MPS. This results in high accumulation of nanoparticles in organs, such as the spleen and the liver, contributing to nonspecific distribution of nanotherapeutics to healthy organs.[148] As mentioned in *Section 2.3.4*., EPR effect allows delivery to the tumor cells using nanocarriers, as nanoparticles due to leaky tumor vasculature are able to passively target tumor cells, and due to the poor lymphatic drainage of tumors their

residence time also increases. However, a number of barriers still exist, which can prevent the efficient extravasation of nanoparticles. These include the tumor interstitium barrier, physiological factors such as low pH, low oxygenation and high interstitial fluid pressure in the tumor microenvironment. Further, the tumor cell membrane and intracellular organelles represent another barrier for the nanoparticles to conquer, for the effective intracellular delivery of drug cargo.[149,150] For the treatment of brain diseases, blood brain barrier (BBB) is a diffusion barrier, consists of the endothelial cells lining the blood vessels in the brain, which impedes influx of most compounds from blood to brain. The cerebral endothelial cells form the tight junctions and create a diffusion barrier, which selectively excludes most blood-borne substances from entering the brain.[151] To overcome these limitations, nanoparticle formulations should possess the ability to encapsulate and protect drugs and release them in a temporally or spatially controlled manner.

2.5.4. Endosomal escape

Endocytosis is the main uptake mechanism of cells for the internalization of any biological agents, such as DNA, siRNA, and proteins.[137] After endocytosis, these molecules become entrapped inside the endosomes from which they transported to the lysosome, and they are degraded by specific enzymes in the lysosome. Thus, another barrier to achieve an effective intracellular drug release is endosomal entrapment. Hence, to facilitate the endosomal escape and ensure cytosolic delivery of the therapeutic molecules, different approaches are required. For example, bacteria and viruses use various mechanisms to penetrate the membranes of their target cells and escape the endosomal pathway. For the carrier-mediated delivery, different approaches can be employed to facilitate the endosomal escape such as pore formation in the endosomal membrane using different peptides, the pH-buffering effect of protonable groups such as PEI and fusion into the lipid bilayer of endosomes.[152]

2.5.5. Drug delivery

A drug delivery system can be defined as a formulation that controls the rate and period of drug delivery (time-release dosage) and targets it to specific areas of the body.[153] Hence, only the pharmacological target is being exposed to the drug, in order to maximize the response and minimize the collateral effects.[154]

2.5.5.1. Oral route

Drugs substances are intended for use in the diagnosis, treatment, or prevention of diseases. Drug therapy is envisioned to result in a specific pharmacologic response of desired intensity

and duration at the same time avoiding adverse drug reactions.[155] The drug response is dependent on the availability of the active drug at the receptor site, which is influenced by the plasma drug concentrations. The solubility and permeability of a compound are therefore a crucial parameter for the drug to be effective at the target site. According to Biopharmaceutical Classification System (BCS), a drug substance is considered highly soluble when the highest dose strength is soluble in 250 ml or less of aqueous media over the pH range of l-7.5. The FDA criterion for solubility classification of a drug in BCS is based on the highest dose strength in an immediate release (IR) oral product.[156] The ability of a compound to diffuse across lipid membranes is termed permeation and it is directly correlated with compound's lipophilicity. The permeability is calculated based on measurements of the rate of mass transfer across the human intestinal membrane. A drug substance is considered to be highly permeable when the extent of absorption in humans is determined to be 90% or more of an administered dose when there was no evidence suggesting instability of the compound in the GI tract. BCS is the fundamental tool in drug development, especially in the development of oral drug products. According to the BCS, drug substances are classified as follows (Figure 14)[157,158]:

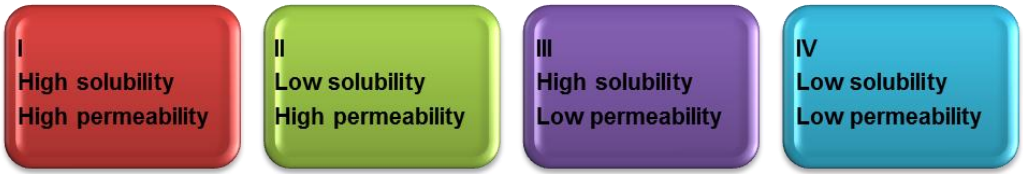

Figure 14. BCS classification of drug molecules.

The oral route is the most widely employed route of drug administration because of its simplicity and patient compliance. In drug discovery, the number of insoluble drug candidates has increased in recent years, with almost 70% of new molecular entities showing poor water solubility.[159] Further, newly designed drugs that are based on biomolecules, such as peptides, oligonucleotides, proteins and DNA often exhibit low bioavailability and require protection against enzymatic breakdown.[160] The major hurdles for oral delivery of many drugs are low aqueous solubility, inadequate penetration through mucosal barriers, low dissolution in the GI fluids, and poor stability in the gastric environment resulting in poor oral bioavailability.[161] In order to overcome these problems associated with drug delivery, and for the reappraisal of drugs that were previously disqualified due to their unfavorable pharmacokinetic properties numerous strategies can be employed.[162] From the various available approaches, carrier-

mediated delivery is a promising method of improving drug bioavailability, in which the drug molecule can be confined within the carrier agent and targeted to its specific site of action and at the same time being shielded from any unwanted degradation.[121,160] Biodegradable mesoporous silica nanomaterials have been widely used as novel drug delivery systems holding promise for oral drug delivery.[163,164]

2.5.5.2. Intravenous route

Compared to oral administration, intravenous route provides advantage such that the entire administered dose reaches the systemic circulation after administration. However, a major challenge to achieve better treatment of disease such as cancer, infection and inflammation is the difficulty of delivering the drug only at a target site after injection, thus reducing severe toxic effects on peripheral tissues and organs. Further, intravenous administration of many newly developed drugs consists of peptides or other bio-macromolecules, which often suffer from degradation in the biological fluids, thus losing their activity. The capability of the targeting ligands or antibodies against cell surface receptors or antigens by active or ligand-mediated cellular targeting can be utilized to increase site-specific actions of drug delivery systems.[165] Thus, drug delivery system along with the therapeutic moiety would be delivered to the interior of the specific cells. Efficient *in vivo* drug delivery and bio-distribution of MSNs after intravenous administration were reported by many research groups.[166,167] Functionalized mesoporous silica nanomaterials are thus possible carriers for targeting therapeutic compounds by intravenous route in order to increase the compound's effectiveness in the diseased tissue and reduce general toxicity.

3. Aim of the study

In spite of the advances in the field of controlled drug delivery, great efforts are still needed for the formulation of poorly soluble drugs, especially chemotherapeutic drug molecules, in order to improve their bio-distribution and pharmacokinetic properties. MSNs have demonstrated beneficial properties for drug delivery; however, the effect of physicochemical properties on drug delivery proficiency and the efficient control of drug release are still being explored.

In this dissertation, MSNs were designed with respect to the cargo molecule to be delivered taking into account its hydrophobicity/hydrophilicity. For hydrophobic (cargo) molecules, surface functionalizations of MSNs with polymers (e.g. different combinations of PEI or PEG) in combination with small-molecular targeting moieties (e.g. folic acid, glucose) were optimized to cross different biological barriers such as the cell membrane (to maximize cellular uptake) or mucosal layers in the GI tract to arrive at its target site. For hydrophilic cargo molecules, lipid bilayers were used as a diffusion barrier to prevent premature release of the water-soluble cargo molecules. This lipid composition was optimized for maximal cellular uptake and proper intracellular trafficking (endosomal escape). To enhance the cellular affinity, targeting moiety (i.e. folic acid) has been employed.

The specific objectives of this dissertation are:

- To evaluate the effect of different surface modifications on the physicochemical properties, and bio-interactions such as protein adsorption, cellular uptake extent, internalization pathways and cytotoxicity *in vitro* **(I, IV**)
- To improve the therapeutic effect of hydrophobic drug molecules by mesoporous silica nanoparticle-mediated delivery and specific cellular targeting *in vitro,* and intestinal targeting *in vivo* via oral route **(I, II, III)**
- To develop lipid bilayer gated mesoporous silica nanocarriers for controlled release and improved therapeutic efficacy of hydrophilic drugs *in vitro,* and to provide *in vivo* delivery to tumor via intravenous route **(IV,V)**

4. Characterization techniques

The standard characterization of periodically-ordered mesoporous silica nanoparticles include use of electron microscopies (scanning electron microscopy; SEM, transmission electron microscopy; TEM), small angle X-ray diffraction (SAXD), gas adsorption analysis, thermogravimetric analysis (TGA) and dynamic light scattering (DLS). The particle morphology is typically studied by SEM, while the ordered arrangement of pores can be detected by TEM. SAXD can be used to determine the periodic-ordered structure of the material. Gas adsorption measurements are used to determine surface area, pore volume, and pore size distributions. DLS is used to confirm redispersibility of the particles in aqueous solution. TG analysis is used to measure the amount of organic content added on the particle surface. Ultraviolet-Visible (UV-Vis) spectroscopy and high performance liquid chromatography (HPLC) are employed to detect and quantify drug amount incorporated into the particles. Important characterization techniques to study fluorescently labeled particles' fate in biological environments are confocal laser scanning microscopy (CLSM) and flow cytometry, were used to evaluate their extent of uptake and specificity towards the target cells.

In the following section, the characterization techniques used will be discussed at a level that is required for understanding the results that will be discussed.

4.1. Electron microscopy

The electron microscope is a type of microscope that uses a beam of electrons to create an image of the specimen; it operates according to the same basic principles as the light microscope but uses electrons instead of light. It is capable of much higher magnifications and has a greater resolving power than a light microscope, allowing it to see much smaller objects in finer detail.

4.1.1. Transmission electron microscopy (TEM)[168,169,170,171]

TEM involves a high voltage electron beam generated by an electron gun that has been focused into a small, thin, coherent beam by condenser lens. The electron beam is restricted by the condenser aperture to remove high angle electrons before it reaches the specimen. It is important that the specimen is thin enough to allow some electrons to transmit through the sample. Electrons that are transmitted through the specimen carry information about the structure of the specimen. The spatial variation in the 'image' is then magnified by a series of magnetic lenses until it is recorded by hitting a fluorescent screen, or light sensitive sensor

such as a CCD (charge-coupled device) camera, which provides a 'shadow image' of the specimen with its different parts displayed in varied darkness according to the atom density in the sample. (Figure 15) Heavy atoms having high electron density result in more interactions between the electrons in the primary beam and those in the sample, which in turn provides a higher contrast in the resultant image. Transmission electron microscopes produce two-dimensional, black and white images.

The successful imaging of nanoparticles using TEM relies on the contrast of the sample relative to the background. Samples are prepared for imaging by drying nanoparticles on a copper grid. Materials which have electron densities significantly higher than amorphous carbon are easy to image.

TEM allows gathering information about particle size, shape, surface coating on the particle e.g. lipid bilayer or polymer coating, and it also provides information about small details of biological structure, such as a cell. Thus, it is an imperative tool in biomedical research. TEM images of the samples in this work were taken by JEM 1400-Plus, JEOL Ltd operated at 200 kV. TEM was also used (under slight underfocus) to verify the presence and arrangement of the pores.

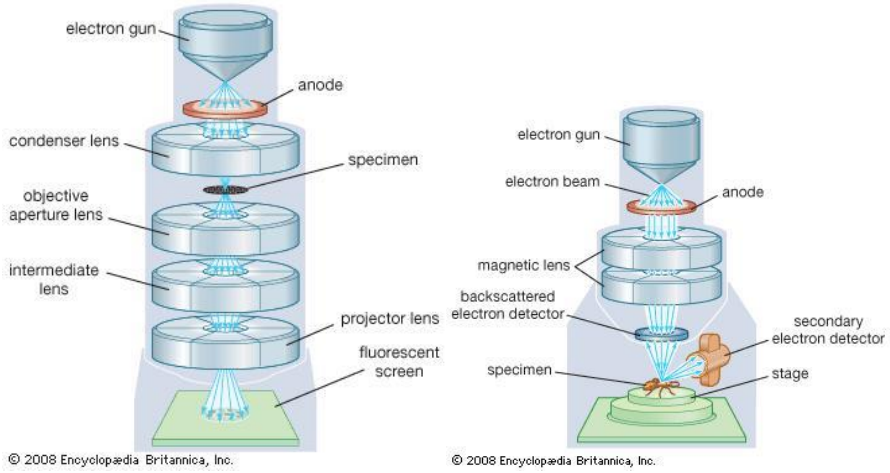

Figure 15. A principal picture of TEM and SEM devices (References 172,173)

4.1.2. Scanning electron microscopy (SEM)[170,174,175]

SEM uses a focused beam of high-energy electrons to generate a variety of signals at the surface of solid specimens. The high voltage electron beam is generated at the top of the microscope by an electron gun and accelerated down the column toward the specimen. The

beam is further focused and directed by electrostatic and electromagnetic lenses, as it moves down the column. (Figure 15) When the beam reaches the specimen, primary electrons of the electron beam can enter the sample and interact with electrons of the atom, and excites the sample by an unchanged energy called backscattered electrons. Some electrons are knocked loose from the surface of the specimen and are referred as secondary electrons. These electrons are 'seen' by a detector that amplifies the signal and sends it to a monitor. The electron beam scans back and forth across the sample and builds up an image from the number of electrons emitted from each spot on the sample. The signals that derive from electron-sample interactions reveal information about the sample, including external morphology, topography, and crystalline structure of the specimen's surface.

Samples to be viewed with the SEM and TEM must be able to withstand a vacuum. For SEM imaging, samples need to be conductive. Samples that are not conductive can be coated with a thin layer of conductive material by a process called sputter coating. SEM images of the samples in this work were captured with LEO Gemini 1530, Leo Ltd. with a Thermo Scientific UltraDry Silicon Drift Detector (SDD).

4.2. Nitrogen sorption analysis[176,177,178,179,180]

Gas adsorption measurements are of major importance for the characterization of various porous materials, as specific surface area, specific pore volume, pore size and its distribution can be determined using this technique. The nitrogen physisorption process is described quantitatively by an adsorption/desorption isotherm, representing the amount of adsorbed/desorbed Nitrogen at a fixed temperature as a function of partial pressure of N_2.

According to IUPAC, the pores can be classified according to their sizes[176]:

(i) macropores: pore width > 50 nm

(ii) mesopores: pore width 2 - 50 nm

(iii) micropores: pore width 0.7 - 2 nm

(iv) ultramicropores: pore width < 0.7 nm

The amount of gas adsorbed by the mass of solid is dependent on the equilibrium pressure, the temperature, and the nature of the gas-solid system. These relationships are represented in what is called the adsorption isotherm. The adsorption isotherms are displayed in graphical form with the amount adsorbed (n_a in mol g^{-1}) plotted against the equilibrium relative pressure (ρ/ρ_0). The majority of physisorption isotherms are grouped into the six types according to the

IUPAC classification shown in Figure 16. The shape of these isotherms is based on the strength of the adsorbent–adsorbate interactions and the type of porosity (or porosities) of the adsorbent.

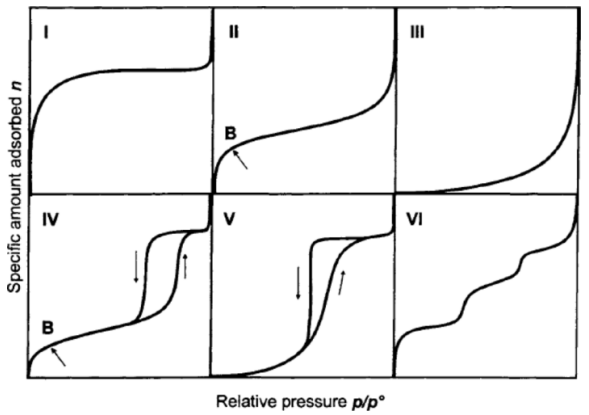

Figure 16. IUPAC classification of physisorption isotherms of porous solids (Reference 176)

Type I isotherms show steep uptake of nitrogen in low relative pressure, which is associated with the microporosity of the material. Adsorption is limited to a few molecular layers, and dependent on the available micropore volume. *Type I* isotherms can be described by the Langmuir equation, which was developed on the assumption that adsorption was limited to at most one monolayer. *Type II* isotherms are indicative of solids that are non-porous and macroporous. Point B indicates the relative pressure at which monolayer coverage is complete. *Type III* isotherms are characteristic for solids where hardly any adsorption occurs due to weak adsorbate-adsorbent interactions. The difference between *Type II and III* isotherms are in terms of strong or weak adsorbent–adsorbate interactions, respectively. Characteristic features of *Type IV* isotherms are the hysteresis loop, the lower branch of which represents measurements obtained by progressive addition and the upper branch by progressive withdrawal of gas of the adsorbent. The shape of the hysteresis loop is associated with the filling and emptying of mesopores by capillary condensation, which reveals additional information about the pore structure. This specific hysteresis loop is of type H1 and is caused by a narrow distribution of uniform pores, such as ordered mesoporous materials. *Type V* isotherms are indicative of weak adsorbent-adsorbate interactions. The hysteresis loop of type H2 is observed, which is common for many inorganic oxides, such as amorphous silica gels. The *type VI* isotherms are associated with layer-by-layer adsorption on a uniform surface. Usually non-polar molecules on uniform surfaces give rise to such isotherms. The

samples prepared in this study are MCM-41 mesoporous materials expressing the *type IV* isotherms.

The Langmuir equation describes microporus material exhibiting Type I Isotherms. The Langmuir model assumes adsorption is limited to one monolayer. The Brunauer-Emmett-Teller (BET) gas adsorption model is the most widely employed procedure for the determination of the specific surface area of finely divided and porous materials using the physisorption isotherm data. For this it is necessary to draw the BET plot and the monolayer volume (Vm) can be derived from the plot.[177]

$$\frac{p}{V(p_0-p)} = \frac{1}{V_m C} + \frac{c-1}{V_m C}\frac{p}{p} \qquad \textit{eq (1)}$$

where V is volume adsorbed, p sample pressure, p_0 saturation pressure and C constant related to the enthalpy of adsorption (BET constant). The constant C is related to the sharpness of point B (Figure 16) and the value is sensitive to both surface polarity and to the presence of microporosity. The C-value for nitrogen adsorption at 77 K on porous silica is normally in the range of 50 to 200. The specific surface area (S_{BET}) is then calculated from V_m by the following equation-

$$S_{BET} = \frac{V_m N_a a_m}{m V_L} \qquad \textit{eq (2)}$$

where N_a is Avogadro constant, a_m the cross sectional area occupied by each nitrogen molecule (0.162 nm^2), m weight of the sample and V_L the molar volume of nitrogen gas (22414 cm^3). The BET surface area can be calculated as long as the BET plot is linear and does not cut the y-axis at x=0 at y-values below zero. The theory is based on the assumption that only monomolecular adsorption takes place, adsorption is localized onto surface sites and the energy of adsorption is independent of the surface coverage. Single point BET involves determining specific surface area using a single point on the isotherm and multipoint BET involves a minimum of three data points.

The pore size can be determined from either the adsorption branch or the desorption branch of the nitrogen isotherm. The Kelvin equation with a correction for the multilayer thickness in the pore walls can be used to evaluate the pore width, or more precisely the pore size distribution, from the pore filling pressure.

$$ln\frac{p}{p_0} = -\frac{2\gamma V_L}{rRT} \qquad \textit{eq (3)}$$

where p/p_0 is the relative pressure, r is the mean radius of curvature of liquid in a pore, γ surface tension of the liquid, V_L molar volume of the liquid, R the gas constant and T absolute temperature.

The most common model for pore size distribution analysis is the Barrett-Joyner-Halenda (BJH) model,[179] which is based on the Kelvin equation. The limitation of the BJH model is that it underestimates the pore size by ~1 nm in the pore size range of 2 - 4 nm. Hence, a model based on the statistical mechanics rather than the Kelvin equation, such as Non local density function theory (NLDFT), provides a more accurate way of determining pore size distribution. NLDFT allows calculation of the pore size distribution in the entire range of micro- and mesopores, i.e. from 0.5 nm to 40 nm. However, NLDFT method is not perfect, the drawback of standard NLDFT method is that it does not take into account chemical and geometrical heterogeneity of the pore walls, instead assume it as a structureless, chemically and geometrically smooth surface. Hence, theoretical NLDFT adsorption isotherms exhibit multiple steps.[181]

Degassing is an important step before measurement of surface area or pore size/volume to clean the surfaces from physisorbed molecules (water/organic vapors). All nitrogen sorption measurements in this work were performed with Autosorb-1 Sorptometer and autosorb software (Quantachrome instruments) was employed to determine surface area using BET theory, and NLDFT theory was used to calculate pore size and the pore size distribution.

4.3. Small angle x-ray diffraction (SAXD)

The technique is based on diffraction of x-rays by the electron clouds of the atoms. In the absence of absorption effects, the intensity of the scattered radiation is directly proportional to the electron density differences in the system. When an x-ray beam with wavelength λ strikes a material with periodic long-range order, characteristic reflections of intensity for planes will be observed in a diffractogram as a result of the constructive interference when the scattering angle (θ) satisfies Bragg's law.

$$n\lambda = 2dsin\theta \qquad \textit{eq (4)}$$

where n- integer number of wavelengths (order of diffraction), λ- wavelength, d- repeating distance between reflecting planes and θ- scattering angle.

Bragg's law shows the relationship between crystal lattices (d) and the observed scattering angle. In Bragg's law, the scattered intensity is measured as a function of scattering angle. In a crystal, a set of crystallographic planes hkl can be defined as the set of parallel equidistant planes, one of which passes through the origin, and the next nearest makes intercepts of a/h, b/k, and c/l on the three crystallographic axes, where a, b, and c are the dimensions of the smallest repeat unit of the crystal (the unit cell). The spacing between diffracting planes is called the *d*-spacing. Compounds with different unit cells have different assemblies of lattice spacings and hence will lead to different diffraction patterns. Thus, the combination of d-spacings and intensities are characteristic for each structure. Consequently, analyzing the positions of the reflected beams information about the size and symmetry of the lattice dimensions can be obtained. In MCM-41, there is no repeat unit in the c axis and so only reflections from the hk planes, in two dimensions, are seen. MCM-41 can be indexed to a hexagonal hk0 lattice and are therefore, indexed as (100), (110), (200), (210) and (300). The repeating distance d directly gives the unit cell (lattice) parameter, a. Center to center distance (a) between the hexagonally arranged channels in MCM-41 is $2/\sqrt{3}$ times the d-spacing for a hexagonal system. (Figure 17)

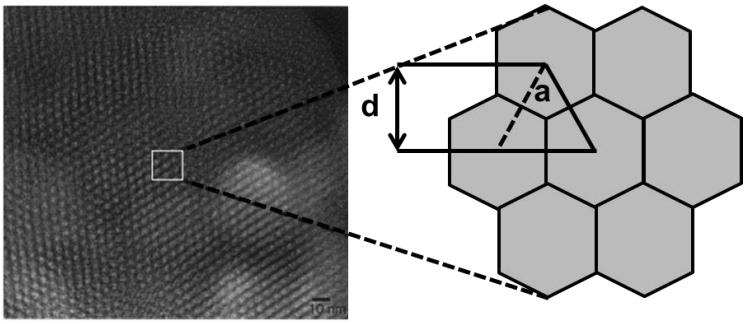

Figure 17. (A) TEM image of MCM-41, (B) illustration of the 2D hexagonally-ordered lattice with d_{100} spacing and unit cell parameter a (Adapted from reference 40)

SAXD experiments were performed on a modified Kratky compact small-angle system (MBraun, Nottinghampshire).

4.4. Thermogravimetric analysis (TGA)[182,183,184]

Thermogravimetric analysis (TGA) measures weight changes in a material as a function of temperature (or time) under a controlled atmosphere. The method offers valuable information for quality control, development and research. TGA can be used to study thermal stability and composition of materials.

A TGA is performed by gradually raising the temperature of a sample in a furnace as its weight is measured on a balance that remains outside of the furnace. The TGA program can be run in different modes- heating or cooling (dynamic), or holding the temperature constant (isothermal), or any combination of these. The measurement can be run up to 2000°C temperatures in controlled gas atmospheres. Changes in the mass of a sample are studied while the sample is subjected to the program. These changes in temperature affect the sample such as e.g. sublimation, vaporization, oxidation, reduction, and decomposition bring a drastic change in mass of the sample. The weight/mass of the sample is plotted against temperature or time to illustrate transformations in the material, and the plot is called thermogram. The thermogram gives information about the changes in sample composition, combustion of and/or evaporation of substances from the sample. The shape of the thermogram is dependent on the rate of heating; therefore, the same temperature program should be chosen in order to compare different samples.

All the TGA measurements in this work were performed using Netzsch STA 449 F1 Jupiter and the data was analyzed by using Netzsch Proteus® Thermal Analysis Software v.5.2.1.

4.5. Dynamic light scattering (DLS)[185,186,187,189]

Dynamic light scattering (DLS) is a non-invasive technique for measuring the size and size distribution of molecules and particles typically in the submicron region. DLS is applied for the characterization of particles, emulsions or molecules, which have been dispersed or dissolved in a liquid. The technique of dynamic light scattering measures the speed of particles undergoing Brownian motion. Smaller particles fluctuate more rapidly than large particles. (Figure 18)

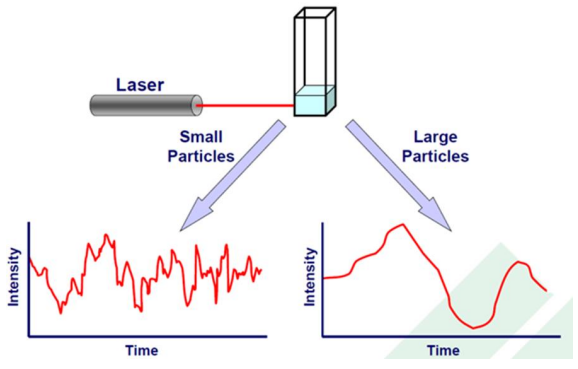

Figure 18. Intensity fluctuation due to Brownian motion (Reference 189)

Analysis of these intensity fluctuations yields the velocity of the Brownian motion (defined by the diffusion coefficient (D)) and hence the particle size can be obtained using the Stokes-Einstein equation.

$$\boldsymbol{D = \frac{kT}{6\pi\eta R}} \qquad \textit{eq (5)}$$

where D= diffusion coefficient, k= Boltzmann constant, T= absolute temperature, η= viscosity of the solvent, and R= hydrodynamic radius of the particle.

When a sample is illuminated by a light source, such as a laser, it scatters light in all directions. In this study, DLS measurements were performed at 298 K, using a monochromatic laser (He-Ne), with a working wavelength of 632.8 nm and a non-invasive backscatter (NIBS), with the detector that is positioned at 173° relative to the laser beam. The speckle pattern is measured in relation to time, first within a certain time point t, next showing the fluctuation in scattering intensity at the time point (t+δ) continuing this way, always correlating the measured data to the previous one. After the determination of the correlation function (Figure 19), it is possible to calculate the particle-size distribution.

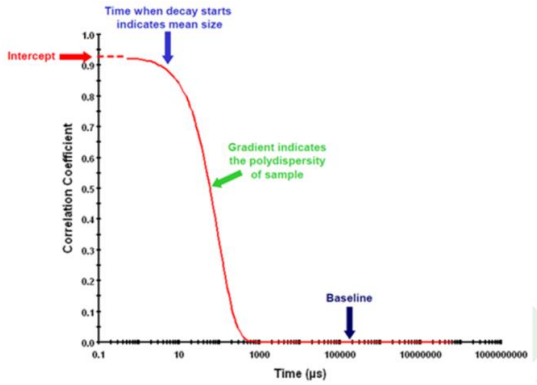

Figure 19. Correlation function (Reference 189)

DLS gives an intensity-weighted distribution, where the contribution of each particle in the distribution relates to the intensity of light scattered by the particle. Rayleigh approximation, which describes the intensity of scattering to be proportional to the sixth power of the particle diameter, for the sample consisting of particles in two size classes equal in number, the bigger particles scatter more light resulting in larger peak area by intensity. When comparing particle size data for the same sample obtained by different techniques, it is important to realize that

the types of distribution being measured and reported can produce very different particle size results. (Figure 20)

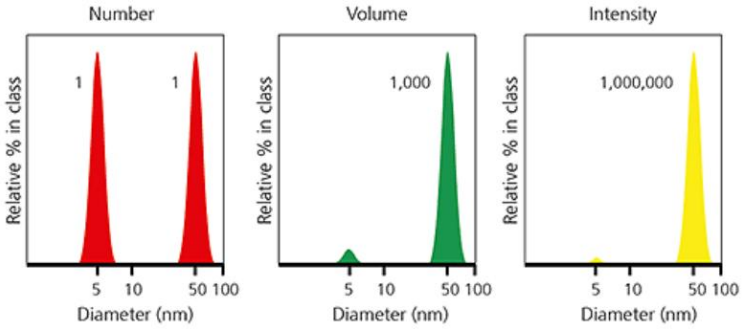

Figure 20. Example of number, volume and intensity weighted particle size distributions for the same sample (Reference 189)

Cumulants analysis has been used for fitting the correlation function. This analysis gives a mean particle size (z-average) and an estimate of the width of the distribution (polydispersity index, PDI). PDI is a dimensionless measure of the broadness of the size distribution. In the Zetasizer software, it ranges from 0 to 1. Low PDI values (lower than 0.1) might be associated with a high homogeneity and high PDI values (greater than 0.7) indicate that the sample has a very broad size distribution and it is not suitable for the DLS measurement.

The diameter measured in DLS is called the hydrodynamic diameter and refers to the way a particle diffuses within a fluid. The diameter obtained by this technique will depend not only on the size of the particle 'core', but also on any surface structure, as well as the concentration and type of ions in the medium. Thus, the size obtained by DLS will be larger than when measured by electron microscopy, where the particle is removed from its native environment.

4.6. Electrokinetic zeta potential measurement[188,189]

Zeta (ζ) potential is a measure of the magnitude of the electrostatic or charge repulsion/attraction between particles, and is one of the fundamental parameters known to affect the stability of a colloidal system. When charged particles are dispersed in aqueous liquid, ions of opposite charge will be attracted to the surface of the particle. The net charge at the particle surface affects the distribution of ions in the surrounding interfacial region, creating an increased concentration of counter ions (ions of opposite charge) close to the surface of the particles and hence creating an electrical double layer around each particle. The liquid layer surrounding the particle consists of two parts: an inner region, or the Stern layer,

where counter ions are strongly bound and an outer region or the diffuse layer, where ions are less firmly attached. Within the outer region or diffuse layer, there is a notional boundary inside which the adsorbed ions and the particle form a stable entity, which implies that when the particle moves in the liquid due to e.g. gravity, the ions within this boundary travels along with the particle, but any ions beyond the boundary do not move with the particle. This boundary is called the surface of hydrodynamic shear or the slipping plane. The potential at the slipping plane (or close to the surface) is known as the zeta (ζ) potential. The potential at this region decays as the distance increases from the surface until it reaches a distance at which the value becomes the same as in the bulk solution, which is conventionally assumed to be zero. It is imperative to note that the ζ potential is an experimentally determined value, an uncertainty arises in that it is not clear at what location within the double layer it is measured, as the precise quantitative meaning of 'close' cannot be defined.[188]

ζ potential magnitude gives a prediction of the colloidal stability of the system. When the particles in the dispersion system have a large negative or positive ζ potential, repulsion exists between them and hence dispersion has no tendency to flocculate and the colloidal system will be stable. The magnitude of the ζ potential around ± 30 mV generally provides electrostatically stabilized systems. The ζ potential varies strongly within the pH and, therefore, the ζ potential should always be noted together with measured pH. As the ζ potential varies with the pH electrokinetic titration, measurements can be exploited to determine the isoelectric point (IEP), which is the pH where the net effective surface charge i.e. the ζ potential is zero, and which means the pH where the colloidal system is least stable. Moreover, the electrolyte concentration should also be taken into consideration, as the added electrolyte will screen the surface charges (reduce the thickness of the double layer) and hence suppress the absolute value of the ζ potential.

When an electric field is applied across an electrolyte solution, charged particles suspended in the electrolyte solution are attracted towards the electrode of opposite charge. Viscous forces acting on the particles tend to oppose this movement. When equilibrium is reached between these two opposing forces, the particles move with constant velocity. The velocity of a particle in an electric field is commonly referred to as its Electrophoretic mobility. The electrophoretic mobility can be determined by performing an electrophoresis measurement using Laser Doppler Velocimetry. Laser Doppler Micro-electrophoresis is used to measure zeta potential.

ζ potential can be measured by determining the electrophoretic mobility and then by applying the Henry equation:

$$\boldsymbol{U_E = \frac{2\varepsilon\zeta}{2\eta} f(Ka)} \qquad \textit{eq (6)}$$

where ε= dielectric constant of the liquid, η=viscosity, U_E= electrophoretic mobility, and f(Ka) = Henry's function.

Two values are generally used as approximations of f(Ka): either 1.5 (the Smoluchowski approximation) or 1.0 (the Hückel approximation). The Smoluchowski approximation is used for the folded capillary cell and the universal dip cell when used with aqueous samples. The Smoluchowski approximation was used throughout this study.

All the ζ potential and DLS measurements in this study were performed using a Zetasizer Nano ZS instrument (Malvern Instruments).

4.7. Fluorescence spectroscopy[190]

Fluorescence spectroscopy measures the intensity of photons emitted from a sample after it has absorbed photons. Fluorescence is an imperative investigation tool in analytical sciences due to its high sensitivity and selectivity.

A photon of an excitation light is absorbed by an electron of a fluorescent particle, which raises the energy level of the electron to an excited state. During this short excitation period, some of the energy is dissipated by molecular collisions or transferred to a proximal molecule, and then the remaining energy is emitted as a photon to relax the electron back to the ground state. Because the emitted photon usually carries less energy and therefore has a longer wavelength than the excitation photon, the emitted fluorescence can be distinguished from the excitation light. (Figure 21) The excitation and photon emission from a fluorophore is recurrent, and until the fluorophore is irreversibly damaged, it can be repeatedly excited.[191]

The fluorescence spectrometer instrument has a light source (xenon lamp), equipped with monochromators to select both the excitation and emission wavelengths. The fluorescence is detected with photomultiplier tubes and quantified with the appropriate electronic devices. The output is usually presented in graphical form.

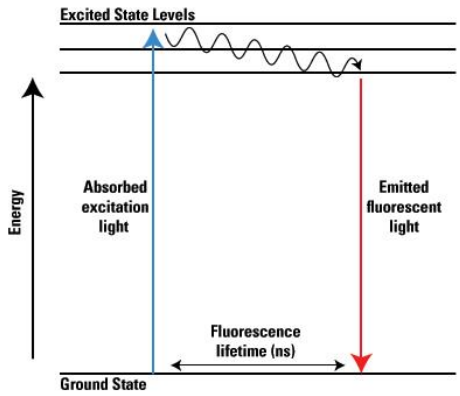

Figure 21. Jablonski energy diagram of fluorescence (Reference 191*)*

The brightness of a given fluorophore is determined by the molar extinction coefficient and quantum yield. The molar extinction coefficient (ε) is defined as the quantity of light that can be absorbed by a fluorophore at a given wavelength and is measured in M^{-1} cm^{-1}. The quantum yield (Φ) is calculated as the number of photons that are emitted by the fluorophore divided by the number of photons that are absorbed, maximum value of it can be 1.

The fluorescence measurements are sensitive to change in temperature, solvent viscosity, and solvent pH. Quantum yield of fluorescence decreases with increasing temperature. As the temperature increases, the frequency of the collision increases which increases the probability of deactivation by external conversion. Solvents with lower viscosity also increase the possibility of deactivation by external conversion. The fluorescence of aromatic compound with basic or acid substituent rings is pH dependent. For example, fluorescein exists in various ionic (cation, monoanion, dianion), neutral and lactone forms depending on the pH of the solution. The monoanion and neutral forms of fluorescein have similar fluorescence spectra in aqueous solution. The dianion form shows a narrower emission band. The lactonic form does not contribute to the fluorescence much, since it does not absorb in the visible spectrum.[192]

Fluorescence measurements in this work are performed on Perkin Elmer LS 50B instrument and data has been analyzed using FLWinLab software.

4.8. Ultraviolet-Visible (UV-Vis) spectroscopy[193,194]

UV-Vis spectroscopy is the most ubiquitous analytical and characterization techniques in qualitative and quantitative analysis. There is a linear relationship between absorbance and

absorber concentration, which makes UV-Vis spectroscopy particularly attractive for making quantitative measurements.

UV-Vis absorption spectroscopy is the measurement of the attenuation of a beam of light after it passes through a sample or after reflection from a sample surface. Absorption measurements can be at a single wavelength or over an extended spectral range. Absorption spectra arise from the transition of electrons within a molecule from a lower level to a higher level. A spectrometer records the degree of absorption by a sample at different wavelengths and the resulting plot of absorbance (A) versus wavelength (λ) is known as spectrum.

In the double beam UV-Vis spectrophotometer, the light is split into two parallel beams, each of which passes through a cell; one cell contains the sample dissolved in a solvent and the other cell contains the solvent alone. The detector measures the intensity of the light transmitted through the solvent alone (I_0) and compares it to the intensity of light transmitted through the sample cell (I).

$$\boldsymbol{T = \frac{I}{I_0}} \qquad \textit{eq (7)}$$

The absorbance is then calculated from transmittance. The relationship between transmittance (T) and absorbance (A) can be expressed by the following equation:

$$\boldsymbol{A = -log_{10} T} \qquad \textit{eq (8)}$$

The Beer-Lambert law defines the relationship between the concentration of a solution and the amount of light absorbed by the solution. The absorbance of a solution is directly proportional to the path length (length of the cell containing the solution) and the concentration of the absorbing molecule (in moles per liter), according to the equation:

$$\boldsymbol{A = \varepsilon bc} \qquad \textit{eq (9)}$$

where, A= absorbance of the sample, ε = molar absorptivity (liter mol^{-1} cm^{-1}), b = length of the light path through the sample (cm), c = the concentration of the sample (mol $liter^{-1}$).

The Beer-Lambert law can be applied to dilute solutions, concentrations ≤0.01 M. At high concentrations, deviations from the law can be observed due to changes in the absorbing species or the properties of the bulk solution. Other causes of nonlinearity include- a scattering of light due to particulates in the sample, fluoresecence or phosphorescence of the

sample, changes in refractive index at high analyte concentration, shifts in chemical equilibria as a function of concentration and stray light.

The equipment used in this work was a Nanodrop 2000c Thermo Scientific Spectrophotometer.

4.9. High performance liquid chromatography (HPLC)[195]

Chromatography is a separation technique which is used to separate a mixture of compounds into its individual components based on their molecular structure and molecular composition. The HPLC instrument consists of a separation column (stationary phase), a reservoir of a mobile phase, a pump, an injector, and a detector. In normal phase HPLC, the stationary phase is polar and the mobile phase is non-polar. In reversed phase HPLC, the stationary phase is non-polar, generally, silica surface modified with long hydrocarbon chain (8 or 18 carbon atoms), and a polar mobile phase, usually water and alcohol or acetonitrile mixture. Reversed phase HPLC is the most commonly used form of HPLC. The process involves the interaction of the compounds in the analyte across an immobile stationary phase. The mobile phase flows through the stationary phase and carries the components of the mixture to be separated with it. Sample components based on their physical and chemical properties (such as polarity, charge, molecular weight and functional group) display stronger/weaker interactions with the stationary phase and they will move slow/fast through the column. These differences in the rates cause the separation of various components. Mobile phase composition and temperature play a major role in the separation process by influencing the interactions taking place between sample components and stationary phase. The separated components pass through the detector located at the end of the column, which detects and quantifies the analytes as they elute from the chromatographic column. Most commonly used detectors are UV-Vis, fluorescence, and mass-spectrometric detectors. The detector provides an output to a computer that result in the chromatogram. (Figure 22)

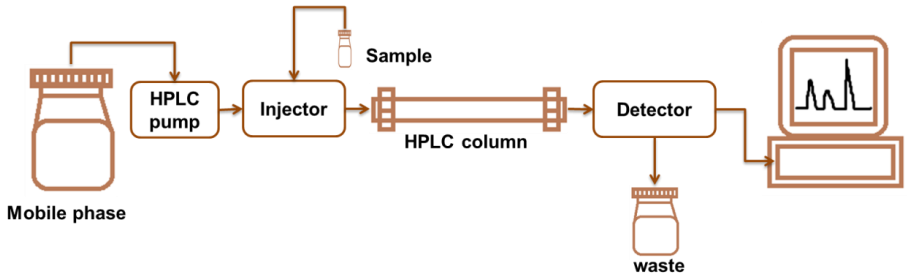

Figure 22. Schematic representation of HPLC instrumentation.

HPLC experiments in the study were performed using an Agilent HPLC system.

4.10. Confocal laser scanning microscopy (CLSM)[196,197]

Confocal laser scanning microscopy (CLSM) is a valuable tool for obtaining high-resolution images and 3-D reconstructions of fluorescent samples. It offers several advantages over conventional optical microscopy, including shallow depth of field, elimination of out-of-focus glare, and the ability to collect serial optical sections from thick specimens. In the biomedical sciences, a major application of confocal microscopy involves imaging of either fixed or living cells and tissues that have usually been labeled with one or more fluorescent probes.

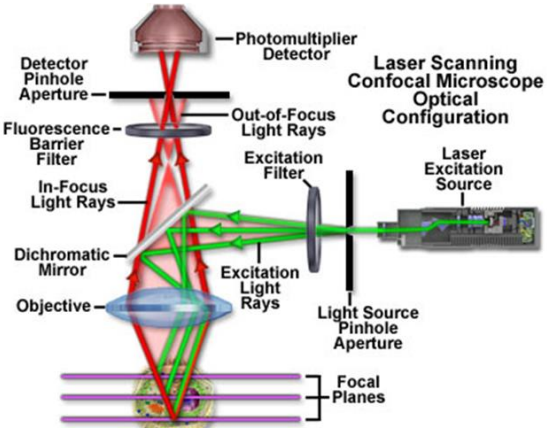

Figure 23. Schematic of light path in confocal microscope (Reference 198)

In the confocal optical system, the objective lens is used to focus a laser beam onto the specimen where it illuminates a small section of the sample. The specimen in a CLSM is irradiated in a pointwise fashion and the physical interaction between the laser beam and the specimen is measured point by point. It is necessary to guide the laser beam across the specimen to obtain information about the entire specimen, and this process is known as 'scanning'. Light proceeds from the illuminated spot on the specimen to the objective where it is directed by a dichroic beam splitter toward the confocal pinhole aperture. (Figure 23) This pinhole positioned in front of the detector, on a plane conjugate to the focal plane of the objective lens, gives the system its confocal property by rejecting light originating from neighboring focal planes. The light coming from planes above or below the focal plane is out of focus when it hits the pinhole, so most of it cannot pass the pinhole and, therefore, does not contribute to forming the image. However, all light rays originating from the plane of focus pass through the pinhole aperture and are collected by the detector. The ability of confocal

microscopes to closely discriminate between light originating at the focal plane from that originating from above or below the focal plane enables known as 'optical sectioning', makes it possible to scan a sample at various x-y planes corresponding to different depths, and, by ordering these planes into a vertical stack, reconstruct a 3-dimensional image of the specimen. Since it does not require physical sectioning of thick samples and precludes the need for extensive specimen processing, CLSM is one of the most efficient methods available to gain three-dimensional information on living biological specimens and biomaterials. In CLSM, instead of a tungsten or mercury lamp, a laser is used as a light source, and is combined with a sensitive photomultiplier tube (PMT) detector, and a computer to control the scanning mirrors or other scanning devices and to facilitate the collection and display of images.

The main goal of confocal microscopy is to explore the structure and structural relationship along the optical (z) axis as well in the x-y plane. For this, preservation of the cells and tissue structure during the preparation of the sample is necessary to obtain a reliable image. It is important to use low laser power for studies of living cells, because it can cause photodynamic damage and consequent alteration in normal cell behavior.

Multiple fluorescent probes within single cells can be incorporated to define the differential distribution of more than one labeled structure or molecular species. Confocal microscopy with a sample containing living cells is dependent on the properties of fluorescent probes, which are the strong signal, high stability in biological environment (e.g. effect of pH and temperature), slow bleaching, and cytocompatibility leading to a high signal-to-noise ratio. The use of nanoparticles as imaging agents has the potential to provide remarkably higher photostability and signal, compared to that of single fluorophores.

Confocal microscopy experiments in this work were performed using Leica TCS SP5 matrix, Leica TCS SP5 STED and Zeiss LSM 510 Meta Confocal microscope and data analysis has been performed using BioImage XD and ImageJ software.

4.11. Flow cytometry[199,200]

Flow cytometry is a well-established technique that integrates light scattering and fluorescence measurements to gather information regarding size, relative granularity or internal complexity of cells and fluorescent intensity, as they flow in a fluid stream through a beam of (laser) light. This technique permits simultaneous multiparametric analysis of the physical and chemical characteristics of up to thousands of particles per second. By using fluorescently labeled nanoparticles it is possible to quantify their internalization in cell

subpopulations, which are identified by specific markers exposed on the cell membrane. Additionally, changes in cell parameters such as side scattering of cells in the presence of specific nanoparticles can be used to recognize cellular internalization.

In flow cytometry, a beam of laser light is directed at a hydrodynamically focused stream of fluid that carries the cells (which may range in size from 0.2 to 150 μm). The optics system consists of lasers to illuminate the particles in the sample stream and optical filters to direct the resulting light to detectors. Several detectors are carefully placed around the stream, at the point where the fluid passes through the light beam. One of these detectors is in line with the light beam and is used to measure Forward Scatter (FSC), and it distinguishes live and dead cells from each other. Another detector is placed perpendicular to the stream and is used to measure Side Scatter (SSC), it detects the granularity of the cells. Fluorescence detectors are used to detect fluorescence signal from different components. The electronics system converts the detected light into electronic data that can be processed by the computer. (Figure 24)

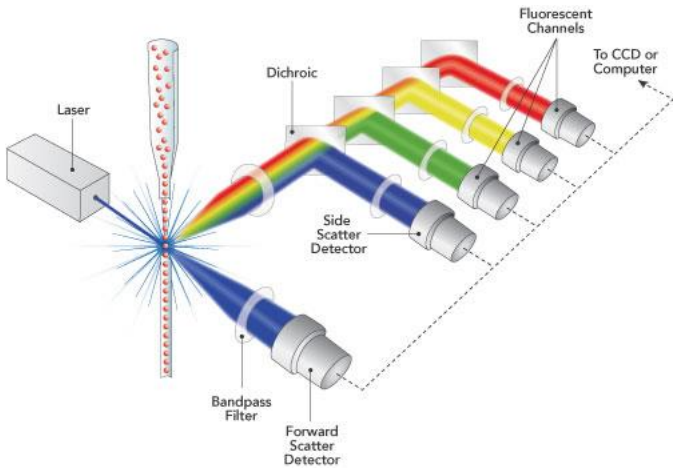

Figure 24. Schematic diagram of a flow cytometer, showing focusing of fluid sheath, laser, optical systems and detectors (Reference 201)

The processing steps should be performed at 4 °C (on ice) and possibly in the dark to reduce negative effects of higher temperatures and lights on the fluorescence. Further, the cytotoxicity of the nanoparticle dose used for the internalization experiments should be empirically tested beforehand. The disadvantages of this technique concern the need of working with monodisperse samples and the inability to localize the site of origin of the fluorescence signal (i.e. different cellular compartments). It also has a limitation in the choice

of fluorochromes to be used in combination because the wavelength of the emission bands must be sufficiently separated to allow their appropriate measurement.

CLSM and flow cytometry are often combined to obtain quantitative data on particle association with cells, and qualitative data on internalization.

Flow cytometry experiments in this work were performed using BD FACSCalibur analyzer and data analysis has been performed using CellQuest Pro™ and Flowing software.

Table 2. ***Summary table showing phenomena studied using above-mentioned techniques:***

Phenomena studied	Technique used	Publication No
Particle size	TEM, SEM, DLS	1-5
Net surface charge	Zeta potential measurement	1-5
Pore size, surface area, pore volume	Nitrogen sorption analysis	2-4
Arrangement of pores	SAXD	1,3,4
Amount of organic surface function	TGA	2-4
Amount of targeting ligand	UV-Vis Spectroscopy, TGA	2-3
Drug loading	UV-Vis Spectroscopy, HPLC	2-5, Supp. Paper 3
Particle fluorescence	Fluorescence spectroscopy	1-4
Particle surface conjugation	FTIR	4
Protein adsorption	UV-Vis Spectroscopy	1
Cytotoxicity	WST-1 assay	1-5
Cellular uptake	CLSM	1-5
	Flow cytometry	1-4
Translocation	CLSM	unpublished
Route of uptake	Flow cytometry	1,5
Permeability	HPLC	unpublished
Heat shock response of celastrol	Western blot analysis	2
***In vitro* apoptotic effect of celastrol**	Flow cytometry	2
***In vivo* bio-distribution**	CLSM	3
Stability of particles and cargo in simulated fluids	TEM, HPLC	3
***In vivo* efficacy of DAPT**	Light microscopy, RT-PCR	3
Bone density	pQCT (Peripheral quantitative computed tomography)	5
***In vivo* efficacy of ZOL**	Measurement of tumor size, light microscopy	5

5. Summary of the results

5.1. Mesoporous nanocarriers for delivery of hydrophobic cargoes

In this thesis, different surface functionalized MSNs of moderate size (250-300 nm) have been developed and step-by-step evaluations of their biophysicochemical interactions have been conducted to arrive at the best particle design for the specific purpose. Further, drug-carrier interactions have been assessed to obtain suitable carrier functionality for the drug delivery application. As observed in our previous studies, MSNs of size 250-300 nm can be employed as an efficient carrier for hydrophobic drug molecules to cancer cells *in vitro*[55] and *in vivo;* via peritumoral and oral routes of administration.[202] These results were promising and, therefore, the same MSN platform has been used for further investigation in this thesis. However, in-depth analysis of surface modification variations on physicochemical aspects as well as bio-interactions was still lacking to some degree in the earlier studies.

In order to fill these gaps, 250-300 nm sized MSNs were thus synthesized using the same protocol as in the previous studies and further functionalized with different polymers and/or targeting ligands (e.g. folic acid and glucose) for drug delivery application. To show the applicability of the MSN platform to deliver various hydrophobic cargoes, and to study the interaction of particles (based on surface charges) with cargo molecules, different hydrophobic molecules were loaded to the MSNs, such as furosemide, celastrol, curcumin and DAPT (γ-secretase inhibitor) and their loading as well as release studies were performed. To evaluate interaction between nanocarriers and cellular environment, the prepared nanocarriers were evaluated for their biocompatibility as well as for their cellular uptake after different surface modifications, and their exocytosis of nanocarriers have been studied. Further, effects of surface charge and surface properties of MSNs on cellular uptake have been examined. MSNs' potential in improving drug permeability across epithelial monolayers has been evaluated. The therapeutic efficacy of drug-loaded MSNs in cancerous cells was studied. Considering the oral delivery application, the stability of drug loaded MSNs in simulated gastric fluid has been assessed. Finally, *in vivo* bio-distribution and efficacy of drug loaded MSNs after oral administration has been studied. The formulation under study and their respective purposes have been summarized in Table 3.

Table 3. ***Overview of the studied formulations for the delivery of hydrophobic cargoes:***

MSN	Surface function	Targeting ligand	Cargo	Main purpose of the study
Co-condensed with 10 % APTES FITC labelled[55,59,202]	PEI-, PEG-, Succ-, PEG-PEI-, Succ-PEI-	-	-	To study effect of surface coating on protein adsorption To study influence of surface charge on the route of uptake
	PEI-, GA_{org}-, GA_{aq}-, Gluc-, GA_{org}-PEI-, GA_{aq}-PEI-, Gluc-PEI-	Glucuronic acid (GA), Glucose (Gluc)	Celastrol	To study effect of glucose targeting on cellular uptake To study apoptosis induction-efficacy of celastrol-loaded MSNs
	PEI-, Succ-PEI-, ACA-PEI-	-	Curcumin	To measure effect of surface charge on the fluorescence property of curcumin
	PEI-, PEG-PEI-, FA-PEG-, FA-PEG-PEI-	Folic acid	Furosemide	To study effect on permeability of furosemide after loading into MSNs.
	FA-PEI-, FA-PEG-PEI-	Folic acid	DAPT	To study *in vivo* oral drug delivery efficiency of MSNs

5.1.1. Design and characterization of mesoporous nanoparticles

Monodisperse mesoporous silica nanoparticles with an average diameter of 250-300 nm were synthesized. Fluorescent MSNs were created by incorporation of fluorophore (FITC), already in the synthesis step via co-condensation approach. Synthesized MSNs were further modified by various surface functionalization routes.

5.1.1.1. Functionalization of MSNs

To investigate the effect of surface functionalization on the interaction between the carrier and drug as well as carrier and environment, amino groups were successfully introduced onto the surface of mesoporous silica nanoparticles in the form of a surface-grown poly(ethylene imine) (PEI) by the method described in the literature section. The monomer aziridine has been used for the polymerization, which is highly reactive and a very small molecule, making it a promising candidate for successful polymer functionalization of porous materials in the nanometer range. PEI is a highly polycationic synthetic polymer which exhibits the highest charge density when fully protonated in aqueous solution.[203] PEI has been mostly investigated and used in nanomedicine due to its ability to deliver DNA with high efficiency and its

excellent performance as a vehicle for gene delivery.[56] The positive charge of PEI facilitates binding to the cell surfaces which are negatively charged, leading to cellular internalization and also enables endosomal release of the particles through their action as 'proton sponges'.[204] PEI has toxic side effects that are directly related to its molecular weight, which would hinder its application for therapeutic drug delivery, but 'charge capping' of PEI with other functional moiety can moderate the toxic effect of pure PEI.[58] To utilize PEI mediated increased cellular internalization PEI-MSNs were synthesized. (PAPER I, II and III)

MSN and PEI-MSNs were further modified with poly (ethylene glycol; PEG), a non-ionic hydrophilic polymer. PEG coating has shown to reduce RES uptake, and increase circulation time in the bloodstream,[61] and therefore, it has been used in drug delivery applications. PEG decreases the particle aggregation by steric stabilization and diminishes association with non-targeted serum and tissue proteins, resulting in so-called 'stealth' behavior. PEG is non-toxic, inexpensive, versatile and approved by US FDA for many pharmaceutical applications.[205] Hence, to evaluate its potential in oral drug delivery hybrid PEG-PEI-MSNs were constructed. (PAPER III)

Further, hyperbranched PEI layer was derivatized with succinic acid to yield terminal carboxylic acid groups, which resulted in a zwitterionic coating containing tertiary, secondary, and probably residual primary amines as basic/positively charged groups and carboxylic acid groups as acidic/negatively charged groups. PEI layer was also capped with acetic acid to provide net neutral charge on the surface. Thus to introduce negative and neutral charge on MSNs' surface, in order to assess surface charge mediated differences in bio-interactions succinic and acetic anhydride modified MSNs were synthesized. (PAPER I, SUPP. PAPER I)

Folate receptors are overexpressed on the surface of several cancer cells, such as ovarian, colorectal, breast, lung, brain metastases derived from epithelial cancer, and neuroendocrine carcinoma.[96] Because of this distinguishing feature between normal and cancer cells, folic acid (FA) was conjugated to the MSNs as a potential affinity ligand for targeted drug delivery to cancerous cells. Further, cancer cells have significantly elevated metabolism, they utilize higher amount of glucose than the normal cells.[206] Therefore, to exploit this phenomenon, MSNs were modified with sugar moiety (glucose) on the surface as targeting strategy. Three different conjugation strategies were employed for coupling of glucose molecules on MSNs' surface. (PAPER II and III, SUPP. PAPER II)

5.1.1.2. Physicochemical characterization of the synthesized MSNs

The synthesized MSNs were characterized by different techniques such as SEM to confirm their size, monodispersity, morphology and non-aggregated state of the particles. (Figure 25A) The mesoscopic ordering of the MSNs was further confirmed by TEM. (Figure 25B) Full redispersibility of dried, extracted and surface-functionalized particles was confirmed by redispersion of dry particles in physiological buffer (HEPES buffer pH 7.2) and subsequent DLS measurements. (Figure 25C)

To determine structural parameters related to the mesoporosity (surface area, pore size, pore volume) N_2-sorption measurements have been performed. (Figure 25D) Ordered arrangement of mesopores was confirmed by SAXD. (Figure 25E) TGA has been used to determine the amount of organic residues or polymers such as PEI, PEG added on the particle surface. (Figure 25F) Effective modification of particles' surface with PEI and further derivatization with PEG, succinic acid or acetyl groups were confirmed by zeta potential measurements.

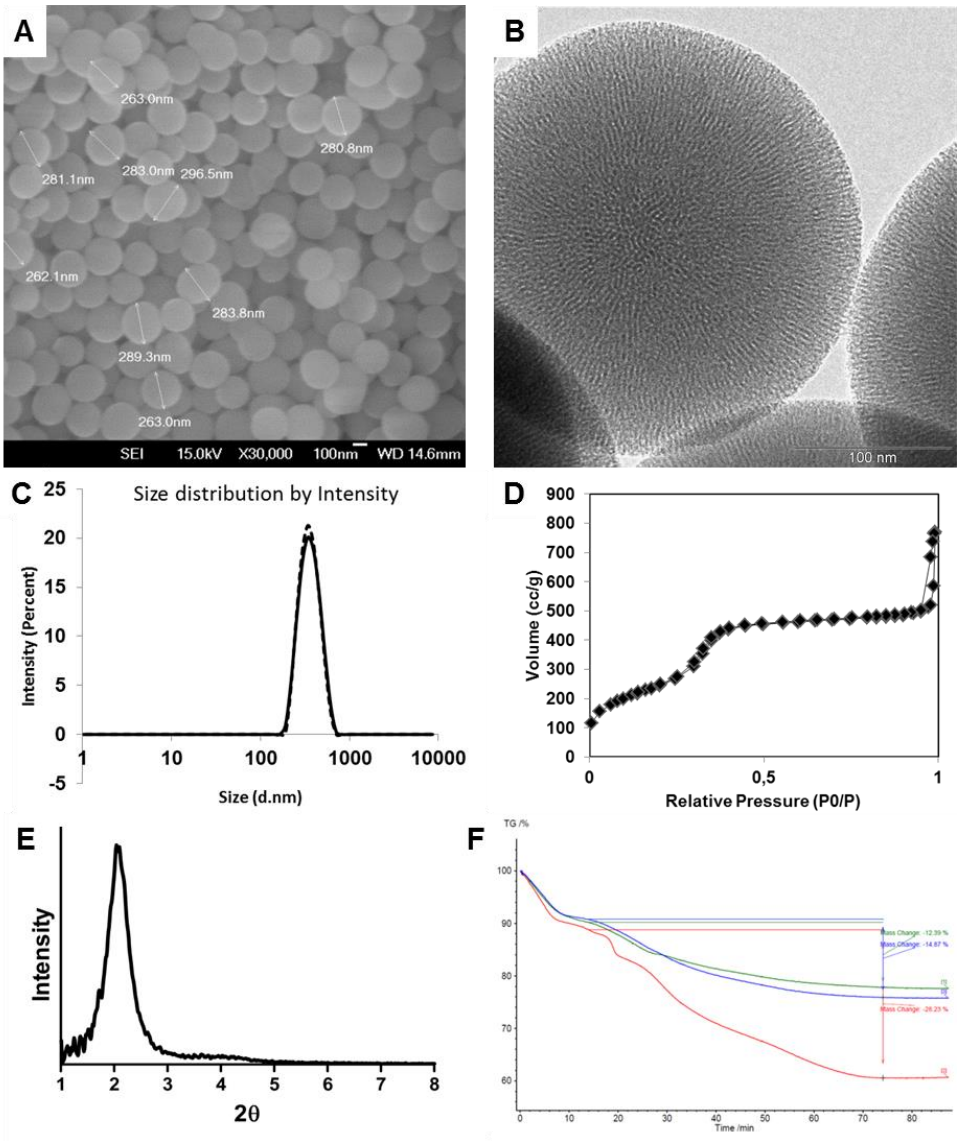

Figure 25. ***Characterization of the MSNs:*** *(A) SEM and (B) TEM images of the synthesized MSNs, (C) size distribution measured by DLS, (D) N_2-sorption isotherm for MSN (SBET=905 m^2/g, Vp=0.79 cc/g, Dp=3.5 nm by nonlocal density functional theory), (E) Powder X-ray diffraction pattern of a typical MSN structure with radially arranged pores (lattice spacing =4.34 nm), (F) TGA analysis of MSNs (green), PEI-MSNs (red), PEG-MSNs (blue). (PAPER I and III)*

Further, to confirm successful conjugation of targeting ligand FA, its amount in weight % with respect to the whole particle system was determined by the spectrophotometric method.

The particles were dissolved in 1 M sodium hydroxide by sonication and overnight stirring. The absorbance of the solution was measured by UV-Vis spectroscopy at λ=285 nm. To estimate the amount of glucose molecules on the particle surface in weight%, the resorcinol sulfuric acid assay method has been employed with slight modifications. MSNs were first dissolved in 1 M sodium hydroxide and diluted with HEPES buffer. Subsequently, the sample has been reacted with resorcinol in presence of sulfuric acid and incubated for 30 minutes. Finally, the sample absorbance was measured by UV-Vis spectroscopy at λ= 430 nm. (TABLE 4)

Table 4. Physicochemical characterization of aqueous particle suspensions

Type of Particle	Zeta Potential (mV)	FA content (weight%)	Organic Portion added (weight%)	Type of Particle	Zeta Potential (mV)	Glucose content (weight%)
MSN	0.8	NA	12	**MSN**	-5.5	-
PEI-MSN	52	NA	28	**MSN-GAaq**	-9.0	0.40
PEG-MSN	-2.1	NA	15	**MSN-GAorg**	-6.1	0.70
PEG-PEI-MSN	10	NA	35	**MSN-Gluc**	-4.9	0.27
FA-MSN	-0.3	0.04	14	**MSN-PEI**	50.3	-
FA-PEI-MSN	40	0.06	34	**MSN-PEI-GAaq**	49.6	1.44
FA-PEG-MSN	-0.9	0.13	21	**MSN-PEI-GAorg**	52.4	0.95
FA-PEG-PEI-MSN	26	0.05	34	**MSN-PEI-Gluc**	49.6	1.04

5.1.1.3. Effect of surface coating on serum protein adsorption

The main rationale for PEGylation of nanomaterials is its expected property in diminishing plasma protein adsorption on the particle surface, and reducing the likelihood of the body defense mechanisms (RES/MPS) of recognizing the particles as foreign substance and, thus, increasing the circulation time of particles in the blood stream.[61] Zwitterionic surface coatings have also been suggested to provide similar 'stealth' properties as PEGylation. Thus, to estimate the effect of different surface charge on protein adsorption, MSNs were incubated at two different concentrations in 1% fecal calf serum (FCS) prepared in HEPES buffer for 4 h. It has been observed that large amounts of serum proteins were adsorbed on the PEI-MSNs, mainly due to highly positive surface charge of the particle surface, since the majority of serum proteins are negatively charged. (Figure 26) Further, the PEGylation of this particle (PEG-PEI-MSNs) led to a decrease in the protein adsorption, but it is not significant and the

effect of PEGylation of the pure MSN was also not drastic but discernible. For the SUCC-PEI-MSNs observed serum protein adsorption was lowest of all samples. The surface charge of these particles was around -60 mV, which is in sharp contrast to the notation that high (both positive and negative) surface charge promotes protein adsorption. Thus, for the given MSNs employing the zwitterionic approach was drastically more efficient than PEGylation in diminishing serum protein adsorption.

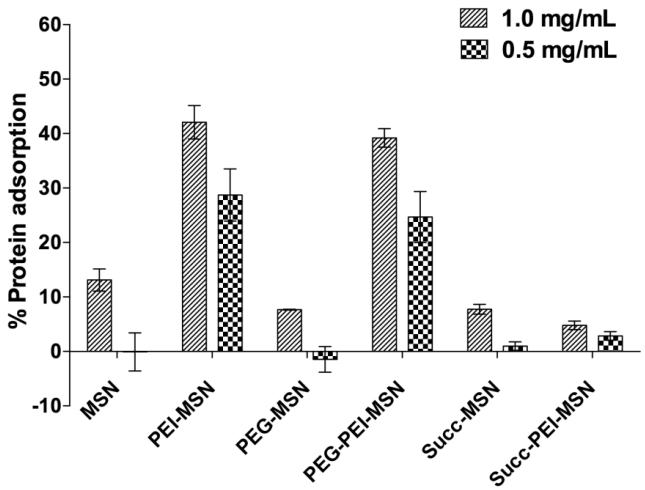

Figure 26. ***Relative serum protein adsorption on MSNs****: Adsorption of serum proteins on different surface charged MSNs after 4 hours incubation at 0.5 and 1.0 mg/ml concentration. Error bar represents ± SEM. (PAPER I)*

Further, the particles were incubated with cell media containing 10% FCS for 2 hours, centrifuged and resuspended in HEPES buffer, to observe the difference in surface charge after incubation with serum proteins. It has been observed that for all studied particles, the surface charge decreased to more negative, except for SUCC-PEI-MSNs, which suggests that the small portion of proteins adsorbed to these particles. (TABLE 5) For the PEG-PEI-MSNs extent of protein adsorption does not reflect the decrease in zeta potential quite well, since high protein adsorption is observed but the reduction in zeta potential is only a few mV. Thus, PEGylated surface probably attracts different kinds of proteins as compared to the pure PEI surface, which makes it difficult to predict resulting surface charge, since no common 'rule' for such protein selection on adsorption to surfaces exists to date.

Table 5. Zeta potential measurements of MSN particle suspensions in HEPES before and after incubation in DMEM cell media containing 10% serum.

Type of particle	in HEPES (200 µg/ml)	after 2 hours incubation in cell media redispersed in HEPES (200 µg/ml)
MSN	+5	-15
PEI-MSN	+48	+3
PEG-MSN	0	-6
PEG-PEI-MSN	+15	+9
SUCC-MSN	-14	-17
SUCC-PEI-MSN	-62	-37

5.1.2. Drug loading and release experiments

To evaluate MSNs' potential as drug delivery carrier, various hydrophobic molecules have been loaded to differently surface functionalized MSNs. To estimate the maximum amount of hydrophobic drug possible to load in MSNs, furosemide has been loaded at various initial loading degrees and the final % drug loading has been calculated. Further, in another study, MSNs were loaded with celastrol at 3 weight % loading degree and *in vitro* release was carried out in HEPES buffer in order to investigate the effect of PEI layer on drug release. In the next study, curcumin has been loaded at 0.3 and 1.0 weight % loading degrees to positive, neutral and negative surface charged MSNs, and the change in fluorescence intensity as function of surface charge has been measured in order to study influence of surface modification on photophysical properties of curcumin.

5.1.2.1. Loading of furosemide in different surface functionalized MSNs

Furosemide has been adsorbed to four different types of MSNs: PEI-, PEG-, FA-PEG-, and FA-PEG-PEI-MSNs at initial loading degrees of 10, 25, 50, 100 and 125 weight percentages to the particulate system. For all the particle systems, the final loading degree is proportional to the initial drug loading. (Figure 27) It has been observed that it is possible to load up to 70 weight % of furosemide to the particles. Further, information obtained from this study is that regardless of surface modification, similar loading degrees are achieved when a non-ideal organic solvent is used for the loading. This notion has been exploited in the following studies (Section 5.1.2.2 and 5.1.2.3)

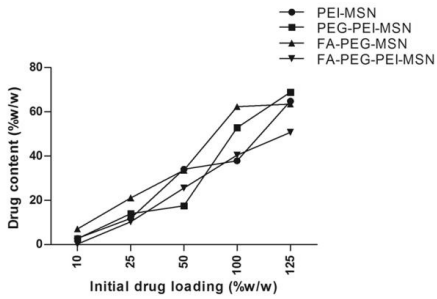

Figure 27. ***Evaluation of drug loading property:*** *% Furosemide loading in four differently functionalized MSNs at various initial loading degrees.*

5.1.2.2. Loading of celastrol and release in buffer

MSN and MSN-PEI were loaded with celastrol at a loading degree of 3 weight %. *In vitro* release of celastrol was carried out in HEPES buffer pH 7.2 and compared to the dissolution of a corresponding amount of free celastrol. For the free celastrol, after 48 hours, 50% drug dissolution has been observed. For the celastrol loaded in MSN-PEI merely 3% cumulative release has been detected. (Figure 28) For the intracellular drug delivery, it is desirable that particles release their cargo once it has reached to the site of action, which is inside the cancer cells for the celastrol. The PEI layer provides protection against premature drug release as for the control MSNs a rapid burst release is observed which is initially faster than the dissolution rate of free drug and after 2 - 6 hours it became the same as free celastrol. After that re-adsorption on to MSNs occurs, probably due to the static condition used, whereas free drug can continue to dissolve due to the absence of adsorbents. Owing to the largely differing conditions in this experiment as compared to biological/physiological situations (such as high drug concentrations used, close to but below the saturation limit of celastrol in an aqueous solvent), these results should be considered indicative only. However, from the observed trend it is evident that the PEI layer can serve as a 'molecular gate' preventing drug release from taking place extracellularly, as speculated previously[55] but now shown in this study. Thus, harmful drug cargo will not be exposed to neighboring cells that do not efficiently internalize the carrier particles. Thus, in line with the results obtained by our group in a different study,[120] the release of cargo molecule in a pure aqueous media depends on the degradation of a silica carrier, whereas physicochemical properties of the cargo molecule and its interaction with surrounding media are the main factors governing release of cargo in media mimicking intracellular conditions. Further, the material degradation has been arrested after loading with

hydrophobic guest molecules, and thus the cargo could be efficiently delivered into live cancer cells and released intracellularly without premature release under extracellular conditions.

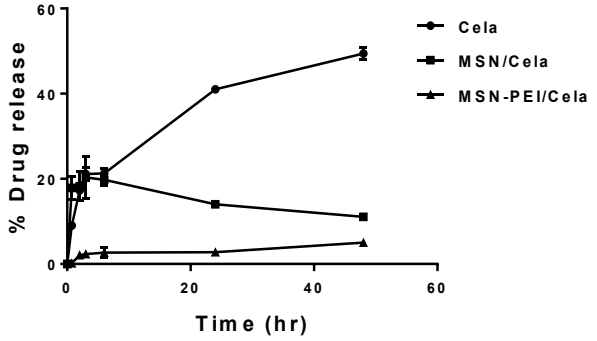

Figure 28. ***Evaluation of drug release property:*** *Release/dissolution kinetics of free celastrol, celastrol-loaded MSNs and celastrol-loaded MSN-PEI in HEPES buffer (pH 7.2) (PAPER II)*

5.1.2.3. Loading of curcumin and measurement of effect on particles fluorescence

Curcumin is natural anti-oxidant and it has anti-inflammatory property. Curcumin is a fluorescent molecule in the visible region. The fluorescence property of curcumin depends on the surrounding environment and it can also be used for physicochemical characterization. MSNs with positive, negative, and neutral surface charge (PEI-MSN, SUCC-PEI-MSN and ACA-PEI-MSN) were loaded with curcumin at two loading degrees, 0.3 and 1.0 weight % with respect to the particles. (SUPP. PAPER III) At higher concentration, fluorescence quenching might occur, therefore, low loading degrees were used for the study. It has been observed that particle surface charge does not affect the loading degree, especially at such low concentrations; but the surface charge has significant influence on the emission spectrum of curcumin. (TABLE 6)

Table 6. ***Amount of curcumin loaded in different surface modified MSNs***

Starting concentration of curcumin/ MSNs (w/w%)	Adsorbed Curcumin/MSNs (µg/mg)
PEI-MSN/CUR-0.3 %	4.75
PEI-MSN/CUR-1 %	8.75
SUCC-PEI-MSN/CUR-0.3 %	2.6
SUCC-PEI-MSN/CUR-1 %	9.42
ACA-PEI-MSN/CUR-0.3 %	3.02
ACA-PEI-MSN/CUR 1 %	13.15

The fluorescence maximum of 0.1 % curcumin loaded MSNs was found at 18975 cm^{-1}, whereas the fluorescence maximum of free curcumin in water was acquired at 18215 cm^{-1}. The higher wave number of curcumin in MSNs might be due to completely different microenvironment inside the pores of MSNs by increasing the energy gap between the ground state and excited state. Different surface chemistries remarkably influence fluorescence of curcumin loaded in MSNs probably due to the local accumulation of protons in the vicinity of the surface. As seen in Figure 29A, neutral net surface charge of charge-capped ACA-PEI-MSNs gave rise to longer wave number scale of curcumin compared to positive or negative net surface charge. The large energy gap between the ground and excited states of curcumin in neutral net surface charge could be due to the effect of pH on curcumin, as the fluorescence of surface modified MSNs is influenced by variation in local pH as opposed to surrounding pH. This trend was similar for both 0.3 and 1.0 weight % loading degrees of curcumin, and the % loading amount of curcumin did not influence appreciably the emission maximum of samples. However, for the neutral charge particles an increase in loading degree increases the fluorescence intensity of curcumin. (Figure 29B) Thus, surface modifications of MSNs influence the spectral behavior of curcumin due to local accumulation of protons. A similar effect of surface modification has been observed in the fluorescence behavior of fluorescein, which has been incorporated into the particles during the synthesis step in PAPER I. These properties are crucial to be aware of, for instance, when attempting to quantify and/or compare the intracellular amount of particles as well as quantifying the drug loading degree based on fluorescence.

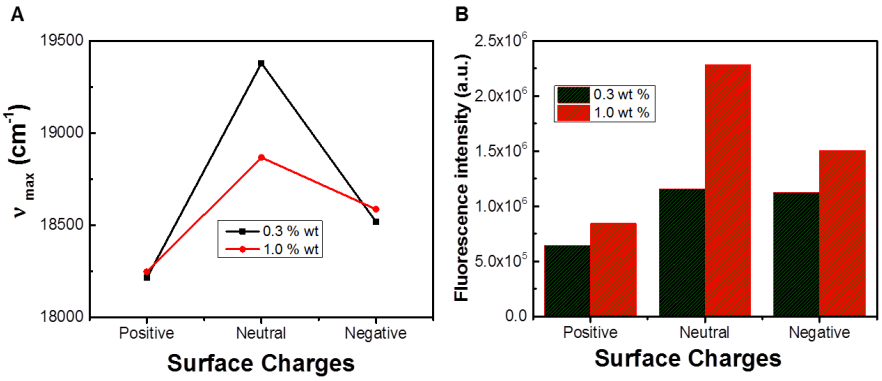

Figure 29. ***Effect of surface charge on fluorescence property of loaded cargo:*** *(A) Change in emission maximum of curcumin in wave number (γ_{max} in cm^{-1}) and (B) change in fluorescence intensity of curcumin as function of net charge on MSNs' surface. (SUPP. PAPER II)*

5.1.3. Cellular interactions

In this part, the interaction of differently surface functionalized MSNs with their environment relevant to their prospective application as drug delivery carriers was investigated.

5.1.3.1. Cytotoxicity assay

Caco-2, human colon adenocarcinoma, cells have been widely used as an *in vitro* model for studying small intestinal epithelial cell function, because they undergo a process of spontaneous differentiation that leads to the formation of a monolayer of cells, expressing several morphological and functional characteristics of the mature enterocytes lining the small intestine.[207] Enterocyte-like Caco-2 cells have been employed as a small intestine epithelial model, to evaluate possible toxicity of MSNs after oral exposure.

The *in vitro* cytocompatibility of all produced MSNs was studied in colon cancer Caco-2 cells using a cell viability assay. All the synthesized MSNs were non-toxic to Caco-2 cells up to 50 µg/ml concentrations, and at 100 µg/ml most of the particles were still non-toxic, except for PEG-PEI-MSNs and FA-PEG-PEI-MSNs, which showed a 20%–30% decrease in cell viability compared to the vehicle control DMSO. (Figure 30) This could be explained by a much higher uptake of these MSNs by the Caco-2 cells. The results show that all the produced MSNs are biocompatible at concentrations as high as 50 µg/ml.

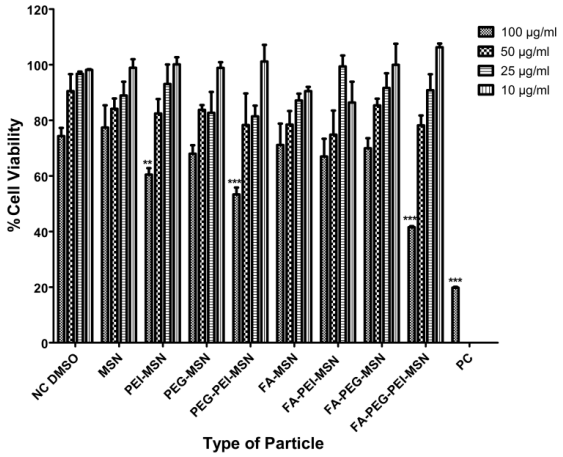

Figure 30. ***Functionalized MSNs are nontoxic to Caco-2 cells:*** *The viability of Caco-2 cells after 48 hours incubation with functionalized MSNs was assessed using the WST-1 assay at indicated MSN concentrations. All data sets were compared with a negative cytotoxicity control cell sample treated with particle vehicle DMSO alone (NC DMSO), and the toxin caliculin A was used as positive control (PC). Error bars represent ± SD (n≥ 3). ** P≤ 0.01, ***P≤0.001 (PAPER III)*

5.1.3.2. Influence of PEI coating on the cell viability

It has been reported that cytotoxicity of PEI has been connected to its molecular weight, as well as the concentration of PEI. To date, we have not observed any adverse effects of PEI-coated MSNs in our previous studies. Thus, it has been speculated that the toxicity of PEI as part of a larger construct could be mitigated/suppressed. The dose-response curve of 25 kDa PEI using HeLa cells has been obtained to find out the LD_{50} dose of the PEI. (Figure 31A) Further, to investigate differences based on: (a) type of particle (non-degrading; polystyrene (PS), very slow degrading; non-porous Stöber, slow degrading; solvent-extracted, fast degrading; calcined), and (b) coating approach (adsorption, grafting), the same kind of PEI has been adsorbed onto PS particles (PEI_{ads}-PS)and three different silica particles (non-porous; PEI_{ads}-Stöber, solvent-extracted; PEI_{ads}-MSN_{Ex} and calcined MSNs; PEI_{ads}-MSN-C) of comparable size via electrostatic interactions, and solvent-extracted particles were surface-grafted with PEI (PEI_{graft}-MSN). The PEI concentration in the toxic range has been selected, in the present case 10 µg/ml of pure PEI. HeLa cells were incubated with pure PEI (10 µg/ml) and the amount of each particle that was coated with the equivalent amount of PEI as well as the corresponding amount of plain particles without PEI, to distinguish the PEI-induced

toxicity. We have speculated that silica dissolution/degradation partly neutralizes extremely high positive charge of PEI and contributes to lessening the toxic effect related to pure PEI. (Figure 31B) Further, the 'biodegradation' of the silica-material itself could create a concentration gradient of silicic acid, which could thus possibly counteract the PEI effect.[208] Thus, PEI mediated toxicity can be restrained by combining it with silica in the construction of hybrid material.

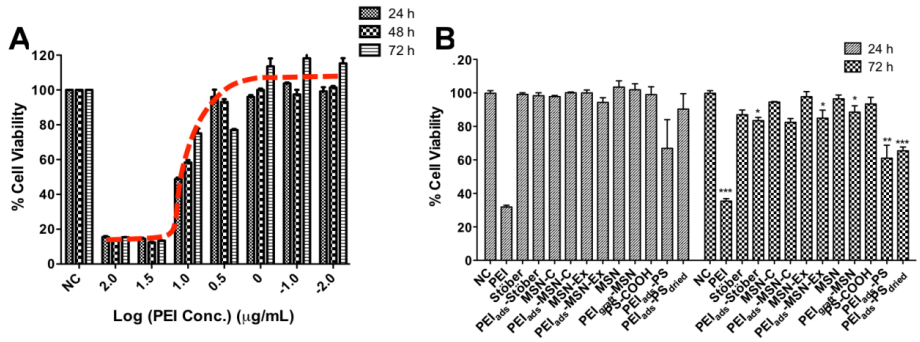

Figure 31. ***MSNs restrains PEI mediated toxicity:*** *Cell viability of HeLa cells incubated with (A) different concentrations of PEI (25 kD) for 24, 48 and 72 hours, (B) different particles with and without coated PEI equivalent to 10 μg/ml PEI (25 kD) for 24 and 72 hours, evaluated by the WST-1 assay. Polystyrene (PS) particles of similar size were included as particle control. Error bar represents ± SEM. *P≤0.05, ** P≤ 0.01, ***P≤0.001 (PAPER I) (broken line is a guide for the eye)*

5.1.3.3. Cellular uptake of differently functionalized MSNs

To investigate the effect of (a) particle surface functionalization, and (b) FA as targeting ligand on the cellular internalization, cellular uptake was assessed by flow cytometry in two different colon cancer cell lines (HT-29 and Caco-2 cells) as model for epithelial cells, as both of them are folate receptor positive cells. Further, for Caco-2 cells, confluent and non-confluent cells have been selected to assess the cellular uptake, as confluent Caco-2 cells can make the tight junctions and have less surface area, and further they can differentiate to form the monolayer of cells. The percent of cells that have internalized particles have been used as a measure of uptake efficiency. (Figure 32a,b) In Caco-2 cells, MSNs were more efficiently internalized in non-confluent cells as compared to confluent cells since more surface area is available for the internalization. (Figure 32b) For the HT-29 cells, MSNs uptake increases with the incubation time. (Figure 32a) Both Caco-2 and HT-29 are folate receptor positive cell lines, but the boosting effect of FA on cellular internalization was detected only in the case

when FA was linked to PEGylated particles (FA-PEG-MSN), where PEG was conjugated directly on the MSN surface, and for which the basal (inherent) cellular uptake was very low. Particles without any polymeric coating or only modified with PEG showed low uptake probably associated with their almost neutral charge as well as their tendency to aggregate at neutral conditions. Confocal microscopy further confirmed that PEG-MSN particles appeared to be aggregated, in contrast to PEI-modified particles which exhibited a more dispersed intracellular pattern. (Figure 32c-l) The combination of PEI and PEG proved most efficient in terms of maximizing the cellular internalization in the studied cell lines.

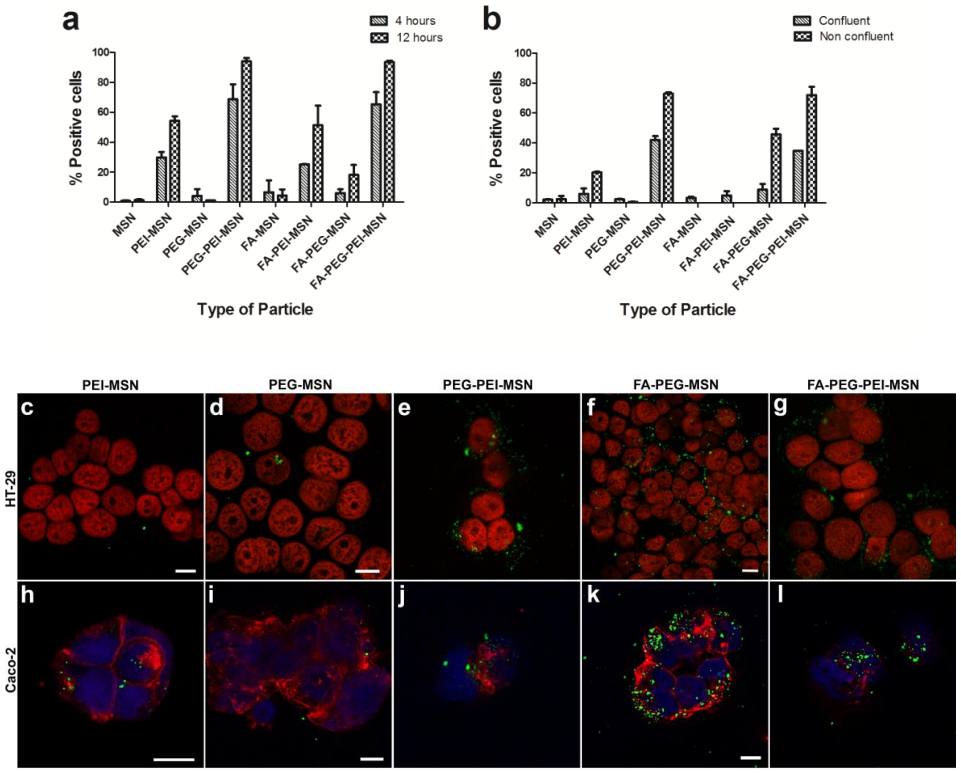

Figure 32. ***Effects of surface functionalization, incubation time and confluency of the cells on uptake of MSNs in the HT-29 and Caco-2 colon cancer cells:*** *(a,b) Flow cytometric analysis of the uptake of functionalized and FITC-labeled MSNs in HT-29 and Caco-2 cells. Error bars represent ± SD (n=4). (c-l) Confocal microscopy images of HT-29 and Caco-2 cells incubated with PEI-MSN, PEG-MSN, PEG-PEI-MSN, FA-PEG-MSN and FA-PEG-PEI-MSNs (green) for 12 hours. Nuclei were stained using PI (shown red in C-G; pseudo blue in h-l) and Caco-2 cell membrane stained with E-catherin Cy 5.0 (shown red in h-l) (Scale bar 10 µm). (PAPER III)*

To estimate the effect of glucose modification on cellular internalization of MSNs, different glucose functionalized MSNs were incubated with three different types of cells: HeLa cells (human cervical carcinoma) and A549 cells (human lung carcinoma); both of them are cancer cells having high glucose consumption, and MEF cells, as representative normal cells with lower glucose consumption. It has been observed that PEI modification increases the uptake of MSNs in both cancer cells. (Figure 33A,B) The distinction between the different sugar functionalization was not possible to discern in terms of percentage uptake efficiency. Therefore, normalized mean fluorescence, i.e. intensity per 10,000 cells against the particle fluorescence, was obtained; from all the studied particles, the MSN-PEI-GAorg particles have provided the highest cellular uptake for HeLa and A549 cells. (Figure 33D,E) The uptake efficiency of PEI-modified MSNs on healthy MEF cells was four to five times lower than cancer cells. (Figure 33C) To confirm the intracellular localization as well as the enhanced affinity toward the cancer cells, MSN-PEI-GAorg was incubated with both MEF and HeLa cells at a concentration of 5µg/ml and imaged by CLSM. (Figure 33F,G) A very negligible fluorescence signal from the FITC channel was detected from the MSN-PEI-GAorg particles within the MEF cells, while bright fluorescence signals could be detected inside the HeLa cells. All fluorescence from the FITC channel was originating from inside the cells, as the cell membrane has been stained with rhodamine-lectin (visible in red channel), confirming that the particles had been internalized. To further confirm the observed differences, image analysis of approx. five hundred cells (FITC channel, Ex. 488 nm/Em. 500–550 nm) was conducted using the BioImageXD software. The MSN-PEI-GAorg particle resulted in the highest FITC intensity per cell, which was significantly higher than the MSN-PEI particle and higher than all other glucose functionalized MSNs. (Figure 33G) Thus, the hyperbranched PEI coating together with glucose moieties as targeting ligand facilitate cellular uptake of MSNs into the targeted cancer cells compared to normal cells.

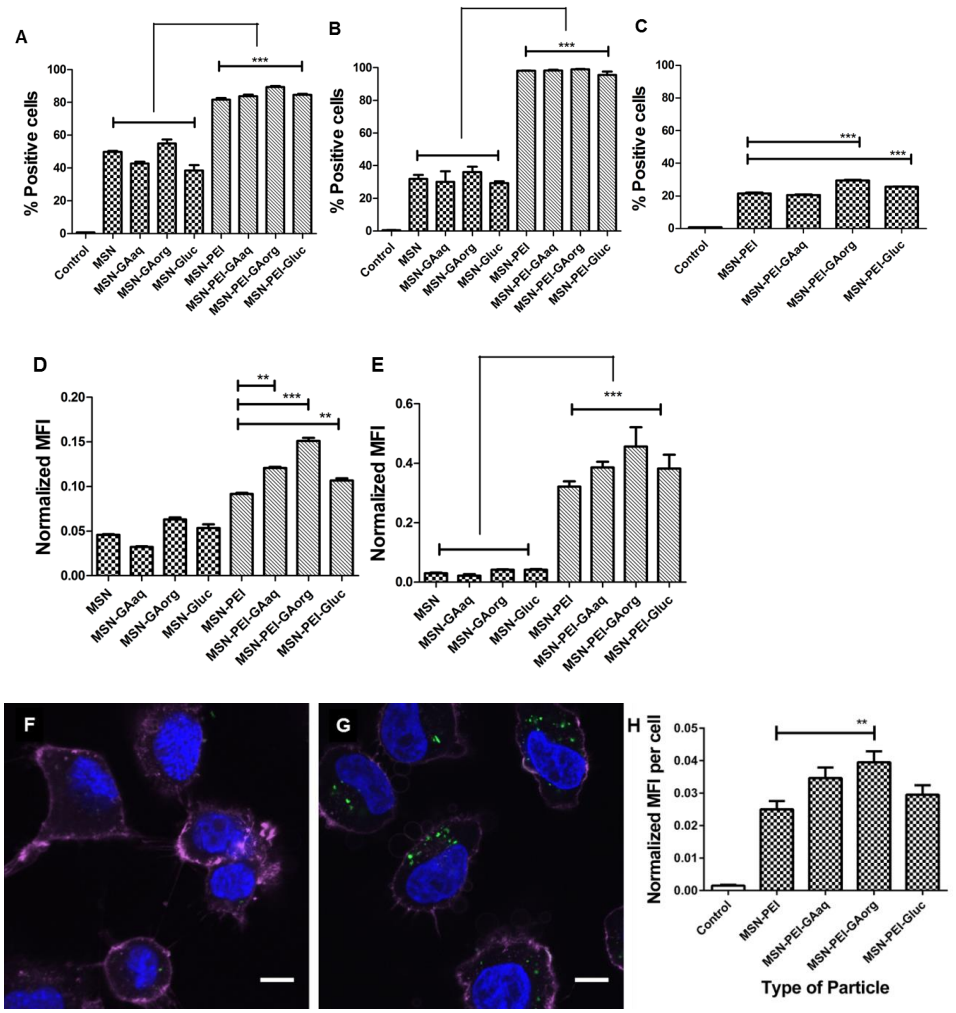

Figure 33. ***Effects of surface functionalization, type and glucose consumption of the cells on uptake of MSNs in the HeLa, A549 and MEF cells:*** *Flow cytometric analysis of uptake of the MSN particles with different glucose functionalization in (A) and (D) HeLa cells,(B) and (E) A549 cells, (C) MEF cells at 5 µg/ml conc. for 3 h. Confocal microscopic images showing endocytosis of MSN-PEI-GAorg particles in D) MEF cells and E) HeLa cells at 5 µg/ml conc. for 3 h. Scale bar-10µm. Quantification of MSN's uptake by using confocal microscopy and BioImageXD software. Normalized mean fluorescence intensity (MFI) of the FITC channel per HeLa cell using 30 µg/ml conc. of MSNs after 3 hours incubation. Error bar represents ± SEM. ** P≤ 0.01, ***P≤0.001 (PAPER II)*

5.1.3.4. Exocytosis of nanoparticles

An exocytosis study was conducted for the PEI-, PEG- and FA- functionalized MSNs to evaluate wether MSNs can be transported across a Caco-2 cell monolayer trans-cellularly without disturbing the integrity of the monolayer. As particles were readily taken up by cells within 12 hours, Caco-2 cells were co-cultured with pre-labelled (cell tracker CMAC blue) acceptor Caco-2 cells. As the exocytosis rate is significantly slower than endocytosis, the co-cultures were incubated for 36 hours. At the end of the experiment, both populations of the cells were labelled with the nuclear dye DRAQ5® to visualize both types of cells, donor cells (red) and the acceptor (red and blue). The results show that both donor cells and acceptor cells contain fluorescent MSN particles, (Figure 34) confirming that the functionalized MSNs tested here can be exocytosed from one cell and taken up by the neighboring cell, and the studied MSNs can transport trans-cellularly through the Caco-2 cells. *(UNPUBLISHED RESULTS)*

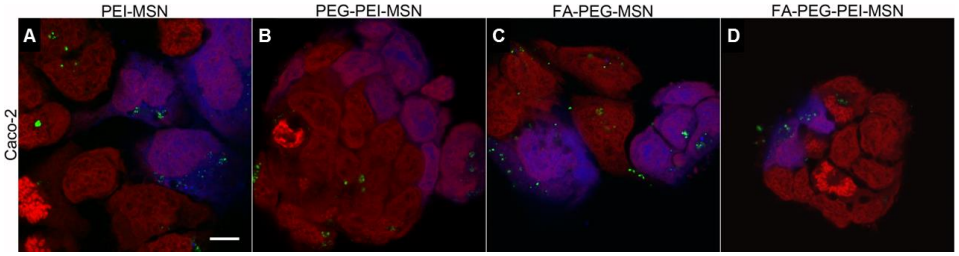

*Figure 34.**MSNs can exocytosed from Caco-2 cells:** Confocal microscopy images of PEI-MSNs, PEG-PEI-MSNs, FA-PEG-MSNs and FA-PEG-PEI-MSNs (green) exocytosed from donor Caco-2 cells (only red) and internalized by co-cultured acceptor Caco-2 cells (red and blue). All nuclei of acceptors and donors are stained using DRAQ5® (pseudo colored red). Scale bar = 10 µm.*

5.1.3.5. Influence of surface charge on route of uptake

MSNs with different surface charge, highly positive, negative and close to the neutral charge, were investigated for their route of uptake to evaluate the effect of surface functionality and surface charge on intracellular trafficking. To determine whether the MSN uptake was an active or passive process, cells were energy depleted using sodium azide (NaN3), which is known to inhibit the respiratory chain in the mitochondria. Macropinocytosis has been inhibited by amiloride, which is a selective inhibitor of Na^+/K^+ exchange, which blocks macropinocytosis by lowering submembraneous pH (cytosolic pH close to the membrane). Clathrin-mediated endocytosis has been inhibited by potassium depletion, or by inhibitors

such as Phenyl arsine oxide and chlorpromazine. Phenyl arsine oxide, a trivalent arsenical, inhibits clathrin-mediated endocytosis by crosslinking the clathrin coat. Caveolae-mediated endocytosis inhibitors include filipin, nystatin, methyl-β-cyclodextrin and genistein, which is a tyrosine kinase inhibitor. The cellular uptake of all investigated MSNs, regardless of their surface charges, were inhibited by the addition of phenyl arsine oxide. (Figure 35) This indicates that all the MSNs were mainly internalized by the clathrin-mediated route regardless of surface functionality. Inhibition by the combination of phenyl arsine oxide and genistein was not further inhibiting the cellular uptake, but it was slightly increasing the total uptake, which indicates that there might be some other (clathrin- and caveolae- independent) pathway, which has been activated by inhibition of both internalization pathways. The indiscernible difference in route of uptake for different surface charge particles might be due to the effect of serum protein adsorption on MSNs, as the experiments were conducted in cell media with serum proteins and the proteins are charged species, which contribute to the overall surface charge of nanoparticles by shielding their surface, as, observed in TABLE 5.

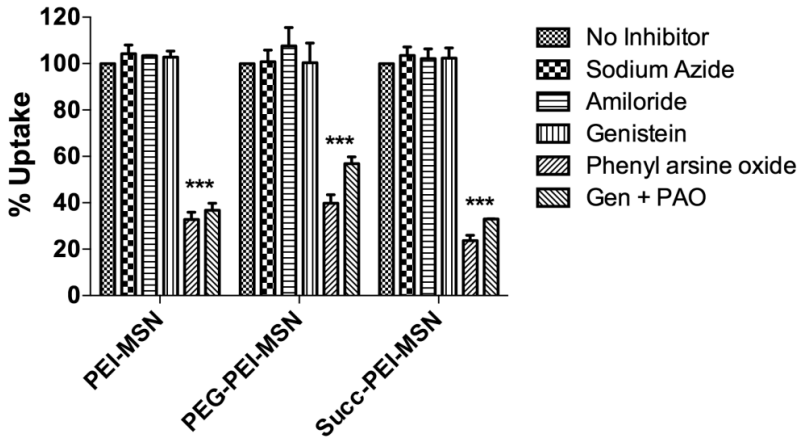

Figure 35. **E*ffects of various cellular uptake inhibitors on uptake of MSNs in Caco-2 cells:*** *Cellular uptake of differently functionalized MSNs after co-treatment with Sodium azide, Amiloride, Genistein, Phenyl arsine oxide and Genistein + Phenyl arsine oxide. Error bar represents ± SEM. * P≤ 0.05, ** P≤ 0.01, ***P≤0.001 (PAPER I)*

5.1.3.6. Influence of loading of hydrophobic cargo on intracellular pathway

MSNs are hydrophilic in nature and by loading MSNs with hydrophobic cargo the properties of MSNs may be altered. To pinpoint if this assumption is true, the uptake of PEI-MSNs and DiD dye (lipophilic dye, used as model drug cargo for visualization using flurescence

microscopy) loaded PEI-MSNs have been evaluated in MDA-MB-231 cells. The early and late endosomes were transfected-using plasmids for EEA1 and Rab7. It has been observed that the intracellular pathways for MSNs before and after dye loading are different. For the PEI-MSNs, the co-localization of a signal with EEA1 or Rab7 has not been observed, whereas for DiD loaded PEI-MSNs a clear co-localization has been observed between signals from MSNs, DiD dye and early/late endosomes after 24 hours. (Figure 36) Further, some amount of dye release from particles has also been observed, which would be expected since cellular release of hydrophobic cargo is required to obtain the therapeutic effects observed in e.g. sections 5.1.3.8 and 5.1.4.3. (SUPP. PAPER IV) This indicates that the intracellular route of MSNs also changes with the loading of the cargo molecule and the physicochemical properties of the cargo molecule. *(UNPUBLISHED RESULTS)*

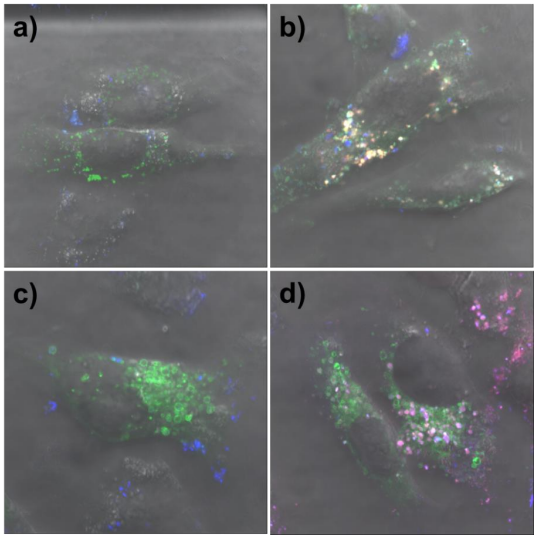

Figure 36. ***Effect of drug loading / hydrophobicity of the particles on the intracellular pathway:*** *MDA-MB-231 cells transfected with EEA1 and Rab7 plasmids to label early and late endosomes showing uptake of (a,c) PEI-MSN and (b,d) DiD/PEI-MSNs (blue) after 24 hours. Early /late endosomes (green) and DiD dye (red).*

5.1.3.7. Effect on permeability of furosemide through Caco-2 monolayers

Cultured human Caco-2 cell monolayers were considered representative models for drug permeability studies in the intestinal epithelium. The ability of selected MSNs from section 5.1.3.3 (PEI-MSNs, PEG-PEI-MSNs, FA-PEG-MSNs and FA-PEI-PEG-MSNs) to deliver the model drug, furosemide, which has low solubility and permeability (BCS Class IV), across a Caco-2 monolayer has been evaluated. The permeability through Caco-2 monolayers by

furosemide alone or furosemide-loaded MSNs was tested by analyzing the level of transport of furosemide from the apical to the basal compartment. Caco-2 cells cultured for 21-28 days showed intact cell monolayers on membrane support and were evaluated by Trans Epithelial Electrical Resistance (TEER) measurement and Lucifer Yellow (LY) rejection. (Data not shown) The amount of drug permeation at different time points starting from 0 to 42 hours indicates a time-dependent increase in furosemide permeation, which was clearly increased by all the studied MSNs as compared to free furosemide. (Figure 37) PEG-PEI-MSNs and FA-PEG-PEI-MSNs showed ~1.3- and ~1.4- fold increase in permeability, respectively, as compared to furosemide alone. Furosemide permeability was increased ~1.5-fold for the particles modified with PEI alone, whereas particles functionalized with FA-PEG-MSNs showed no increase in permeability. These results indicate that PEI-functionalization achieves better permeability than PEGylation, of which the latter has previously been regarded as a permeability enhancing agent, and that the combination of PEI and PEG constitutes a particularly good drug permeability enhancing surface coating. *(UNPUBLISHED RESULTS)*

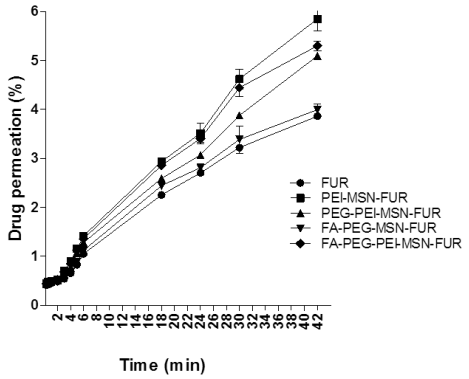

Figure 37. ***MSNs improve the permeability of Class IV drug:*** *%Drug permeation of furosemide across Caco-2 monolayer loaded in different surface functionalized MSNs as function of time.*

5.1.3.8. Apoptotic effect of celastrol loaded MSNs on cancer cells

To confirm a therapeutic response could be attained for drug loaded MSNs, the cytoprotective effect of free celastrol was first validated in HeLa and A549 cells by measuring the heat shock response using Western blot analysis. (Figure 38a,b) An apoptosis assay using propidium iodide staining was employed using different concentrations of free celastrol for 24 and 48 hours to establish the drug dose as well as time point to evaluate the particle-mediated drug delivery. (PAPER II) The assay showed that 24 hours is enough time for celastrol to induce

apoptosis in HeLa cells. This is probably due to the mitotic rate of HeLa cells, which is about 8-12 hours; therefore, 24 hours can be regarded as sufficient time for celastrol to induce apoptosis through microtubule destabilization. The optimal dose to induce apoptosis in HeLa cells found to be around 5.3 µM after 24 hours. The toxicity of empty-MSNs (without celastrol drug load) was evaluated after 24 hours incubation with HeLa cells, and it has been observed that at all the studied concentrations they are non-toxic. (Figure 38c) Further, HeLa cells were incubated with celastrol loaded MSNs corresponding to 5.3 µM of celastrol to assess their potential anticancer properties. At the same celastrol concentrations, significant enhancement in drug efficacy (in terms of apoptosis) was observed for all PEI modified MSNs. For the MSN-PEI-GA_{aq} particles, the effect was lower compared to the other particles at the studied concentration. This could be due to structural changes of the porous matrix upon GA-conjugation, which was carried out in aqueous conditions and disordered structure of pores might have occurred due to exposure to water, as observed in PAPER I using X-ray diffraction, which may have repercussions on drug release.

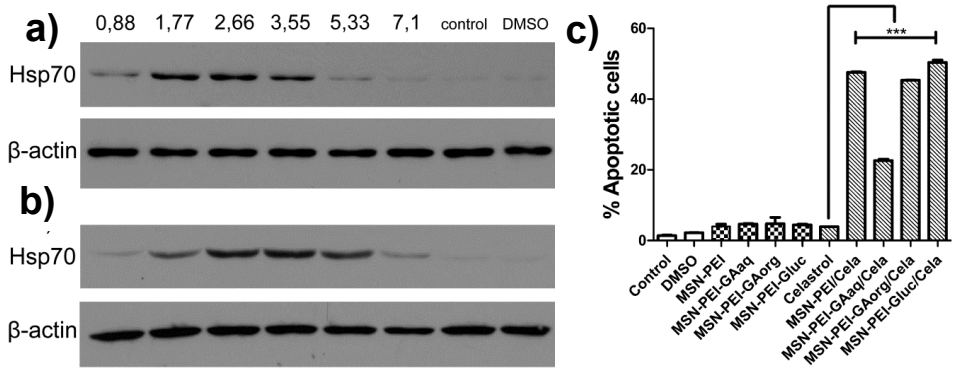

*Figure 38.**MSNs can improve the apoptotic effect of celastrol:** Celastrol induces the heat shock response in (a) HeLa cells and (b) A549 cells at different concentrations. Expression of heat shock protein 70 (Hsp70) can be seen as band in western blot image, β-actin is used as standard. (c) Apoptotic effect of control, DMSO (vehicle), empty MSNs, celastrol and celastrol loaded MSNs after 24 hours incubation with HeLa cells at concentration corresponding to 5.3 µM of free celastrol. Error bar represents ± SEM. * P≤ 0.05, ** P≤ 0.01, ***P≤0.001 (PAPER II)*

5.1.4. *In vivo* bio-distribution and pharmacodynamics studies

After successful *in vitro* studies, selected particles were further tested *in vivo* to confirm their applicability in a more clinically relevant and complex setting.

5.1.4.1. In vivo bio-distribution of fluorescent MSNs in the gastrointestinal tract

Different techniques can be employed for tracking the bio-distribution of MSNs (i) by labelling the particles inherently with a fluorescent dye, and measuring fluorescence intensity using spectroscopy or microscopy; or (ii) coupling a radioisotope with particles and following the radioactivity, or (iii) by use of inductively coupled plasma mass spectrometry (ICP-MS) or inductively coupled plasma optical emission spectrometry (ICP-OES) to directly quantify the amount of metal (silicon) in each tissue sample. MRI can also be used for the tracking of MSNs, in case of iron oxide or gadolinium oxide core-shell nanoparticles or gadolinium ions doped MSNs.[209,210] Two different techniques were employed to determine whether orally administered MSNs with different types of polymeric coatings were taken up by the intestinal epithelial cells *in vivo*. For *in vivo* uptake studies, eight adult male mice were orally gavaged with different MSN samples and a control daily for four consecutive days. The health of the mice was monitored each day and they were sacrificed at the end of the experiment by cervical dislocation. The whole GI tract was removed, and divided into stomach, small intestine corresponding to duodenum, jejunum, ileum, cecum, proximal colon and distal colon. The tissue samples of 6 μm thickness were imaged using confocal microscope. The tissue sections of the control mice gavaged with vehicle alone show only autofluorescence from the tissue in the green channel, whereas tissue sections from the mice fed with fluorescent MSNs showed brighter green particulate fluorescence from the FITC-labeled MSNs either attached to the mucosal barrier or internalized by epithelial cells. This was evident in all studied GI sections but easily discernible in the stomach and the small intestinal villi. (Figure 39a-p)

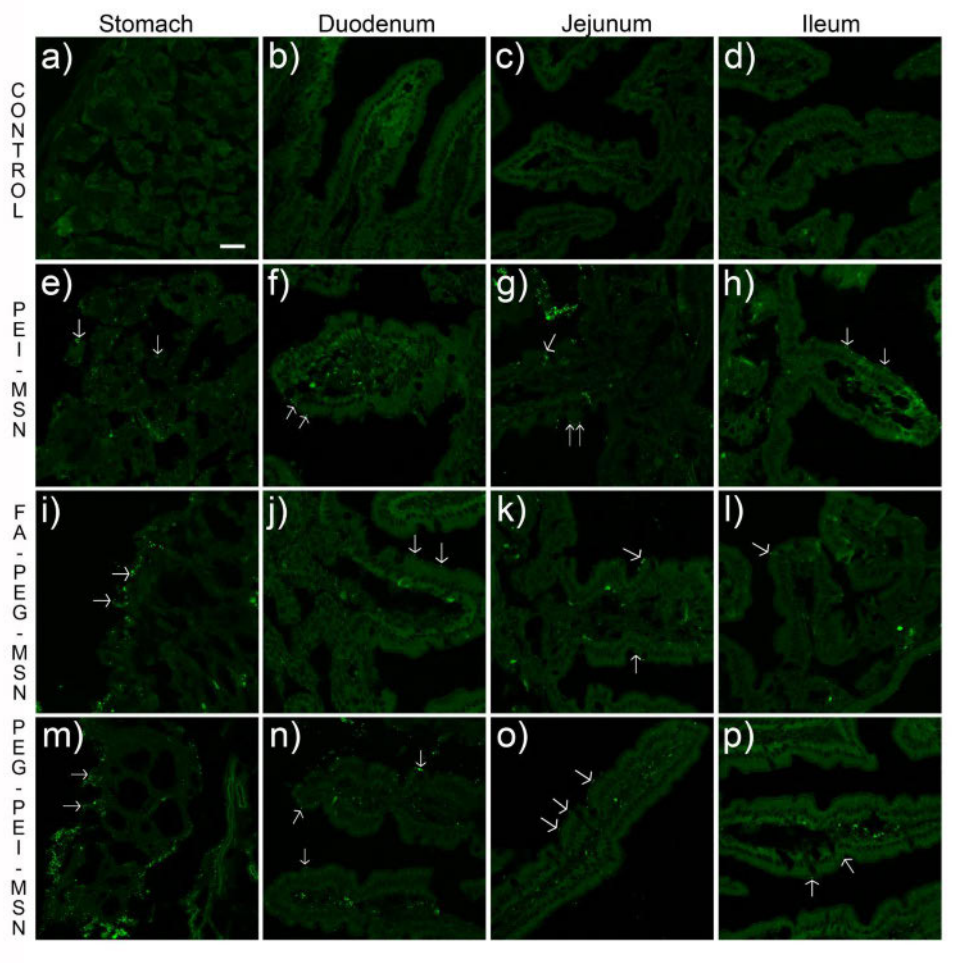

Figure 39. ***Internalization of fluorescent MSNs in intestinal epithelia:*** *MSNs fed by oral gavage, tissue sections were excised, fixed in 4% paraformaldehyde and imaged. Confocal microscopy images of the tissue sections of stomach, duodenum, jejanum and ileum section of the mice fed with Control (HEPES)(a-d), PEI-MSNs(e-h), FA-PEG-MSNs(i-l) and PEG-PEI-MSNs(m-p). Arrow indicated internalized nanoparticles. (Scale bar 25 µm) (PAPER III)*

The uptake of PEG-PEI-MSNs was further confirmed by staining for F-actin in tissue sections from mice to highlight epithelial apical microvilla toward the lumen and DRAQ5® to visualize nuclei. The frozen tissue sections were subsequently analyzed by fluorescence spectroscopy and inductively coupled plasma mass spectrometry to determine the amount of internalized MSNs. However, neither fluorescence spectroscopy of homogenized tissue samples nor quantification of elemental silicon by inductively coupled plasma measurements proved to be sensitive enough to detect changes in fluorescence or Silicon (Si) level in

different tissue samples in comparison with control mice gavaged with vehicle (HEPES) alone due to autofluorescence from the tissue samples and high endogenous Si background in the tissue. (PAPER III)

5.1.4.2. Stability of drug loaded MSNs in simulated gastric fluid

After oral administration, the nanocarriers encounter the harsh physicochemical environment of the GI tract. These biological fluids influence the stability of particles even before they come in to contact with the intestinal cells. Hence, *in vitro* tests in gastric and intestinal simulated fluids are important to investigate if particles are stable in the GI environment and if they are able to protect the incorporated drug/cargo. The PEG-PEI-MSNs and DAPT loaded PEG-PEI-MSNs were exposed to simulated gastric and intestinal fluids, thereafter the particle morphology was analyzed by transmission electron microscopy (TEM). The TEM images after treatments with simulated gastric fluid (SGF) and simulated intestinal fluid (SIF) show that the MSNs were intact and the structure was virtually unaltered compared to the untreated particles. (Figure 40) In addition, to evaluate if MSNs can protect the loaded cargo/drug while passing the gastrointestinal fluids, the cargo (DAPT) has been eluted from MSNs samples collected before and after SGF and SIF treatment, and analyzed by high performance liquid chromatography, which showed that DAPT is intact and it has not been degraded by exposure to SGF and SIF, confirmed by no change in shape of HPLC chromatogram peak. (PAPER III) These results indicate that functionalized MSNs can serve as an effective carrier to deliver cargo to the target site without losing its integrity.

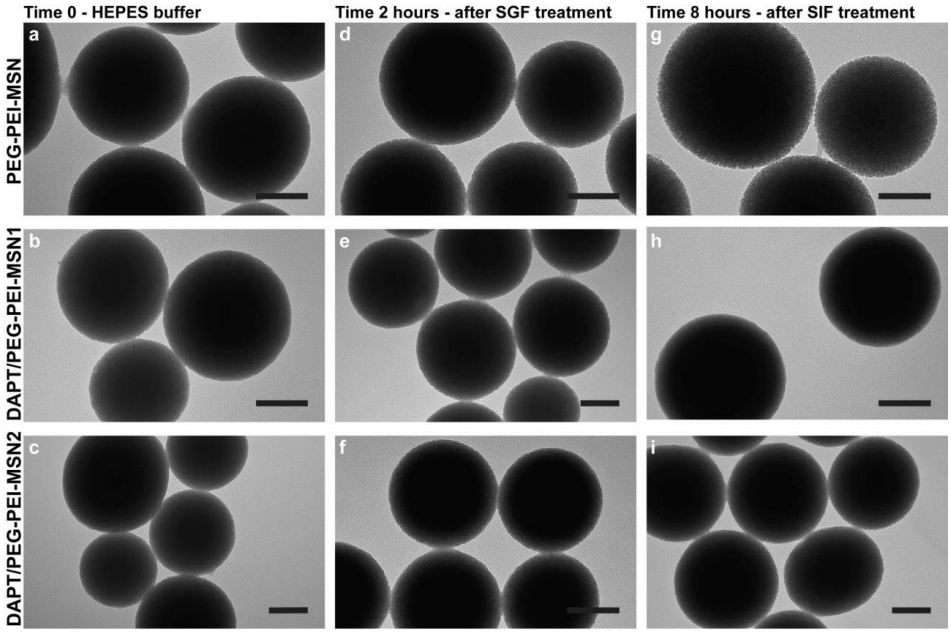

Figure 40. ***Functionalized and DAPT loaded MSNs are stable in simulated gastric and intestinal fluid:*** *Transmission electron microscopy images of PEG-PEI-MSNs and DAPT/PEG-PEI-MSNs (n=2) (a-c) at time 0 hour in HEPES buffer, (d-f) after 2 hours incubation with SGF and (g-i) after further 6 hours incubation in SIF. Scale bar = 100 nm. (PAPER III)*

5.1.4.3. In vivo oral drug delivery efficiency

The γ-secretase inhibitors block activation of the Notch pathway, which regulates a broad spectrum of cell fate decisions. The intestinal epithelium has stem cell and progenitor cell populations. Replicating crypt base columnar stem cells can self-renew or give rise to rapidly dividing transit-amplifying cells, which differentiate into mature cell types, including absorptive enterocytes, enteroendocrine cells, mucus-secreting goblet cells, antimicrobial peptide-secreting Paneth cells and chemosensing tuft cells. Notch signaling is a critical regulator of epithelial cell fate in the intestinal epithelium; with Notch promoting the absorptive cell fate over the secretory cell fate. Thus γ -secretase inhibitors by blocking the Notch pathway cause the transformation of proliferative intestinal crypt cells into post-mitotic goblet cells. To evaluate the therapeutic potential of MSNs as drug delivery vehicles *in vivo* for oral drug delivery to the intestinal epithelium, the effect on Notch activity by MSNs loaded with the γ-secretase inhibitor-DAPT was measured. Adult male mice were subjected to gastric gavage once a day for three consecutive days with different MSN particles and a

control. The uptake and effects were tested both in the small intestine, and in colon, which are the target tissues in most intestinal diseases. The readout of Notch mediated cell fate switches was monitored by counting the number of goblet cells using Periodic Acid-Schiff (PAS) staining, MUC2 mRNA analysis, and determining stool hydration. The DAPT alone (in vehicle buffer solution) increases the number of goblet cells in the colon as well as in the small intestine after oral gavage compared to controlled mice given vehicle buffer solution. The number of goblet cells in the colon of mice given DAPT/FA-PEG-PEI-MSNs was significantly higher than of those given DAPT alone or control particles without DAPT and they were also able to increase the expression of MUC2, a predominant intestinal mucin in the colon. (Figure 41) However, DAPT/FA-PEI-MSNs were not able to improve the colonic Notch inhibition. Goblet cell hyperplasia was observed in the small intestine, where DAPT/FA-PEI-MSNs showed a significantly better inhibition of Notch compared to DAPT alone. This effect was seen in both crypts and villi but more prominently in the villi, which have a bigger cell compartment and more goblet cells. The results were also confirmed by an increased level of stool hydration only in the mice fed with DAPT alone or DAPT/FA-PEG-PEI-MSNs, which reflect the Notch inhibition-induced cell fate switch from water-absorbing colonocytes to mucus-producing goblet cells. (PAPER III) The inconsistency in drug effect between small intestine and colon could be associated with the fact that the particles come into contact with the small intestine first and might be exposed to it for a slightly longer time than the colon, and due to that DAPT/FA-PEI-MSNs were more efficiently internalized by the intestinal cells leading to a more efficient drug delivery. The other possible reason might be that differences in the colon and small intestine mucus layers influence particle penetration, for instance, the pore size and charge of mucin molecules may vary considerably along the GI tract. It has been observed that particles more easily penetrate the mucus in the small intestine and hence there might be no beneficial effect of PEGylation, while this modification may be necessary for the colon, which has a thicker mucus barrier than the small intestine. Since colorectal cancer and inflammatory bowel disease, the main intestinal disorders, occur in the colon and not in the small intestine, the PEGylation of MSNs should provide a useful tool for nanomedical drug development targeting the colon. The PEI coating provides surface charge for stabilization of particles, PEG facilitates the penetration of the particles through the mucus layer or increase residence time of the adhered fraction of particles in the mucosa, and FA acts as a targeting moiety for folate receptor expressed on the intestinal epithelial cells.

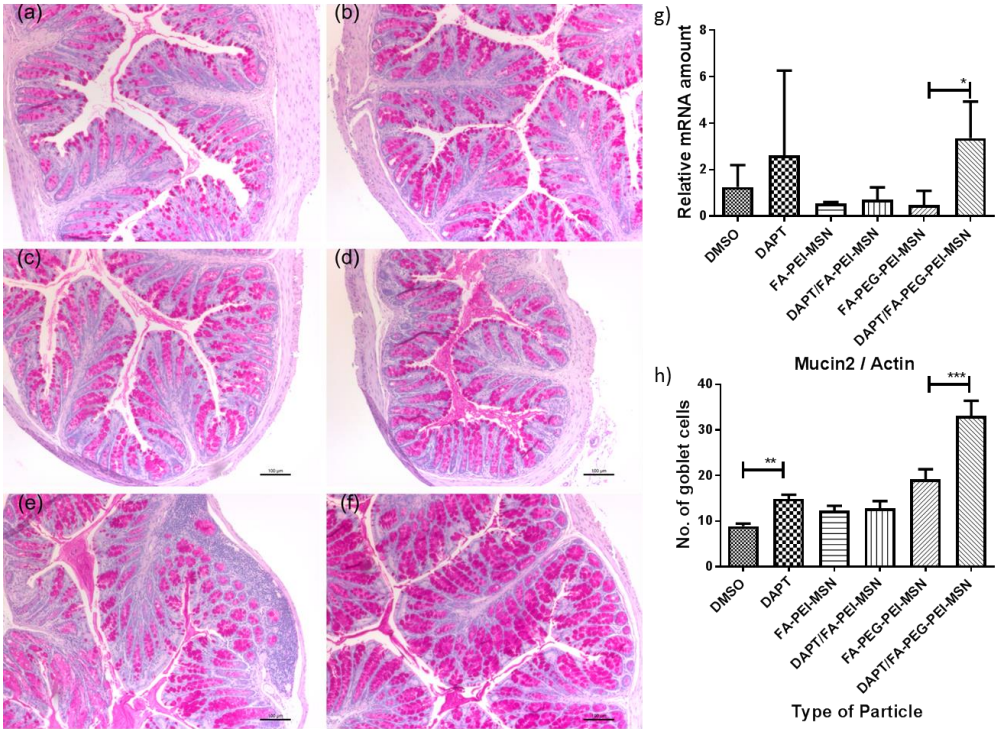

Figure 41. ***Notch Inhibitor loaded MSNs induce goblet cell differentiation and mucus secretion:*** *Colon sections stained for Goblet cells by Periodic-Shiff (PAS)-staining from mice fed with (a) vehicle control, (c,e) control particles (FA-PEI-MSN, FA-PEG-PEI-MSN) and (b) Notch inhibitor;DAPT, (d,f) DAPT-loaded MSNs (DAPT/FA-PEI-MSN, DAPT/FA-PEG-PEI-MSN) by oral gavage. (Scale bar 100µm). (g) Mucin-2 content in colon section was determined by RT-PCR and (h) goblet cells in colon were counted using Image J software. Student's t-test. Error bars represent ± SEM (n= 3). *P≤ 0.05, ** P≤ 0.01, ***P≤0.001 (PAPER III)*

5.2. Mesoporous nanocarriers for delivery of hydrophilic cargoes

As mentioned in the literature review, smaller particles may be more effectively taken up by the cells than larger particles. Therefore, mesoporous silica nanoparticles of approximately 70 nm size were synthesized, as sub-100 nm size is reported to be an optimal particle size to reach maximum cellular uptake.[31] For the delivery of hydrophobic molecules, they can be adsorbed to the pore walls and the release is mediated by degradation of the silica matrix, or by the physicochemical properties such as solubility and oil-in-water partition coefficient of the cargo molecule. However, for hydrophilic (BCS Class I) guest molecules, since their solubility is very high in an aqueous environment, drug release is achieved immediately by diffusion. Therefore, to prevent the immediate drug release in an aqueous medium and to achieve targeted intracellular drug delivery, the pore openings should be gated/ sealed after drug loading and it should be released after activation by a specific stimulus. Here, MSNs were coated with lipid bilayers as diffusion barriers, using DOPE lipid (a neutral lipid) as an inner leaflet of the bilayer, and POPG lipid (negatively charged lipid), DOPC lipid (neutrally charged lipid) and DOTAP lipid (positively charged lipid) were used as an outer leaflet of the bilayer. Different outer lipids were used to investigate the effect of different surface charges on cellular uptake and intracellular drug release. The MSNs have been loaded with hydrophilic molecules, such as calcein and zoledronic acid. The prepared lipid bilayer coated MSNs have been evaluated for their stability. The synthesized lipid bilayer coated MSNs were evaluated for their cytocompatibility as well as their cellular internalization. Further, the influence of the outer leaflet of the lipid layer on cellular uptake has been assessed. Efficacy of the MSNs loaded with zoledronic acid (ZOL) has been evaluated using breast cancer cells to find out the suitable candidate for *in vivo* studies. Finally, *in vivo* delivery and safety of the empty and zoledronic acid loaded MSNs have been studied.

5.2.1. Design and characterization of mesoporous nanoparticles

Highly ordered, uniform, spherically shaped mesoporous silica nanoparticles with an average diameter of approx. 70 nm having radially aligned pore structure and pore sizes approx. 5 nm were synthesized. The pore size enlargement was achieved through joint incorporation of swelling agents 1,3,5-triisopropylbenzene (TMB) and decane in a CTAB templating system.

5.2.1.1. Surface functionalization and coating of MSNs with lipid bilayers

Fluorescent MSNs were created by incorporation of FITC, already in the synthesis step via co-condensation approach, whereas amino groups were successfully introduced by hyperbranching polymerization of PEI, which improves the cargo loading by electrostatic adsorption to the pore surfaces, as calcein/ZOL both are negatively charged molecules. Further, the PEI layer provides a soft cushion to produce a defect-free and durable lipid bilayer on silica nanocarriers. (Figure 42)

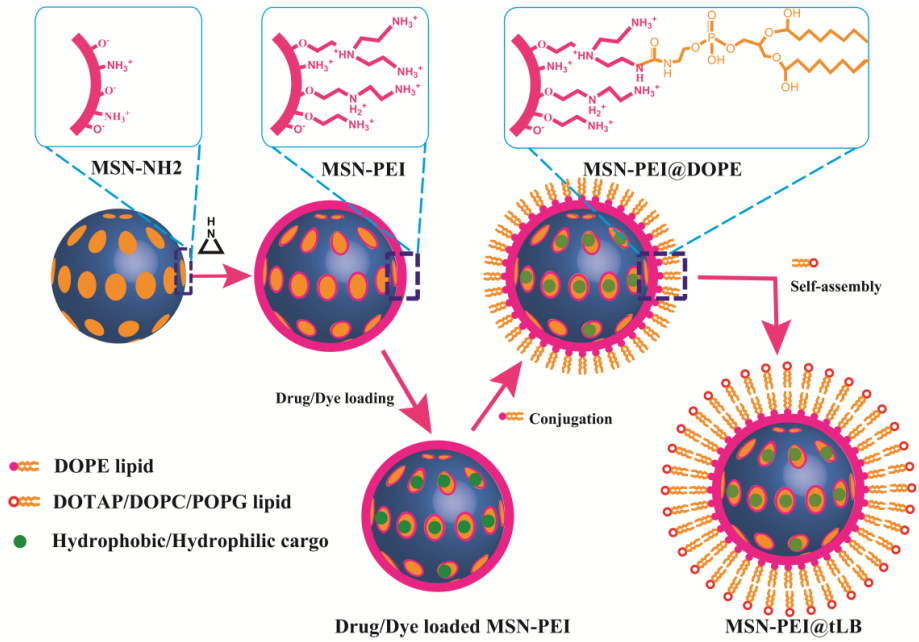

Figure 42. Scheme demonstrating the lipid bilayer (LB) tethering approach on MSN surface by hyperbranched PEI. Hyperbranched PEI (pink) was anchored onto the surface of amino group co-condensed MSN (MSN-NH_2) for the subsequent loading of negatively charged drug (green dots). Thereafter, the conjugation of DOPE lipid as an inner leaflet of LB was realized by using a coupling agent N, N'-disuccinimidyl carbonate (DSC). The self-assembly of the outer leaflet of LB driven by hydrophobic interactions was carried out through a dual solvent exchange method in the final step. (PAPER IV)

MSNs were further coated with a tethered lipid bilayer (tLB). Lipid bilayer gated MSNs can act as potential carriers for controlled drug delivery. The sophisticated architecture of those particles mimics the cell membrane's property on the impermeability towards hydrophilic molecules by the hydrophobic bilayer.[211]The MSNs can carry high payloads of guest

molecules due to their high surface area and large accessible pore volumes, while the LB elegantly functions as a biomimetic cap and provides barrier formation towards hydrophilic drugs loaded in MSNs. This system offers an advantage for the retention of hydrophilic drugs in the mesopores without premature leakage and intracellular drug release. The inner leaflet of the LB has been composed of DOPE lipids, which was tethered via the covalent conjugation between primary amines of DOPE and that of the PEI. DOPE is commonly used as a helper lipid; it has reported to have an ability to reduce the cytotoxicity of cationic liposomes. The DOPE lipid obtains spherical micelle morphology above pH 9.0 and transforms to an inverted hexagonal (HII) morphology at acidic pH. The densely packed hydrophobic tails of DOPE lipids extending outwards therefore led to the self-assembly of another phospholipid driven by van der Waals interactions using a dual solvent exchange method, resulting in the formation of the outer leaflet of tLB. (Figure 42) The outer leaflet of the lipid bilayer is composed of either DOPC lipid, POPG lipid or DOTAP lipid. PC and PG lipids, accounting for a large portion of the phospholipids in most mammalian cells, are also common constituents of the widely used liposomal formulations in nanomedicine. The DOTAP lipid is the most popular cationic lipid used in lipoplex formation. The addition of PEG to the lipid bilayer can further decrease recognition by the reticuloendothelial system and hence extend the circulation time of MSNs in biological fluids. To improve delivery efficiency of the PEGylated nanoparticles comprising transient PEG coating, attachment of targeting ligands at the distal end of PEG moieties can be utilized. Therefore, a small fraction (2 mol%) of DOPC lipid was replaced with DSPE-PEG(2000)-Maleimide for the further conjugation with targeting ligand folic acid.

5.2.1.2. Physicochemical characterization of the synthesized MSNs

The SEM and TEM image reveals uniform spherical MSN-NH_2 particles with an average diameter of 70 nm. (Figure 43A-B) The TEM image of the MSN-PEI particles stained with osmium shows the reduction in the contrast of the mesopores via the presence of a large amount of scattered black dots. (Figure 43C) These dots can be attributed to the hyperbranched polymers on the exterior and interior surface of particles; however, the thickness of the PEI modification layer on the mesopore surface is thinner than that on the exterior particle surface. The typical nitrogen adsorption-desorption type IV isotherm for MSN-NH_2 and MSN-PEI confirmed the mesoporous nature of the particles. (Figure 43D) Compared with MSN-NH_2, the isotherm of MSN-PEI displays an apparently decreased specific surface area (from 1043 m^2g^{-1} to 566 m^2g^{-1}) and pore volume (from 0.85 cm^3g^{-1} to 0.58 cm^3g^{-1}), suggesting an efficient polymer modification. However, the peak position in the

pore size distribution remained virtually unchanged (4.8 nm). Substantial reduction in the intensity of X-ray diffraction peak (Figure 43E) and substantial weight loss (23 wt%) in the TGA curve further supports the efficacious surface polymerization. (Figure 44B)

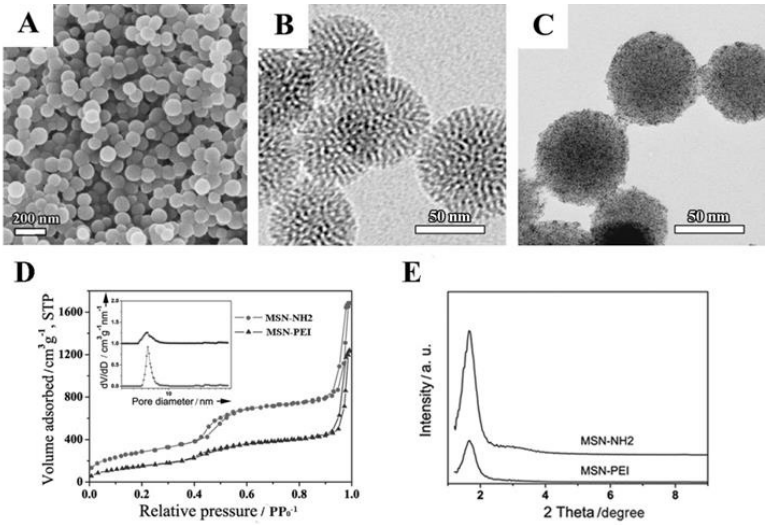

Figure 43. ***Characterization of the nanocarriers:*** *(A) Representative SEM image of the small-MSN-NH2, (B) TEM images of MSN-NH2 and (C) the hyperbranched PEI modified MSNs (MSN-PEI) stained with osmium tetraoxide to show the presence of PEI. Scale bar represents 50 nm. (D) Typical nitrogen sorption isotherms, the corresponding pore size distributions (inset), (E) small angle X-ray diffraction patterns of MSN-NH2 and MSN-PEI. (PAPER IV)*

The tethering of NHS group activated DOPE lipids has been verified by a weight-loss increase of 8.4 wt% for the MSN-PEI@DOPE. (Figure 44B) Osmium-stained TEM image for the MSN-PEI@tLB particles approves the self-assembly of the outer leaflet of the LB. As shown in Figure 44A, individually encapsulated particles with typical core-shell morphology were obtained. The core region is darker than the shell, probably because of the penetration of osmium into the pores of MSN-PEI particles. The thickness of the shell is around 9 nm, which should be contributed by a PEI tether layer and a lipid bilayer. Furthermore, a weight-loss increase of 9.0 wt% in the TGA curve was found after the self-assembly step. This demonstrates that the outer leaflet of DOPC has the same molecular packing density as that of the inner leaflet of DOPE. (Figure 44B) The tethering of activated DOPE lipids with primary amines of PEI can be observed by the amide vibration peaks in the FTIR spectrum at 1650 cm^{-1} and 1560 cm^{-1}. (Figure 44C)

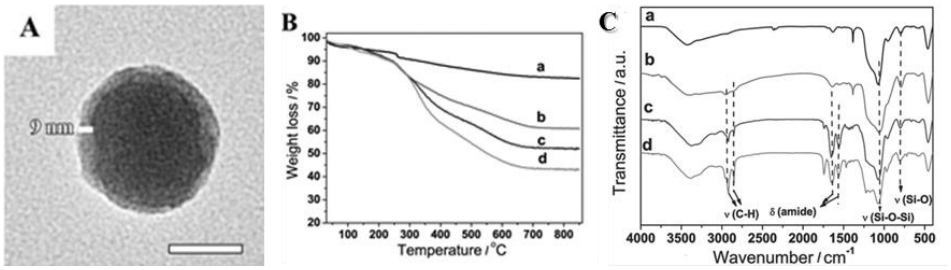

*Figure 44.**Confirmation of lipid bilayer coating on nanocarriers:** (A) Lipid bilayer tethered nanocomposites (MSN@tLB) sample stained with osmium tetroxide to show the presence of LB. Scale bar represents 50 nm. (B) TGA curves of and (C) FT-IR spectra of (a) MSN-NH2, (b) MSN-PEI, (c) MSN-PEI@DOPE, and (d) MSN-PEI@tLB. The peaks at 1650 cm^{-1} and 1560 cm^{-1} in FTIR spectrum for DOPE conjugated MSN-PEI can be ascribed to the vibrations of amide I and amide II from the conjugation between the primary amines of PEI and DOPE by DSC. The greatly enhanced bands at 2927 cm^{-1} and 2854 cm^{-1} correspond to the asymmetric and symmetric methylene stretching modes, respectively, from the alkyl tails of DOPE and DOPC. (PAPER IV)*

5.2.2. Drug loading and release experiments

5.2.2.1. Loading of calcein and zoledronic acid

Before the conjugation of the DOPE inner leaflet, hydrophilic guests, either calcein or ZOL, were loaded in to MSN-NH_2 and MSN-PEI particles. As the conjugation reaction was carried out in organic solvents, no escape of the hydrophilic cargos (calcein or ZOL) was observed in the tethering process due to their low solubility in these solvents. The use of hyperbranched PEI, which is positively charged in aqueous solutions below pH 10, allows for electrostatic adsorption of the negatively charged hydrophilic guest molecules onto the polyelectrolyte-grafted substrate. The saturated loading degree of calcein and ZOL for MSN-PEI was 42 wt% and 9 wt% with respect to particle weight, obtained by adsorption from MES buffer (pH 5.0). (Figure 45) Then, calcein or ZOL adsorption capacities were normalized to the total amount of accessible primary amines, which gave calcein/primary amine molar ratios of 0.46 and 0.099 for calcein and ZOL, respectively. The observed difference between loading capacity of calcein and ZOL might be due to the size as well as pKa of the molecules.

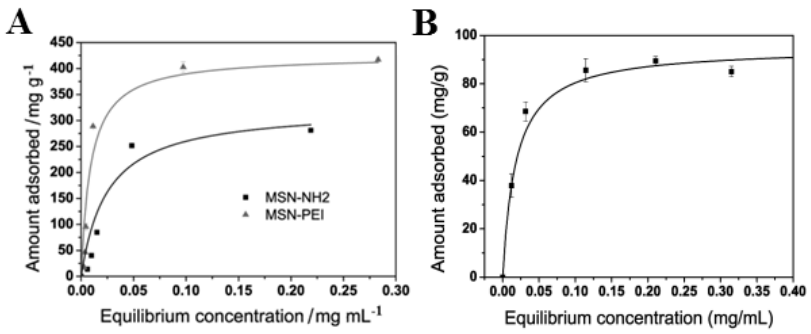

Figure 45. ***Evaluation of drug loading and release properties of the nanocarriers:*** *(A) Typical adsorption isotherms of calcein on MSN-NH_2 and MSN-PEI in MES buffer (pH 5) solution. The loading capacity is around 280 mg/g and 420 mg/g for MSN-NH_2 and MSN-PEI, respectively. (B) Typical adsorption isotherm of ZOL on MSN-PEI particles in MES buffer (pH 5) solution. The loading capacity calculated by the Langmuir model is 90 mg/g. (PAPER IV, V)*

5.2.2.2. Stability of lipid bilayer after drug loading and change in zeta potential as function of pH

The advantage of tethered lipid bilayer coating results from their ability to retain the hydrophilic guest molecules. In the absence of tLB gating, calcein and ZOL loaded in MSN-PEI was quickly replaced by anions in the release media, resulting in a complete premature release. The tLB approach encompasses generation of a closely packed outer leaflet of the LB with extended durability. Synthesis of tLB was done through dual solvent exchange method, by gradually changing the solvent from chloroform to DMSO to water, to generate a slow increase of solvent polarity for inducing the self-assembly. The volume ratio of water/DMSO was optimized to maximize the retention efficiency of hydrophilic drug and to testify the influence of solvent polarity on sealing efficiency of LB. By increasing the DMSO volume, the premature release of calcein was reduced dramatically by 77–100% compared to release from MSN-PEI without any lipid bilayer. (Figure 46A) Zero release was achieved by utilizing 95 vol% water in the self-assembly process, indicative of an intact LB and high enough sequestering of hydrophilic guests at this polarity. Additionally, after one week of incubation in phosphate buffer indicated that there was still quite low release (less than 10%), confirming their long-term stability. The presence of a membrane-disrupting agent, Triton X-100, in the release medium did not lead to rapid and continuous release of the loaded cargo and suggests enhanced durability of the tethered lipid bilayer. (Figure 46B) ZOL loaded tLB@MSNs also

showed very little premature release. (Figure 46C) Interactions of cationic polymers like PEI with lipid bilayers and live cell membranes can induce two basic types of membrane disruption, by hole-formation and thinning via the re-orientation of lipids or the removal of a layer of lipid from the lipid bilayers. However, these kinds of LB disruption require a close spatial proximity (<1 nm) between the headgroups of phospholipids and polymer. In the case of tLB, the local interaction between PEI and the inner leaflet of LB was scheduled by covalent conjugation, whereas the interaction between the head group of outer lipid with the charged amine groups of PEI has been separated by the thickness of LB. More importantly, it has been observed that the Coulombic repulsion between amino groups would make the PEI chains in the external surface adopt a rigid-like conformation and be pushed away toward the pore openings, which would also be beneficial for the PEI tethered lipid bilayer to span over the pore openings in the self-assembly process. The combination of these factors may lead tethered lipid bilayer in this strategy to produce more defect-free and durable packing.

Zeta potential measurements were performed to compare the surface properties of tLB@MSNs with different compositions, which may have implications for cellular uptake and intracellular trafficking and drug release. The LB coating shifted the isoelectric point (IEP) of MSN-PEI particles from 10.4 to approx. 7.5, 7.0 and 5.8 for DOTAP-, DOPC- and POPG-DOPE@MSNs, respectively. (Figure 46D) The inner PEI layer has influenced the charging of the whole particle by its strong ‘proton sponge’ ability. However, the outer surface of tLB@MSNs is composed of the lipids with high packing density, and thus difference in surface charge is most closely associated with outer lipid. The difference in the pH-dependent surface charging after LB tethering should be due to the long-range influence of the underlying PEI layer on the outer lipids. Monodispersity of all the lipid bilayer coated MSNs has been confirmed by hydrodynamic size measurement. (Figure 46E)

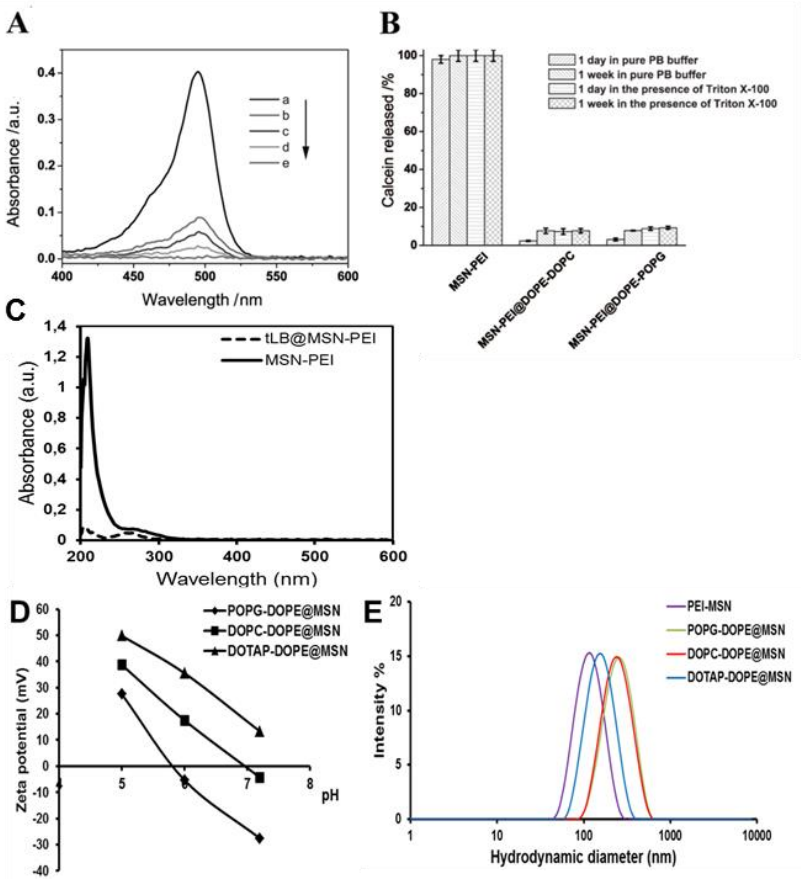

Figure 46. ***Characterization of nanocarriers:*** *(A) Absorption spectra of the release supernatant from calcein loaded (a) PEI-MSN and tLB@PEI-MSN particles prepared by using different volume fractions of water in the phase transfer step of the LB self-assembly process: (b) 0 vol%, (c) 80 vol%, (d) 90 vol%, and (e) 95 vol%. Calcein was loaded into MSNs at a loading degree of 90 μg/mg and the particles were incubated in 20 mM phosphate buffer (pH 7.4) at a concentration of 0.5 mg/ml. (B) Long term calcein release evaluated by the absorbance at 497 nm for the supernatant from different calcein loaded particles in PB buffer with or without Triton X-100 (a membrane disrupting agent) after different time periods. (C) UV-vis spectra of the release supernatant from the model bisphosphonate drug loaded PEI-MSN particles with/without the presence of lipid bilayer coating. (D) Plots of zeta potential changing as a function of pH for tLB@ PEI-MSN with different composition of the outer leaflet (E) Hydrodynamic diameter distributions of PEI-MSNs, and tLB@ PEI-MSN with different composition. (PAPER IV and V)*

5.2.3. Cellular interactions

In this section, the interaction of different lipid bilayer coated MSNs with cellular environment has been investigated.

5.2.3.1. Cytotoxicity assay

The cell viability in the presence of tLB@MSNs carriers have been confirmed by cell viability assay using HeLa cells, as they are most commonly used human cell lines. All the particles, PEI-MSN, DOPC-DOPE@MSN and POPG-DOPC@MSN demonstrated viability higher than 90% for HeLa cells at 10 μg/ml and 25 μg/ml concentrations. (Figure 47)

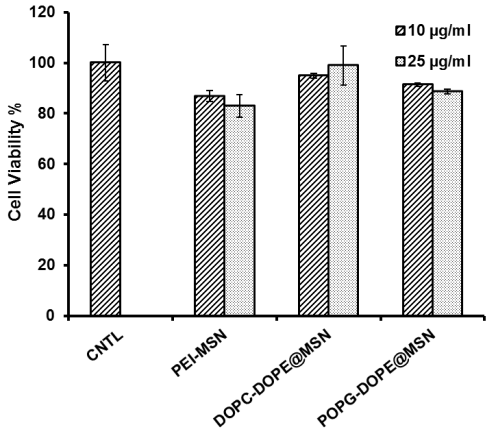

Figure 47. ***Lipid bilayer gated MSNs are not toxic to HeLa cells:*** *Cell viability assay after treating HeLa cells with Control (Vehicle), PEI-MSNs, DOPC-DOPE@MSN and POPG-DOPE@MSNs for 24 hours. Error bars represents ± SEM (n≥3) (PAPER IV)*

5.2.3.2. Cellular uptake and effect of outer leaflet of lipid coating on cargo release

The potential of tLB@MSN system to deliver hydrophilic guest molecules to cancer cells has been investigated by the degree of cellular internalization of hydrophilic cargo, calcein. Increase of PEI-MSNs concentration from 10 to 25 μg/ml did not lead to a significant enhancement of the mean fluorescence obtained from intracellular calcein in the HeLa cells. However, a significant particle-dose-dependent increase in the mean fluorescence intensity was found for both DOPC-DOPE@MSN and POPG-DOPC@MSNs. (Figure 48A) PEI-MSNs without any lipid bilayer coating does not protect the calcein release in cell media, and the calcein molecule itself is not able to permeate the cell membrane; hence very little or no enhancement in mean fluorescence intensity has been observed for PEI-MSN/calcein

compared to the control without any treatment. However, DOPC- and POPG-DOPE@MSNs both are efficient to transport calcein inside the cell. (Figure 48B)

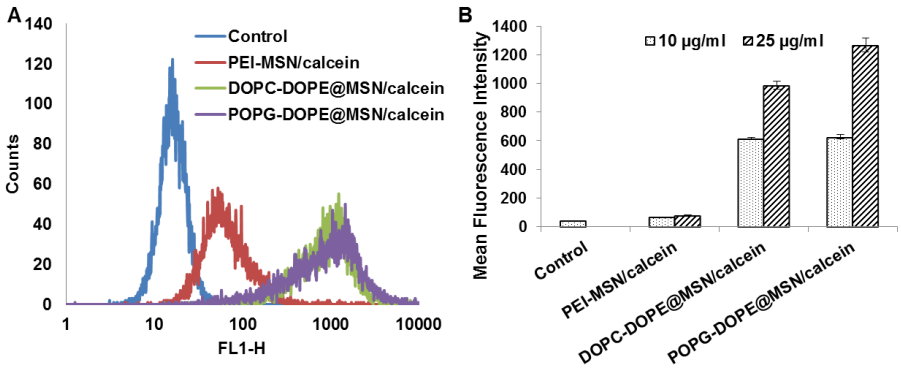

Figure 48. ***Lipid bilayer gated MSNs are efficiently internalized by HeLa cells:*** *(A) Determination of the mean fluorescence intensity of intracellular calcein from the flow cytometry of HeLa cells incubated with Vehicle alone (Control), PEI-MSN/calcein, DOPC-DOPE@MSN/calcein and POPG-DOPE@MSNs/calcein for 24 hours. (B) Flow cytometry histogram of HeLa cells after incubating with 10 µg/ml of PEI-MSNs or tLB@MSNs loaded with calcein for 24 hours. Error bars represents ± SEM (n≥3) (PAPER IV)*

MSNs loaded with calcein were incubated with HeLa cells at 10 µg/ml concentrations for 24 hours and the fluorescence of calcein recorded in the green channel with a confocal fluorescence microscope. No green signal has been visible for PEI-MSNs suggesting that most of the calcein might have been released already outside the cells prior to the cellular uptake of particles. (Figure 49a-c) LB tethered particles produced a significantly strong fluorescence signal inside the cells, suggesting improved calcein retention before and during the cellular internalization of the carrier particles. For the POPG- and DOTAP-DOPE@PEI-MSNs mostly co-localization of red signal from MSNs (TRITC-labelled, Tetramethylrhodamine-5-isothiocyanate) and green signal from calcein (visible as yellow signal) has been observed after 24 hours, whereas for DOPC-DOPE@PEI-MSNs some amount of calcein release from the MSNs (only green signal) has been observed mainly from the cytoplasm, suggesting it can provide endosomal escape and eventual delivery of the cargo to the cytoplasm. (Figure 49d-l) DOTAP has been used as fusogenic lipid in a liposomal preparation; however, in this system calcein release has not been observed from the DOTAP-DOPE@PEI-MSNs even after 72 hours [Data not shown].

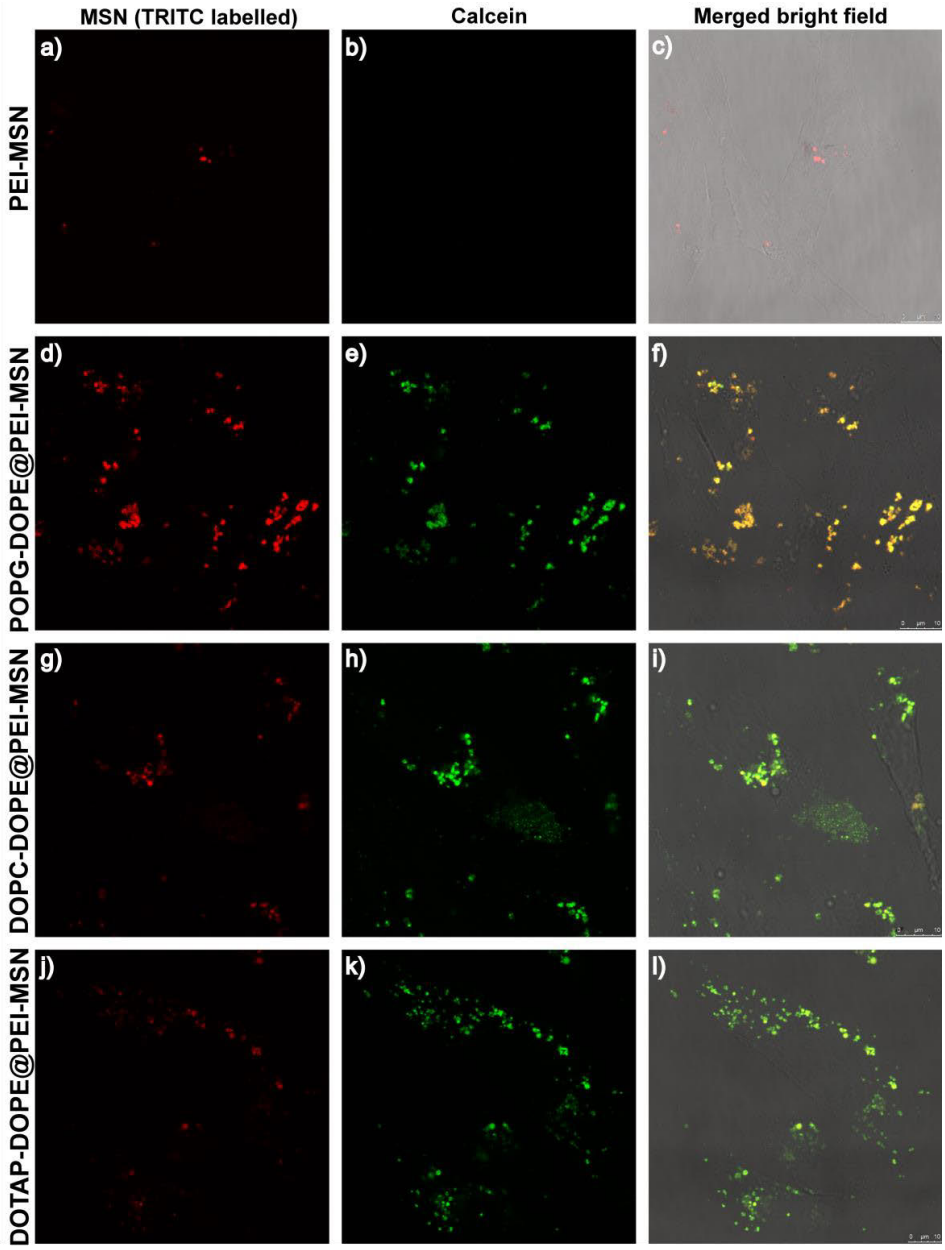

Figure 49. ***Lipid bilayer coated MSNs efficiently deliver cargo intracellularly:*** *Confocal fluorescence microscopy images of HeLa cells incubated with calcein-loaded PEI-MSNs (a-c), POPG-DOPE@PEI-MSN (b-f), DOPC-DOPE@PEI-MSNs g-i), and DOTAP-DOPE@PEI-MSNs (J-L) for 24 hours. Red channel shows MSNs (labelled with TRITC), green shows the presence of calcein and merged channel with bright field. (PAPER V)*

5.2.3.3. Influence of outer leaflet of lipid coating on the route of uptake

The influence of lipid bilayer coating and surface charge of the lipid from the outer leaflet of a lipid bilayer on the route of cellular uptake has been evaluated by measuring cellular internalization in the presence of different cellular uptake inhibitors. For the PEI-MSNs, as observed before for large approx. 250-300 nm MSNs, the cellular uptake was inhibited by phenylarsine oxide, which is the inhibitor of clathrin-mediated endocytosis. (Figure 50) However, when inhibited by both genistein and phenylarsine oxide cellular uptake has been slightly increased, which might be due to activation of other internalization pathways.

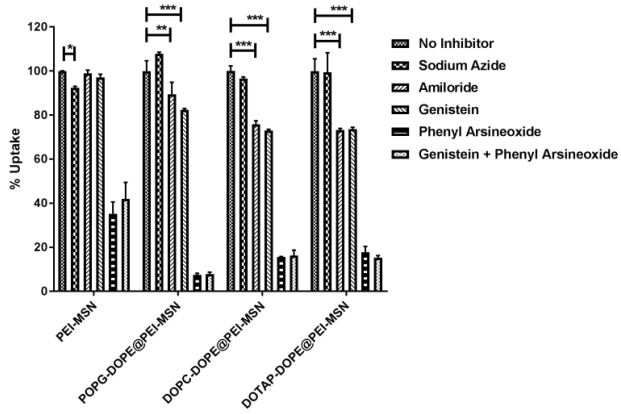

Figure 50. ***Surface coating influence the route of internalization:*** *The effects of various cellular uptake inhibitors on internalization of tLB@MSNs in MDA-MB-231cells. Cellular uptake of PEI-MSNs and different lipid bilayer coated MSNs after co-treatment with Sodium azide, Amiloride, Genistein, Phenyl arsine oxide and Genistein + Phenyl arsine oxide. Error bar represents ± SEM. (n≥3) *P<0.05, **P<0.01and ***P<0.001.(PAPER V)*

For all three lipid bilayer coated MSNs, the statistical significant uptake inhibition has been observed in the presence of amiloride and genistein, which are inhibitors of macropinocytosis and caveolae-mediated endocytosis, respectively. The cellular internalization has also been inhibited significantly by the presence of phenylarsine oxide alone and by the combination of genistein and phenylarsine oxide at the same extent. The discrepancy between different outer lipids of lipid bilayer is not evident, however, a clear difference between the route of uptake of PEI-MSNs and tLB@MSNs has been observed. In the literature, it has also been reported that lipid nanoparticles have high affinity for the lipid bilayer of the cells and they can be targeted to cholesterol rich caveolae domains on the cell surface, hence inhibition of caveolae-mediated endocytosis has shown significant inhibition in percentage cellular uptake for lipid

bilayer coated MSNs.[140] These results suggest that surface coating and surface properties such as hydrophobicity has a significant effect on the route of cellular internalization and further intracellular routing.

5.2.3.4. Evaluation of in vitro efficacy of the drug loaded lipid bilayer coated MSNs in breast cancer cells

The drug delivery competence of the ZOL loaded nanoparticles was evaluated using WST-1 assay and Incucyte™ instrument using toll-like receptor (TLR 9) transfected MDA-MB-231 breast cancer cells, as they are more sensitive to the ZOL treatment.[212] For the WST-1 assay, empty MSNs with different lipid bilayer coating, free ZOL and ZOL loaded MSNs at concentrations equivalent to 1, 10 and 20 μM of free ZOL were incubated with MDA-MB-231 TLR9 transfected cells for 72 and 96 hours. At the end of the incubation period, cytotoxicity of samples was evaluated by employing WST-1 reagent. The obtained results indicate that indeed the ZOL loaded MSNs are effective to induce cytotoxicity in breast cancer cells. (Figure 51) Although, at lower concentrations there is no difference between the effect of free ZOL and ZOL loaded MSNs, a clear difference between the toxicity of free ZOL and ZOL loaded lipid bilayer coated MSNs has been observed at higher concentrations. To further confirm the influence of drug loaded MSNs on cell viability Incucyte™ live cell imaging was performed. Cell growth was followed for one week after incubation with empty and ZOL loaded DOPC-DOPE@PEI-MSNs at concentrations equivalent to 1 and 10 μM of free ZOL. These results further approve efficient drug release and effectiveness of ZOL loaded MSNs on the reduction of cancer cells growth. (PAPER V)

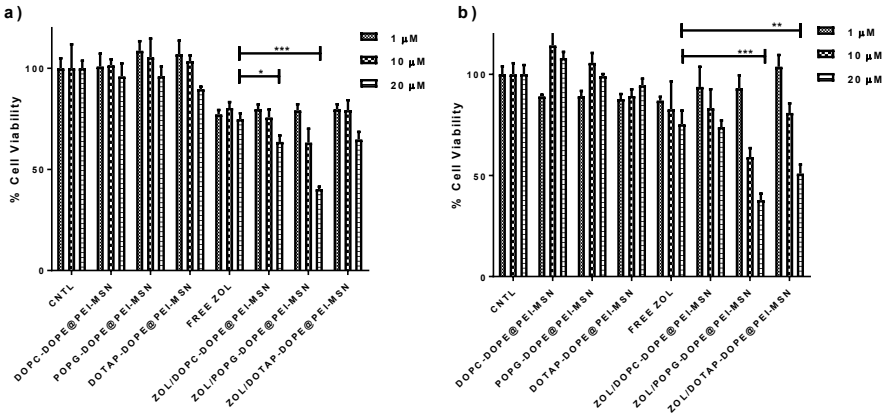

Figure 51. ***ZOL loaded lipid bilayer coated MSNs produce cytotoxic effect:*** *The effect of ZOL loaded MSNs on MDA-MB-231 TLR9 siRNA cells. The cytotoxicity of ZOL/tLB@MSNs has*

*been evaluated after (a) 72 and (b) 96 hours incubation with MDA-MB-231 cells at different concentrations using the WST-1 assay. Error bars represent ± SD (n≥ 3) *P<0.05, **P<0.01and ***P<0.001 (PAPER V)*

5.2.4. *In vivo* delivery and safety studies

After successful *in vitro* studies, the selected particle was further applied *in vivo* to confirm its functionality and safety in more clinically relevant environment.

5.2.4.1. *In vivo delivery of the drug loaded lipid bilayer coated MSNs*

To evaluate the efficiency of FA-DOPC-DOPE@PEI-MSNs to deliver ZOL *in vivo*, ZOL/FA-DOPC-DOPE@PEI-MSNs at two different concentrations were intravenously injected to mice xenografted with MDA-MB-231 tumor cells. Mice were randomly distributed into three different groups and each group consisted of 8 mice. The mice were injected one week after the tumor cells' inoculation, with vehicle alone:group 1, low dose ZOL/FA-DOPC-DOPE@PEI-MSNs:group 2 and high dose:group 3, three times a week for three weeks. Tumor growth was monitored for four weeks, at the end of the experiment mice were sacrificed by CO_2 inhalation and cervical dislocation; further tumor and liver samples were collected for histology. Tumor volumes were calculated using the formula $V = (\pi/6)(d_1 \times d_2)^{3/2}$, where d_1 and d_2 are the perpendicular tumor diameters. It has been observed that the tumor grew normally for mice injected with vehicle alone, whereas the tumor growth very marginally reduced for low dose ZOL loaded FA-DOPC-DOPE@PEI-MSNs and a statistically significant reduction in tumor growth has been observed for high dose ZOL loaded FA-DOPC-DOPE@PEI-MSNs. (Figure 52) In conclusion, it has been observed that ZOL loaded FA-DOPC-DOPE@PEI-MSNs were able to suppress tumor growth.

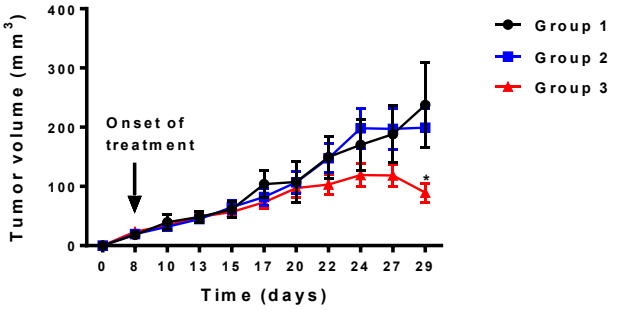

*Figure 52. **ZOL loaded lipid bilayer coated MSNs suppress tumor growth:** Tumor size reduction followed for four weeks. Group 1:vehicle control, group 2:ZOL/FA-DOPC-*

*DOPE@PEI-MSNs (0.1 mg/kg free ZOL) and group3: ZOL/FA-DOPC-DOPE@PEI-MSNs (0.3 mg/kg free ZOL). *P<0.05 (PAPER V)*

5.2.4.2. *Safety evaluation of lipid bilayer coated MSNs after in vivo administration*

Since nanoparticles are typically prone to accumulate in liver and spleen after clearance from the circulation, the liver samples were collected from the mice injected with control, low and high dose ZOL loaded particles. The particles have not shown any necrotic effect on the liver. (Figure 53) Hence, the effects induced by ZOL loaded FA-DOPC-DOPE@PEI-MSNs were specifically observed in tumor tissues and were not observed in normal livers of the treated animals, indicating that the developed system can be used for *in vivo* drug delivery.

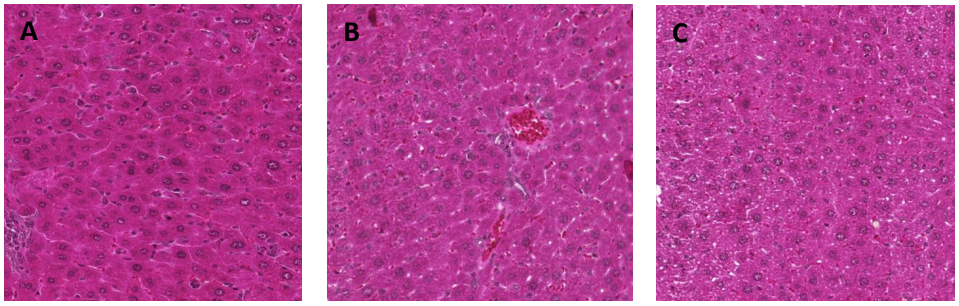

Figure 53. ***ZOL loaded lipid bilayer coated MSNs are not toxic to liver cells:*** *Hematoxylin eosin staining of the liver sections of (A) vehicle control, (B) low dose ZOL-loaded DOPC-DOPE@PEI-MSNs and (C) high dose ZOL-loaded DOPC-DOPE@PEI-MSNs after intravenous administration showing no necrosis effect on the liver. (PAPER V)*

6. Conclusions and future outlook

In this dissertation, different surface functionalization strategies on MSNs employing different polymers and lipids were utilized to fabricate advanced drug delivery nanocarriers for hydrophobic and hydrophilic drugs, in order to improve the efficacy of poorly aqueous soluble drugs and to achieve sustained or triggered drug release. In addition, the potential of MSNs as drug delivery carriers via the oral route of administration was evaluated. The applicability of MSNs for cancer therapy was assessed *in vitro* and *in vivo*.

Modification of the surface characteristics of MSNs possesses great impact on the fate of particles in physiological environment. Adequate surface functionalization as well as surface charge provide colloidal stability, and reduce protein adsorption on the particle surface, which determines the particles' interaction with RES. In this study, it has been observed that application of the zwitterionic coating on the MSN surface diminishes protein adsorption on the particle surface. (PAPER I) Further, hydrophobic cargo has been loaded to the different functionalized MSNs and loading degrees up to 70 w/w% can be achieved, however, surface modification did not influence the loading efficiency when drug loading has been performed using non-ideal organic solvent conditions. In addition, surface coating with PEI layer serves as a 'molecular gate' and prevents drug release extracellularly; moreover, efficient intracellular drug release was subsequently achieved. (PAPER II)

MSNs' properties can also be exploited for diagnostic applications, for example, fluorescence imaging. The variation in fluorescence properties of fluorescent molecules upon incorporation into MSNs has not been devoted as proper attention in the literature as it should deserve. The effect of surface properties and different loading degrees on the fluorescent properties of fluorescent cargo molecules was studied in this thesis. The surface properties, the environment to which the fluorophore has been exposed due to their incorporation in MSN matrices, were determined to be the most critical parameter influencing the spectral behavior of fluorophore. (PAPER I, Supp Paper 3)

Further, defect free and highly durable lipid bilayer coating on MSNs' surface intended for the delivery of hydrophilic guest molecules was successfully produced, which successfully hindered drug leakage in physiological conditions. However, efficient drug/cargo release was achieved intracellularly, whereby the cytoplasmic release depended on the composition (net surface charge) of the lipid bilayer. (PAPER IV)

In additional to surface modification with different polymers, a small-molecular targeting moiety (glucose or folic acid) was successfully conjugated onto the particle surface, which provided better therapeutic efficacy and fewer side effects of drug loaded MSN nanocarriers towards cancer cells. (PAPER II,III)

For delivery of hydrophilic anticancer drugs, lipid bilayer gated MSNs with DOPC lipid as an outer leaflet have provided efficient anticancer activity. The covalently coupled lipid bilayer coated nanocarriers provided good retention of the drug molecules and enabled them to be delivered to the cancer cells, and no hepatic toxicity has been observed. (PAPER V)

For the oral administration, out of the different surface modifications explored, PEGylation in combination with PEI as the particle surface coating is superior to enhance the internalization of MSNs to intestinal epithelial cells. Additionally, MSNs were also able to be exocytosed after internalization, showing that they can transport across the Caco-2 monolayer without disturbing its integrity. The carrier MSNs are capable of protecting the loaded drug after exposure to the harsh conditions of the stomach and the intestine. The MSNs mediated drug delivery *in vivo* provided a significant therapeutic benefit after oral administration compared to an administered free drug. (PAPER III)

In conclusion, the developed hybrid systems in this thesis represent a novel contribution to the field of drug delivery employing MSNs as a versatile drug delivery platform. The results presented in the thesis are assumed to provide importance of surface modification needed according to the properties of cargo molecule and appropriate evaluation of biophysicochemical interactions of nanocarriers for their future drug delivery applications. This knowledge facilitates preparation of nanocarriers with desired properties, and can be utilized further to prepare multidrug carrying nanoparticles for therapy of drug resistant cancer. For example, different hydrophobic molecules can be loaded in MSNs while hydrophilic therapeutic molecules can be conjugated on the surface, which can act as a targeting ligand simultaneously.

Many aspects of the MSN mediated drug delivery still remain to be studied in future. The safety of the developed nanoformulations in systemic administration needs to be verified by thorough animal experiments. In addition to nanoparticle-tumor interactions, in-depth knowledge is required concerning how the materials behave in healthy tissues particularly the liver, spleen, and kidney, which are main factors affecting the ability of nanopharmaceuticals to circulate in the bloodstream. Further, evaluation of oral drug delivery efficiency of MSNs needs to be done using a proper disease model such as Crohn's disease or ulcerative colitis.

In addition, more detailed knowledge is required regarding the transport of MSNs, to explore whether alternative routes, in which particles travel through instead of around endothelial cells lining the blood vessels, exist for reaching the tumor. Further information is needed regarding how nanoparticles leave tumor vessels, their extravasation and how they then interact with tumor tissues. How does particle design affect the penetration depth of these particles into tumor tissues? These obstacles due to non-uniform extravasation in the tumor interstitium are needed to be overcome for improved drug delivery by nanomedicines. For example, nanoparticles can be developed which are capable of lowering interstitial fluid pressure or modifying tumor vasculature together with carrying potent anticancer agents. Many other hurdles are to be overcome before MSNs could reach clinical use, such as scaling up the synthesis of the particles to meet Good Manufacturing Practice (GMP) and cost of the formulation. However, cancer is still the leading cause of death after heart diseases, and treatment of this condition requires improvements in efficacy, safety, and patient comfort, and thus, a smart drug delivery system is the need of current time.

7. Acknowledgements

The present work was carried out at the Laboratory of Pharmaceutical Sciences and at the Laboratory of Physical Chemistry, Åbo Akademi University, Turku, Finland.

First and foremost, I would like to express my deepest respect and profound gratitude to my supervisor Professor Jessica M. Rosenholm for the invaluable advice, support, inspiring guidance, and positive attitude during working with my thesis.

I would like to thank Professor Niklas Sandler for providing me an opportunity to finalize my thesis at the Department of Pharmaceutical Sciences. I am honored to have Professor Jörg Huwyler from Department of Pharmaceutical Sciences, University of Basel, Switzerland and Professor Vesa-Pekka Lehto from the Department of Applied Physics, University of Eastern Finland, Finland as reviewers of this thesis.

I would also like to express my gratitude to Dr. Diana Toivola for providing me the opportunity to work in her lab and for her useful inputs. Furthermore, I would also like to thank Prof. Cecilia Sahlgren, Dr. Johanna Tuomela and Dr. Jouko Sandholm for the collaboration. I would like to express my most sincere gratitude to all my colleagues and friends Didem, Tina, Helene, Neeraj, Ezgi, Jixi, Eva and Eudald (BionanoMaterials group), for their friendship, and for sharing with me the best and the worst of these years, always cheering me up, and for creating a positive atmosphere. I also like to thank the Toivola lab members Julia, Iris, Joel and Nadeem for their invaluable support. I would like to express my gratitude to Erik Niemelä, for all the discussions and collaboration during these years.

Many thanks to all the personnel at the Laboratory of Pharmaceutical Sciences and Laboratory of Physical Chemistry, Åbo Akademi University, for their support and most of all creating a cheerful working environment.

I am grateful for the financial support of the CIMO Finland Fellowship, Otto A. Malm Foundation, Erasmus Mundus Fellowship, Akademi of Finland project#260599, Finnish Cultural Foundation, and Jane-Aatos Erkko foundation.

I would like to express my everlasting gratitude to my fiancé Nisarg, for his unflagging love and support.

Finally, I would like to dedicate this work to my parents (મમ્મી-પપ્પા) and grandparents (બા-બાપા) to whom I owe my deepest gratitude for their love and unconditional support with every decision I have made, always encouraging me to pursue my dreams; and to my little sister (Payal) for lighting up my life and for her positive wishes.

Diti Desai

Åbo, 2016

8. References

[1] Theresa M. Allen and Pieter R. Cullis, 'Drug Delivery Systems: Entering the Mainstream', *Science (New York, N.Y.)* **303** (2004): 1818–22.

[2] Volker Wagner, Anwyn Dullaart, Anne-Katrin Bock, and Axel Zweck, 'The Emerging Nanomedicine Landscape', *Nature Biotechnology* **24** (2006): 1211–17.

[3] Kristina Riehemann, Stefan W. Schneider, Thomas A. Luger, Biana Godin, Mauro Ferrari, and Harald Fuchs, 'Nanomedicine--Challenge and Perspectives', *Angewandte Chemie (International Ed. in English)* **48** (2009): 872–97.

[4] Wendy R. Sanhai, Jason H. Sakamoto, Richard Canady, and Mauro Ferrari, 'Seven Challenges for Nanomedicine', *Nature Nanotechnology* **3** (2008): 242–44.

[5] Spomenka Simovic, Nasrin Ghouchi-Eskandar, Aw Moom Sinn, Dusan Losic, and Clive A. Prestidge, 'Silica Materials in Drug Delivery Applications', *Current Drug Discovery Technologies* **8** (2011): 269–76.

[6] Lewis & Harrison, LLC, 'Generally Recognized As Safe Determination For Silicon Dioxide When Added Directly And/Or Indirectly To Human Food', 2010, http://www.fda.gov/ucm/groups/fdagov-public/@fdagov-foods-gen/documents/document/ucm269494.pdf.

[7] Miriam Benezra, Oula Penate-Medina, Pat B. Zanzonico, David Schaer, Hooisweng Ow, Andrew Burns, Elisa DeStanchina, Valerie Longo, Erik Herz, Srikant Iyer, Jedd Wolchok, Steven M. Larson, Ulrich Wiesner, and Michelle S. Bradbury, 'Multimodal Silica Nanoparticles Are Effective Cancer-Targeted Probes in a Model of Human Melanoma', *Journal of Clinical Investigation* **121** (2011): 2768–80.

[8] Daniel Arcos and María Vallet-Regí, 'Bioceramics for Drug Delivery', *Acta Materialia*, The Diamond Jubilee IssueMaterials Challenges in Tomorrow's World Selected Topics in Materials Science and Engineering, **61** (2013): 890–911.

[9] Alina Maria Holban and Alexandru Mihai Grumezescu, *Nanoarchitectonics for Smart Delivery and Drug Targeting* (William Andrew, 2016).

[10] Elena Aznar, Mar Oroval, Lluís Pascual, Jose Ramón Murguía, Ramón Martínez-Máñez, and Félix Sancenón, 'Gated Materials for On-Command Release of Guest Molecules', *Chemical Reviews* **116** (2016): 561–718.

[11] R. Seigneuric, L. Markey, D. S. A. Nuyten, C. Dubernet, C. T. A. Evelo, E. Finot, and C. Garrido, 'From Nanotechnology to Nanomedicine: Applications to Cancer Research', *Current Molecular Medicine* **10** (2010): 640–52.

[12] Pilar Rivera Gil, Dominik Hühn, Loretta L. del Mercato, Daniel Sasse, and Wolfgang J. Parak, 'Nanopharmacy: Inorganic Nanoscale Devices as Vectors and Active Compounds', *Pharmacological Research* **62** (2010): 115–25.

[13]Mortality-European commission, http://ec.europa.eu/health/major_chronic_diseases/mortality/ index_en.htm accessed 25 August 2016.

[14] Andreas Wicki, Dominik Witzigmann, Vimalkumar Balasubramanian, and Jörg Huwyler, 'Nanomedicine in Cancer Therapy: Challenges, Opportunities, and Clinical Applications', *Journal of Controlled Release* **200** (2015): 138–57.

[15] Kewal K. Jain, *The Handbook of Nanomedicine* (Springer Science & Business Media, 2012).

[16] 'Home - ClinicalTrials.gov', accessed 16 August 2016, https://clinicaltrials.gov/.

[17] Zhen Guo and Li Tan, *Fundamentals and Applications of Nanomaterials* (Artech House, 2009).

[18] Xiaohua J. Huang, *Nanotechnology Research: New Nanostructures, Nanotubes and Nanofibers* (Nova Publishers, 2008).

[19] 'Bottom-up Methods for Making Nanotechnology Products', *AZoNano.com*, 2004, http://www.azonano.com/article.aspx?ArticleID=1079.

[20] C. Jeffrey Brinker and George W. Scherer, *Sol-Gel Science: The Physics and Chemistry of Sol-Gel Processing*, 1 edition (Boston: Academic Press, 1990).

[21] Bo Jönsson, Björn Lindman, Krister Holmberg, and Bengt Kronberg, *Surfactants and Polymers in Aqueous Solution* (Wiley, 2000).

[22] Qiannan Liu, Ziqi Sun, Yuhai Dou, Jung Ho Kim, and Shi Xue Dou, 'Two-Step Self-Assembly of Hierarchically-Ordered Nanostructures', *Journal of Materials Chemistry A* **3** (2015): 11688–99.

[23] C. T. Kresge, M. E. Leonowicz, W. J. Roth, J. C. Vartuli, and J. S. Beck, 'Ordered Mesoporous Molecular Sieves Synthesized by a Liquid-Crystal Template Mechanism', *Nature* **359** (1992): 710–12.
[24] J. S. Beck, J. C. Vartuli, W. J. Roth, M. E. Leonowicz, C. T. Kresge, K. D. Schmitt, C. T. W. Chu, D. H. Olson, and E. W. Sheppard, 'A New Family of Mesoporous Molecular Sieves Prepared with Liquid Crystal Templates', *Journal of the American Chemical Society* **114** (1992): 10834–43.
[25] Frank Hoffmann, Maximilian Cornelius, Jürgen Morell, and Michael Fröba, 'Silica-Based Mesoporous Organic-Inorganic Hybrid Materials', *Angewandte Chemie (International Ed. in English)* **45** (2006): 3216–51.
[26] Ying Wan and Zhao, 'On the Controllable Soft-Templating Approach to Mesoporous Silicates', *Chemical Reviews* **107** (2007): 2821–60.
[27] Paul Ducheyne, Kevin Healy, Dietmar E. Hutmacher, David W. Grainger, and C. James Kirkpatrick, *Comprehensive Biomaterials* (Newnes, 2015).
[28] Kai Schumacher, Peter I. Ravikovitch, Alexander Du Chesne, Alexander V. Neimark, and Klaus K. Unger, 'Characterization of MCM-48 Materials', *Langmuir* **16** (2000): 48.
[29] María Vallet-Regí and Daniel Arcos Navarette, *Nanoceramics in Clinical Use: From Materials to Applications 2nd Edition* (Royal Society of Chemistry, 2015).
[30] Dharitri Rath, Surjyakanta Rana, and K. M. Parida, 'Organic Amine-Functionalized Silica-Based Mesoporous Materials: An Update of Syntheses and Catalytic Applications', *RSC Advances* **4** (2014): 57111–24.
[31] Fang Lu, Si-Han Wu, Yann Hung, and Chung-Yuan Mou, 'Size Effect on Cell Uptake in Well-Suspended, Uniform Mesoporous Silica Nanoparticles', *Small* **5** (2009): 1408–13.
[32] Robert I. Nooney, Dhanasekaran Thirunavukkarasu, Yimei Chen, Robert Josephs, and Agnes E. Ostafin, 'Synthesis of Nanoscale Mesoporous Silica Spheres with Controlled Particle Size', *Chemistry of Materials* **14** (2002): 4721–28.
[33] Si-Han Wu, Chung-Yuan Mou, and Hong-Ping Lin, 'Synthesis of Mesoporous Silica Nanoparticles', *Chemical Society Reviews* **42** (2013): 3862–75.
[34] C. E. Fowler, D. Khushalani, B. Lebeau, and S. Mann, 'Nanoscale Materials with Mesostructured Interiors', *Advanced Materials* **13** (2001): 649–52.
[35] A. Galarneau, J. Iapichella, K. Bonhomme, F. Di Renzo, P. Kooyman, O. Terasaki, and F. Fajula, 'Controlling the Morphology of Mesostructured Silicas by Pseudomorphic Transformation: A Route Towards Applications', *Advanced Functional Materials* **16** (2006): 1657–67.
[36] Shengpu Ma, Yanqin Wang, and Yingchun Zhu, 'A Simple Room Temperature Synthesis of Mesoporous Silica Nanoparticles for Drug Storage and Pressure Pulsed Delivery', *Journal of Porous Materials* **18** (2010): 233–39.
[37] D. Maldonado, N. Tanchoux, P. Trens, A. Galarneau, E. Garrone, F. Di Renzo, and F. Fajula, 'Condensation Enthalpies of N-Hexane in Micelle-Templated Mesoporous Silicas', *Journal of Porous Materials* **14** (2007): 279–84.
[38] Antonio B. Fuertes, Patricia Valle-Vigón, and Marta Sevilla, 'Synthesis of Colloidal Silica Nanoparticles of a Tunable Mesopore Size and Their Application to the Adsorption of Biomolecules', *Journal of Colloid and Interface Science* **349** (2010): 173–80.
[39] Michal Kruk, Mietek Jaroniec, and Abdelhamid Sayari, 'New Insights into Pore-Size Expansion of Mesoporous Silicates Using Long-Chain Amines', *Microporous and Mesoporous Materials* **35–36** (2000): 545–53.
[40] Gerhard Ertl, H. Knözinger, and Jens Weitkamp, *Handbook of Heterogeneous Catalysis* (Wiley-VCH, 1997).
[41] S. Kawi and M. W. Lai, 'Supercritical Fluid Extraction of Surfactant from Si-MCM-41', *AIChE Journal* **48** (2002): 1572–80.
[42] S. Hitz and R. Prins, 'Influence of Template Extraction on Structure, Activity, and Stability of MCM-41 Catalysts', *Journal of Catalysis* **168** (1997): 194–206.
[43] A. Stein, B. J. Melde, and R. C. Schroden, 'Hybrid Inorganic–Organic Mesoporous Silicates—Nanoscopic Reactors Coming of Age', *Advanced Materials* **12** (2000): 1403–19.
[44] S. Angelos, E. Johansson, J. F. Stoddart, and J. I. Zink, 'Mesostructured Silica Supports for Functional Materials and Molecular Machines', *Advanced Functional Materials* **17** (2007): 2261–71.

[45] Supratim Giri, Brian G. Trewyn, Michael P. Stellmaker, and Victor S.-Y. Lin, 'Stimuli-Responsive Controlled-Release Delivery System Based on Mesoporous Silica Nanorods Capped with Magnetic Nanoparticles', *Angewandte Chemie* **117** (2005): 5166–72.

[46] Fei Fei Fang, Hyoung Jin Choi, and Wha Seung Ahn, 'Electroactive Response of Mesoporous Silica and Its Nanocomposites with Conducting Polymers', *Composites Science and Technology*, Smart Composites and Nanocomposites Special Issue with Regular Papaers, **69** (2009): 2088–92.

[47] Chang Ok Kim, Sung Ju Cho, and Joon Won Park, 'Hyperbranching Polymerization of Aziridine on Silica Solid Substrates Leading to a Surface of Highly Dense Reactive Amine Groups', *Journal of Colloid and Interface Science* **260** (2003): 374–78.

[48] Dominik Brühwiler, 'Postsynthetic Functionalization of Mesoporous Silica', *Nanoscale* **2** (2010): 887.

[49] Greg T. Hermanson, *Bioconjugate Techniques* (Academic Press, 2013).

[50] X. S. Zhao and G. Q. Lu, 'Modification of MCM-41 by Surface Silylation with Trimethylchlorosilane and Adsorption Study', *The Journal of Physical Chemistry B* **102** (1998): 1556–61.

[51] Myong H. Lim and Andreas Stein, 'Comparative Studies of Grafting and Direct Syntheses of Inorganic−Organic Hybrid Mesoporous Materials', *Chemistry of Materials* **11** (1999): 3285–95.

[52] Krishna K. Sharma, Abhishek Anan, Robert P. Buckley, Wayne Ouellette, and Tewodros Asefa, 'Toward Efficient Nanoporous Catalysts: Controlling Site-Isolation and Concentration of Grafted Catalytic Sites on Nanoporous Materials with Solvents and Colorimetric Elucidation of Their Site-Isolation', *Journal of the American Chemical Society* **130** (2008): 218–28.

[53] Neil Ayres, Stephen G. Boyes, and William J. Brittain, 'Stimuli-Responsive Polyelectrolyte Polymer Brushes Prepared via Atom-Transfer Radical Polymerization', *Langmuir: The ACS Journal of Surfaces and Colloids* **23** (2007): 182–89.

[54] Roxana-Viorela Ostaci, Denis Damiron, Simona Capponi, Guillaume Vignaud, Liliane Léger, Yves Grohens, and Eric Drockenmuller, 'Polymer Brushes Grafted To "passivated" silicon Substrates Using Click Chemistry', *Langmuir: The ACS Journal of Surfaces and Colloids* **24** (2008): 2732–39.

[55] Jessica M. Rosenholm, Annika Meinander, Emilia Peuhu, Rasmus Niemi, John E. Eriksson, Cecilia Sahlgren, and Mika Lindén, 'Targeting of Porous Hybrid Silica Nanoparticles to Cancer Cells', *ACS Nano* **3** (2008): 197–206.

[56] W. T. Godbey, K. K. Wu, and A. G. Mikos, 'Size Matters: Molecular Weight Affects the Efficiency of Poly(ethylenimine) as a Gene Delivery Vehicle', *Journal of Biomedical Materials Research* **45** (1999): 268–75.

[57] Arkadi Zintchenko, Alexander Philipp, Ali Dehshahri, and Ernst Wagner, 'Simple Modifications of Branched PEI Lead to Highly Efficient siRNA Carriers with Low Toxicity', *Bioconjugate Chemistry* **19** (2008): 1448–55.

[58] Thomas Merdan, Klaus Kunath, Holger Petersen, Udo Bakowsky, Karl Heinz Voigt, Jindrich Kopecek, and Thomas Kissel, 'PEGylation of Poly(ethylene Imine) Affects Stability of Complexes with Plasmid DNA under in Vivo Conditions in a Dose-Dependent Manner after Intravenous Injection into Mice', *Bioconjugate Chemistry* **16** (2005): 785–92.

[59] Jessica M. Rosenholm, Alain Duchanoy, and Mika Lindén, 'Hyperbranching Surface Polymerization as a Tool for Preferential Functionalization of the Outer Surface of Mesoporous Silica†', *Chemistry of Materials* **20** (2008): 1126–33.

[60] J. Milton Harris and Robert B. Chess, 'Effect of Pegylation on Pharmaceuticals', *Nature Reviews. Drug Discovery* **2** (2003): 214–21.

[61] Donald E. Owens and Nicholas A. Peppas, 'Opsonization, Biodistribution, and Pharmacokinetics of Polymeric Nanoparticles', *International Journal of Pharmaceutics* **307** (2006): 93–102.

[62] Y. Huang, W. Leobandung, A. Foss, and N. A. Peppas, 'Molecular Aspects of Muco- and Bioadhesion: Tethered Structures and Site-Specific Surfaces', *Journal of Controlled Release: Official Journal of the Controlled Release Society* **65** (2000): 63–71.

[63] Alejandro Baeza, Montserrat Colilla, and María Vallet-Regí, 'Advances in Mesoporous Silica Nanoparticles for Targeted Stimuli-Responsive Drug Delivery', *Expert Opinion on Drug Delivery* **12** (2015): 319–37.

[64] Simona Mura, Julien Nicolas, and Patrick Couvreur, 'Stimuli-Responsive Nanocarriers for Drug Delivery', *Nature Materials* **12** (2013): 991–1003.

[65] Zhengyang Zhou, Shenmin Zhu, and Di Zhang, 'Grafting of Thermo-Responsive Polymer inside Mesoporous Silica with Large Pore Size Using ATRP and Investigation of Its Use in Drug Release', *Journal of Materials Chemistry* **17** (2007): 2428–33.

[66] Nawal Kishor Mal, Masahiro Fujiwara, and Yuko Tanaka, 'Photocontrolled Reversible Release of Guest Molecules from Coumarin-Modified Mesoporous Silica', *Nature* **421** (2003): 350–53.

[67] Wei Guo, Chunyu Yang, Huiming Lin, and Fengyu Qu, 'P(EO-Co-LLA) Functionalized Fe3O4@mSiO2 Nanocomposites for Thermo/pH Responsive Drug Controlled Release and Hyperthermia', *Dalton Transactions (Cambridge, England: 2003)* **43** (2014): 18056–65.

[68] Weiwei Gao, Juliana M. Chan, and Omid C. Farokhzad, 'pH-Responsive Nanoparticles for Drug Delivery', *Molecular Pharmaceutics* **7** (2010): 1913–20.

[69] Xuejuan Wan, Di Wang, and Shiyong Liu, 'Fluorescent pH-Sensing Organic/Inorganic Hybrid Mesoporous Silica Nanoparticles with Tunable Redox-Responsive Release Capability', *Langmuir* **26** (2010): 15574–79.

[70] Andrea Bernardos, Elena Aznar, María Dolores Marcos, Ramón Martínez-Máñez, Félix Sancenón, Juan Soto, José Manuel Barat, and Pedro Amorós, 'Enzyme-Responsive Controlled Release Using Mesoporous Silica Supports Capped with Lactose', *Angewandte Chemie* **121** (2009): 5998–6001.

[71] Shenmin Zhu, Zhengyang Zhou, Di Zhang, Chan Jin, and Zhiqiang Li, 'Design and Synthesis of Delivery System Based on SBA-15 with Magnetic Particles Formed in Situ and Thermo-Sensitive PNIPA as Controlled Switch', *Microporous and Mesoporous Materials* **106** (2007): 56–61.

[72] Q. Fu, G.v.r. Rao, L.k. Ista, Y. Wu, B.p. Andrzejewski, L.a. Sklar, T.l. Ward, and G.p. López, 'Control of Molecular Transport Through Stimuli-Responsive Ordered Mesoporous Materials', *Advanced Materials* **15** (2003): 1262–66.

[73] Juan L. Vivero-Escoto, Igor I. Slowing, Chian-Wen Wu, and Victor S.-Y. Lin, 'Photoinduced Intracellular Controlled Release Drug Delivery in Human Cells by Gold-Capped Mesoporous Silica Nanosphere', *Journal of the American Chemical Society* **131** (2009): 3462–63.

[74] Tania M. Guardado-Alvarez, Lekshmi Sudha Devi, Melissa M. Russell, Benjamin J. Schwartz, and Jeffrey I. Zink, 'Activation of Snap-Top Capped Mesoporous Silica Nanocontainers Using Two Near-Infrared Photons', *Journal of the American Chemical Society* **135** (2013): 14000–3.

[75] Alidad Amirfazli, 'Nanomedicine: Magnetic Nanoparticles Hit the Target', *Nature Nanotechnology* **2** (2007): 467–68.

[76] Xia Wang, Hangrong Chen, Yuanyi Zheng, Ming Ma, Yu Chen, Kun Zhang, Deping Zeng, and Jianlin Shi, 'Au-Nanoparticle Coated Mesoporous Silica Nanocapsule-Based Multifunctional Platform for Ultrasound Mediated Imaging, Cytoclasis and Tumor Ablation', *Biomaterials* **34** (2013): 2057–68.

[77] Ying Wang, Ning Han, Qinfu Zhao, Ling Bai, Jia Li, Tongying Jiang, and Siling Wang, 'Redox-Responsive Mesoporous Silica as Carriers for Controlled Drug Delivery: A Comparative Study Based on Silica and PEG Gatekeepers', *European Journal of Pharmaceutical Sciences* **72** (2015): 12–20.

[78] Dong Xiao, Hui-Zhen Jia, Ning Ma, Ren-Xi Zhuo, and Xian-Zheng Zhang, 'A Redox-Responsive Mesoporous Silica Nanoparticle Capped with Amphiphilic Peptides by Self-Assembly for Cancer Targeting Drug Delivery', *Nanoscale* **7** (2015): 10071–77.

[79] N. A Peppas, 'Devices Based on Intelligent Biopolymers for Oral Protein Delivery', *International Journal of Pharmaceutics*, Selected Papers from The 11th International Pharmaceutical Technology Symposium, **277** (2004): 11–17.

[80] Panayiotis Bilalis, Leto-A. Tziveleka, Spyridon Varlas, and Hermis Iatrou, 'pH-Sensitive Nanogates Based on poly(L-Histidine) for Controlled Drug Release from Mesoporous Silica Nanoparticles', *Polymer Chemistry* **7** (2016): 1475–85.

[81] Juewen Liu, Alison Stace-Naughton, Xingmao Jiang, and C. Jeffrey Brinker, 'Porous Nanoparticle Supported Lipid Bilayers (Protocells) as Delivery Vehicles', *Journal of the American Chemical Society* **131** (2009): 1354–55.

[82] Juewen Liu, Xingmao Jiang, Carlee Ashley, and C. Jeffrey Brinker, 'Electrostatically Mediated Liposome Fusion and Lipid Exchange with a Nanoparticle-Supported Bilayer for Control of Surface Charge, Drug Containment, and Delivery', *Journal of the American Chemical Society* **131** (2009): 7567–69.

[83] Carlee E. Ashley, Eric C. Carnes, Genevieve K. Phillips, David Padilla, Paul N. Durfee, Page A. Brown, Tracey N. Hanna, Juewen Liu, Brandy Phillips, Mark B. Carter, Nick J. Carroll, Xingmao Jiang, Darren R.

Dunphy, Cheryl L. Willman, Dimiter N. Petsev, Deborah G. Evans, Atul N. Parikh, … C. Jeffrey Brinker, 'The Targeted Delivery of Multicomponent Cargos to Cancer Cells by Nanoporous Particle-Supported Lipid Bilayers', *Nature Materials* **10** (2011): 389–97.

[84] Valentina Cauda, Hanna Engelke, Anna Sauer, Delphine Arcizet, Christoph Bräuchle, Joachim Rädler, and Thomas Bein, 'Colchicine-Loaded Lipid Bilayer-Coated 50 Nm Mesoporous Nanoparticles Efficiently Induce Microtubule Depolymerization upon Cell Uptake', *Nano Letters* **10** (2010): 2484–92.

[85] Qianjun He and Jianlin Shi, 'MSN Anti-Cancer Nanomedicines: Chemotherapy Enhancement, Overcoming of Drug Resistance, and Metastasis Inhibition', *Advanced Materials* **26** (2014): 391–411.

[86] Chung Yen Ang, Si Yu Tan, and Yanli Zhao, 'Recent Advances in Biocompatible Nanocarriers for Delivery of Chemotherapeutic Cargoes towards Cancer Therapy', *Organic & Biomolecular Chemistry* **12** (2014): 4776–4806.

[87] Edgar Pérez-Herrero and Alberto Fernández-Medarde, 'Advanced Targeted Therapies in Cancer: Drug Nanocarriers, the Future of Chemotherapy', *European Journal of Pharmaceutics and Biopharmaceutics* **93** (2015): 52–79.

[88] L. E. Gerlowski and R. K. Jain, 'Microvascular Permeability of Normal and Neoplastic Tissues', *Microvascular Research* **31** (1986): 288–305.

[89] Nicolas Bertrand, Jun Wu, Xiaoyang Xu, Nazila Kamaly, and Omid C. Farokhzad, 'Cancer Nanotechnology: The Impact of Passive and Active Targeting in the Era of Modern Cancer Biology', *Advanced Drug Delivery Reviews*, Cancer nanotechnology, **66** (2014): 2–25.

[90] Erkki Ruoslahti, Sangeeta N. Bhatia, and Michael J. Sailor, 'Targeting of Drugs and Nanoparticles to Tumors', *The Journal of Cell Biology* **188** (2010): 759–68.

[91] Vahid Mirshafiee, Morteza Mahmoudi, Kaiyan Lou, Jianjun Cheng, and Mary L. Kraft, 'Protein Corona Significantly Reduces Active Targeting Yield' **49** (2013): 2557–59.

[92] Kathleen F. Pirollo and Esther H. Chang, 'Does a Targeting Ligand Influence Nanoparticle Tumor Localization or Uptake?', *Trends in Biotechnology* **26** (2008): 552–58.

[93] Twan Lammers, Fabian Kiessling, Wim E. Hennink, and Gert Storm, 'Drug Targeting to Tumors: Principles, Pitfalls and (Pre-) Clinical Progress', *Journal of Controlled Release*, Drug Delivery Research in Europe, **161** (2012): 175–87.

[94] Rihe Liu, Brian K. Kay, Shaoyi Jiang, and Shengfu Chen, 'Nanoparticle Delivery: Targeting and Nonspecific Binding', *MRS Bulletin* **34** (2009): 432–440.

[95] Adam D. Friedman, Sarah E. Claypool, and Rihe Liu, 'The Smart Targeting of Nanoparticles', *Current Pharmaceutical Design* **19** (2013): 6315–29.

[96] Nikki Parker, Mary Jo Turk, Elaine Westrick, Jeffrey D. Lewis, Philip S. Low, and Christopher P. Leamon, 'Folate Receptor Expression in Carcinomas and Normal Tissues Determined by a Quantitative Radioligand Binding Assay', *Analytical Biochemistry* **338** (2005): 284–93.

[97] Xiaobin Zhao, Hong Li, and Robert J. Lee, 'Targeted Drug Delivery via Folate Receptors', *Expert Opinion on Drug Delivery* **5** (2008): 309–19.

[98] Jessica M. Rosenholm, Cecilia Sahlgren, and Mika Lindén, 'Towards Multifunctional, Targeted Drug Delivery Systems Using Mesoporous Silica Nanoparticles--Opportunities & Challenges', *Nanoscale* **2** (2010): 1870–83.

[99] Fabiola Porta, Gerda E. M. Lamers, Jess Morrhayim, Antonia Chatzopoulou, Marcel Schaaf, Hans den Dulk, Claude Backendorf, Jeffrey I. Zink, and Alexander Kros, 'Folic Acid-Modified Mesoporous Silica Nanoparticles for Cellular and Nuclear Targeted Drug Delivery', *Advanced Healthcare Materials* **2** (2013): 281–86.

[100] Jessica Rosenholm, Cecilia Sahlgren, and Mika Lindén, 'Cancer-Cell Targeting and Cell-Specific Delivery by Mesoporous Silica Nanoparticles', *Journal of Materials Chemistry* **20** (2010): 2707–13.

[101] Satoru Sonoke, Toshihiro Ueda, Kae Fujiwara, Kenji Kuwabara, and Junichi Yano, 'Galactose-Modified Cationic Liposomes as a Liver-Targeting Delivery System for Small Interfering RNA', *Biological & Pharmaceutical Bulletin* **34** (2011): 1338–42.

[102] David Brevet, Magali Gary-Bobo, Laurence Raehm, Sébastien Richeter, Ouahiba Hocine, Kassem Amro, Bernard Loock, Pierre Couleaud, Céline Frochot, Alain Morère, Philippe Maillard, Marcel Garcia, and Jean-Olivier Durand, 'Mannose-Targeted Mesoporous Silica Nanoparticles for Photodynamic Therapy', *Chemical Communications* (2009): 1475–77.

[103] Jing Li, Fang-Kui Ma, Qi-Feng Dang, Xing-Guo Liang, and Xi-Guang Chen, 'Glucose-Conjugated Chitosan Nanoparticles for Targeted Drug Delivery and Their Specific Interaction with Tumor Cells', *Frontiers of Materials Science* **8** (2014): 363–72.

[104] Dong Xiao, Hui-Zhen Jia, Jing Zhang, Chen-Wei Liu, Ren-Xi Zhuo, and Xian-Zheng Zhang, 'A Dual-Responsive Mesoporous Silica Nanoparticle for Tumor-Triggered Targeting Drug Delivery', *Small* **10** (2014): 591–98.

[105] Chih-Pin Tsai, Chao-Yu Chen, Yann Hung, Fu-Hsiung Chang, and Chung-Yuan Mou, 'Monoclonal Antibody-Functionalized Mesoporous Silica Nanoparticles (MSN) for Selective Targeting Breast Cancer Cells', *Journal of Materials Chemistry* **19** (2009): 5737–43.

[106] Yuetong Wang, Hsin-Yi Huang, Liu Yang, Zhanxia Zhang, and Hongbin Ji, 'Cetuximab-Modified Mesoporous Silica Nano-Medicine Specifically Targets EGFR-Mutant Lung Cancer and Overcomes Drug Resistance', *Scientific Reports* **6** (2016): 25468.

[107] Penghui Zhang, Fangfang Cheng, Ri Zhou, Juntao Cao, Jingjing Li, Clemens Burda, Qianhao Min, and Jun-Jie Zhu, 'DNA-Hybrid-Gated Multifunctional Mesoporous Silica Nanocarriers for Dual-Targeted and MicroRNA-Responsive Controlled Drug Delivery', *Angewandte Chemie International Edition* **53** (2014): 2371–75.

[108] Shaobin Wang, 'Ordered Mesoporous Materials for Drug Delivery', *Microporous and Mesoporous Materials* **117** (2009): 1–9.

[109] Monty Liong, Jie Lu, Michael Kovochich, Tian Xia, Stefan G. Ruehm, Andre E. Nel, Fuyuhiko Tamanoi, and Jeffrey I. Zink, 'Multifunctional Inorganic Nanoparticles for Imaging, Targeting, and Drug Delivery', *ACS Nano* **2** (2008): 889–96.

[110] Juan L. Vivero-Escoto, Igor I. Slowing, Brian G. Trewyn, and Victor S.-Y. Lin, 'Mesoporous Silica Nanoparticles for Intracellular Controlled Drug Delivery', *Small* **6** (2010): 1952–67.

[111] Charu Bharti, Upendra Nagaich, Ashok Kumar Pal, and Neha Gulati, 'Mesoporous Silica Nanoparticles in Target Drug Delivery System: A Review', *International Journal of Pharmaceutical Investigation* **5** (2015): 124–33.

[112] Sooyeon Kwon, Rajendra K. Singh, Roman A. Perez, Ensanya A. Abou Neel, Hae-Won Kim, and Wojciech Chrzanowski, 'Silica-Based Mesoporous Nanoparticles for Controlled Drug Delivery', *Journal of Tissue Engineering* **4** (2013): 2041731413503357.

[113] María Vallet-Regí, Francisco Balas, and Daniel Arcos, 'Mesoporous Materials for Drug Delivery', *Angewandte Chemie (International Ed. in English)* **46** (2007): 7548–58.

[114] Amirali Popat, Sandy Budi Hartono, Frances Stahr, Jian Liu, Shi Zhang Qiao, and Gao Qing Max Lu, 'Mesoporous Silica Nanoparticles for Bioadsorption, Enzyme Immobilisation, and Delivery Carriers', *Nanoscale* **3** (2011): 2801–18.

[115] Jenny Andersson, Jessica Rosenholm, Sami Areva, and Mika Lindén, 'Influences of Material Characteristics on Ibuprofen Drug Loading and Release Profiles from Ordered Micro- and Mesoporous Silica Matrices', *Chemistry of Materials* **16** (2004): 4160–67.

[116] Renato Mortera, Juan Vivero-Escoto, Igor I. Slowing, Edoardo Garrone, Barbara Onida, and Victor S.-Y. Lin, 'Cell-Induced Intracellular Controlled Release of Membrane Impermeable Cysteine from a Mesoporous Silica Nanoparticle-Based Drug Delivery System', *Chemical Communications* (2009): 3219–21.

[117] Amirali Popat, Benjamin P. Ross, Jian Liu, Siddharth Jambhrunkar, Freddy Kleitz, and Shi Zhang Qiao, 'Enzyme-Responsive Controlled Release of Covalently Bound Prodrug from Functional Mesoporous Silica Nanospheres', *Angewandte Chemie International Edition* **51** (2012): 12486–89.

[118] Li Yuan, Wulian Chen, Jianhua Hu, Jin Z. Zhang, and Dong Yang, 'Mechanistic Study of the Covalent Loading of Paclitaxel via Disulfide Linkers for Controlled Drug Release', *Langmuir: The ACS Journal of Surfaces and Colloids* **29** (2013): 734–43.

[119] Paulo Costa and José Manuel Sousa Lobo, 'Modeling and Comparison of Dissolution Profiles', *European Journal of Pharmaceutical Sciences* **13** (2001): 123–33.

[120] Eva von Haartman, Desiré Lindberg, Neeraj Prabhakar, and Jessica M. Rosenholm, 'On the Intracellular Release Mechanism of Hydrophobic Cargo and Its Relation to the Biodegradation Behavior of Mesoporous Silica Nanocarriers', *European Journal of Pharmaceutical Sciences*, accessed 7 June 2016.

[121] Prakash Khadka, Jieun Ro, Hyeongmin Kim, Iksoo Kim, Jeong Tae Kim, Hyunil Kim, Jae Min Cho, Gyiae Yun, and Jaehwi Lee, 'Pharmaceutical Particle Technologies: An Approach to Improve Drug Solubility, Dissolution and Bioavailability', *Asian Journal of Pharmaceutical Sciences* **9** (2014): 304–16.

[122] Dan Peer, Jeffrey M. Karp, Seungpyo Hong, Omid C. Farokhzad, Rimona Margalit, and Robert Langer, 'Nanocarriers as an Emerging Platform for Cancer Therapy', *Nature Nanotechnology* **2** (2007): 751–60.

[123] K. R. Martin, 'The Chemistry of Silica and Its Potential Health Benefits', *The Journal of Nutrition, Health & Aging* **11** (2007): 94–97.

[124] M. Vallet-Regi, A. Rámila, R. P. del Real, and J. Pérez-Pariente, 'A New Property of MCM-41: Drug Delivery System', *Chemistry of Materials* **13** (2001): 308–11.

[125] Nai-Tzu Chen, Shih-Hsun Cheng, Jeffrey S. Souris, Chin-Tu Chen, Chung-Yuan Mou, and Leu-Wei Lo, 'Theranostic Applications of Mesoporous Silica Nanoparticles and Their Organic/Inorganic Hybrids', *Journal of Materials Chemistry B* **1** (2013): 3128–35.

[126] Cheng-Yu Lai, Brian G. Trewyn, Dusan M. Jeftinija, Ksenija Jeftinija, Shu Xu, Srdija Jeftinija, and Victor S.-Y. Lin, 'A Mesoporous Silica Nanosphere-Based Carrier System with Chemically Removable CdS Nanoparticle Caps for Stimuli-Responsive Controlled Release of Neurotransmitters and Drug Molecules', *Journal of the American Chemical Society* **125** (2003): 4451–59.

[127] Si-Han Wu, Yu-Shen Lin, Yann Hung, Yi-Hsin Chou, Yi-Hua Hsu, Chen Chang, and Chung-Yuan Mou, 'Multifunctional Mesoporous Silica Nanoparticles for Intracellular Labeling and Animal Magnetic Resonance Imaging Studies', *ChemBioChem* **9** (2008): 53–57.

[128] Alexandre Albanese, Peter S. Tang, and Warren C. W. Chan, 'The Effect of Nanoparticle Size, Shape, and Surface Chemistry on Biological Systems', *Annual Review of Biomedical Engineering* **14** (2012): 1–16.

[129] Ayush Verma and Francesco Stellacci, 'Effect of Surface Properties on Nanoparticle–Cell Interactions', *Small* **6** (2010): 12–21.

[130] Motao Zhu, Guangjun Nie, Huan Meng, Tian Xia, Andre Nel, and Yuliang Zhao, 'Physicochemical Properties Determine Nanomaterial Cellular Uptake, Transport, and Fate', *Accounts of Chemical Research* **46** (2013): 622–31.

[131] Hervé Hillaireau and Patrick Couvreur, 'Nanocarriers' Entry into the Cell: Relevance to Drug Delivery', *Cellular and Molecular Life Sciences* **66** (2009): 2873–96.

[132] Joanna Rejman, Volker Oberle, Inge S. Zuhorn, and Dick Hoekstra, 'Size-Dependent Internalization of Particles via the Pathways of Clathrin- and Caveolae-Mediated Endocytosis', *Biochemical Journal* **377** (2004): 159–69.

[133] Ling Hu, Zhengwei Mao, Yuying Zhang, and Gao Changyou, 'Influences of Size of Silica Particles on the Cellular Endocytosis, Exocytosis and Cell Activity of HepG2 Cells', *Journal of Nanoscience Letters* **1** (2011): 1–16.

[134] Wen Jiang, Betty Y. S. Kim, James T. Rutka, and Warren C. W. Chan, 'Nanoparticle-Mediated Cellular Response Is Size-Dependent', *Nature Nanotechnology* **3** (2008): 145–50.

[135] Xiaopin Duan and Yaping Li, 'Physicochemical Characteristics of Nanoparticles Affect Circulation, Biodistribution, Cellular Internalization, and Trafficking', *Small (Weinheim an Der Bergstrasse, Germany)* **9** (2013): 1521–32.

[136] Zhan-Guo Yue, Wei Wei, Pi-Ping Lv, Hua Yue, Lian-Yan Wang, Zhi-Guo Su, and Guang-Hui Ma, 'Surface Charge Affects Cellular Uptake and Intracellular Trafficking of Chitosan-Based Nanoparticles', *Biomacromolecules* **12** (2011): 2440–46.

[137] Amir K. Varkouhi, Marije Scholte, Gert Storm, and Hidde J. Haisma, 'Endosomal Escape Pathways for Delivery of Biologicals', *Journal of Controlled Release: Official Journal of the Controlled Release Society* **151** (2011): 220–28.

[138] Igor Slowing, Brian G. Trewyn, and Victor S.-Y. Lin, 'Effect of Surface Functionalization of MCM-41-Type Mesoporous Silica Nanoparticles on the Endocytosis by Human Cancer Cells', *Journal of the American Chemical Society* **128** (2006): 14792–93.

[139] Parag Aggarwal, Jennifer B. Hall, Christopher B. McLeland, Marina A. Dobrovolskaia, and Scott E. McNeil, 'Nanoparticle Interaction with Plasma Proteins as It Relates to Particle Biodistribution, Biocompatibility and Therapeutic Efficacy', *Advanced Drug Delivery Reviews*, Identifying and Assessing Biomaterial Nanotoxicity in Translational Research for Preclinical Drug Development, **61** (2009): 428–37.

[140] Mariam Samadi Moghaddam, Markus Heiny, and V. Prasad Shastri, 'Enhanced Cellular Uptake of Nanoparticles by Increasing the Hydrophobicity of Poly(lactic Acid) through Copolymerization with Cell-Membrane-Lipid Components', *Chemical Communications* **51** (2015): 14605–8.

[141] Changhui Fu, Tianlong Liu, Linlin Li, Huiyu Liu, Dong Chen, and Fangqiong Tang, 'The Absorption, Distribution, Excretion and Toxicity of Mesoporous Silica Nanoparticles in Mice Following Different Exposure Routes', *Biomaterials* **34** (2013): 2565–75.

[142] Qianjun He, Zhiwen Zhang, Fang Gao, Yaping Li, and Jianlin Shi, 'In Vivo Biodistribution and Urinary Excretion of Mesoporous Silica Nanoparticles: Effects of Particle Size and PEGylation', *Small (Weinheim an Der Bergstrasse, Germany)* **7** (2011): 271–80.

[143] Jaeyun Kim, Hoe Suk Kim, Nohyun Lee, Taeho Kim, Hyoungsu Kim, Taekyung Yu, In Chan Song, Woo Kyung Moon, and Taeghwan Hyeon, 'Multifunctional Uniform Nanoparticles Composed of a Magnetite Nanocrystal Core and a Mesoporous Silica Shell for Magnetic Resonance and Fluorescence Imaging and for Drug Delivery', *Angewandte Chemie (International Ed. in English)* **47** (2008): 8438–41.

[144] Ji Eun Lee, Nohyun Lee, Hyoungsu Kim, Jaeyun Kim, Seung Hong Choi, Jeong Hyun Kim, Taeho Kim, In Chan Song, Seung Pyo Park, Woo Kyung Moon, and Taeghwan Hyeon, 'Uniform Mesoporous Dye-Doped Silica Nanoparticles Decorated with Multiple Magnetite Nanocrystals for Simultaneous Enhanced Magnetic Resonance Imaging, Fluorescence Imaging, and Drug Delivery', *Journal of the American Chemical Society* **132** (2010): 552–57.

[145] Jie Lu, Monty Liong, Zongxi Li, Jeffrey I. Zink, and Fuyuhiko Tamanoi, 'Biocompatibility, Biodistribution, and Drug-Delivery Efficiency of Mesoporous Silica Nanoparticles for Cancer Therapy in Animals', *Small* **6** (2010): 1794–1805.

[146] Linlin Li, Tianlong Liu, Changhui Fu, Longfei Tan, Xianwei Meng, and Huiyu Liu, 'Biodistribution, Excretion, and Toxicity of Mesoporous Silica Nanoparticles after Oral Administration Depend on Their Shape', *Nanomedicine: Nanotechnology, Biology and Medicine* **11** (2015): 1915–24.

[147] Laura M. Ensign, Richard Cone, and Justin Hanes, 'Oral Drug Delivery with Polymeric Nanoparticles: The Gastrointestinal Mucus Barriers', *Advanced Drug Delivery Reviews*, Advances in Oral Drug Delivery: Improved Biovailability of Poorly Absorbed Drugs by Tissue and Cellular Optimization, **64** (2012): 557–70.

[148] Elvin Blanco, Haifa Shen, and Mauro Ferrari, 'Principles of Nanoparticle Design for Overcoming Biological Barriers to Drug Delivery', *Nature Biotechnology* **33** (2015): 941–51.

[149] Rakesh K. Jain, 'Understanding Barriers to Drug Delivery: High Resolution in Vivo Imaging Is Key', *American Association for Cancer Research* **5** (1999): 1605–6.

[150] Shravan Kumar Sriraman, Bhawani Aryasomayajula, and Vladimir P Torchilin, 'Barriers to Drug Delivery in Solid Tumors', *Tissue Barriers* **2** (2014).

[151] Praveen Ballabh, Alex Braun, and Maiken Nedergaard, 'The Blood-Brain Barrier: An Overview: Structure, Regulation, and Clinical Implications', *Neurobiology of Disease* **16** (2004): 1–13.

[152] Monika Dominska and Derek M. Dykxhoorn, 'Breaking down the Barriers: siRNA Delivery and Endosome Escape', *J Cell Sci* **123** (2010): 1183–89.

[153] Guozhong Cao, *Annual Review of Nano Research* (World Scientific, 2010).

[154] Carmen Alvarez-Lorenzo and Angel Concheiro, 'Smart Drug Delivery Systems: From Fundamentals to the Clinic', *Chemical Communications* **50** (2014): 7743–65.

[155] Leon Shargel and Andrew Yu, *Applied Biopharmaceutics & Pharmacokinetics, Seventh Edition* (McGraw Hill Professional, 2015).

[156] Lawrence X. Yu, Gordon L. Amidon, James E. Polli, Hong Zhao, Mehul U. Mehta, Dale P. Conner, Vinod P. Shah, Lawrence J. Lesko, Mei-Ling Chen, Vincent H. L. Lee, and Ajaz S. Hussain, 'Biopharmaceutics Classification System: The Scientific Basis for Biowaiver Extensions', *Pharmaceutical Research* **19** (2002): 921–25.

[157] G. L. Amidon, H. Lennernäs, V. P. Shah, and J. R. Crison, 'A Theoretical Basis for a Biopharmaceutic Drug Classification: The Correlation of in Vitro Drug Product Dissolution and in Vivo Bioavailability', *Pharmaceutical Research* **12** (1995): 413–20.

[158] Waiver of In Vivo Bioavailability and Bioequivalence Studies for Immediate-Release Solid Oral Dosage Forms Based on a Biopharmaceutics Classification System Guidance for Industry - ucm070246.pdf, accessed 4

May2016,
http://www.fda.gov/downloads/drugs/guidancecomplianceregulatoryinformation/guidances/ucm070246.pdf.
[159] S. Stegemann, F. Leveiller, D. Franchi, H. de Jong, and H. Lindén, 'When Poor Solubility Becomes an Issue: From Early Stage to Proof of Concept', *European Journal of Pharmaceutical Sciences: Official Journal of the European Federation for Pharmaceutical Sciences* **31** (2007): 249–61.
[160] Sönke Svenson, 'Carrier-Based Drug Delivery', in *Carrier-Based Drug Delivery*, vol. 879, 0 vols, ACS Symposium Series 879 (American Chemical Society, 2004), 2–23, http://dx.doi.org/10.1021/bk-2004-0879.ch001.
[161] Christopher A. Lipinski, 'Poor Aqueous Solubility - an Industry Wide Problem in Drug Discovery', *Am Pharm Rev* **5** (2002): 82–85.
[162] R. Langer, 'Drug Delivery and Targeting', *Nature* **392** (1998): 5–10.
[163] Amirali Popat, Siddharth Jambhrunkar, Jun Zhang, Jie Yang, Honwei Zhang, Anand Meka, and Chengzhong Yu, 'Programmable Drug Release Using Bioresponsive Mesoporous Silica Nanoparticles for Site-Specific Oral Drug Delivery', *Chemical Communications (Cambridge, England)* **50** (2014): 5547–50.
[164] K. Yoncheva, M. Popova, A. Szegedi, J. Mihaly, B. Tzankov, N. Lambov, S. Konstantinov, V. Tzankova, F. Pessina, and M. Valoti, 'Functionalized Mesoporous Silica Nanoparticles for Oral Delivery of Budesonide', *Journal of Solid State Chemistry* **211** (2014): 154–61.
[165] Lisa Brannon-Peppas and James O. Blanchette, 'Nanoparticle and Targeted Systems for Cancer Therapy', *Advanced Drug Delivery Reviews* **56** (2004): 1649–59.
[166] Jie Lu, Zongxi Li, Jeffrey I. Zink, and Fuyuhiko Tamanoi, 'In Vivo Tumor Suppression Efficacy of Mesoporous Silica Nanoparticles-Based Drug-Delivery System: Enhanced Efficacy by Folate Modification', *Nanomedicine: Nanotechnology, Biology and Medicine* **8** (2012): 212–20.
[167] Xiaoyu Li, Meiying Wu, Limin Pan, and Jianlin Shi, 'Tumor Vascular-Targeted Co-Delivery of Anti-Angiogenesis and Chemotherapeutic Agents by Mesoporous Silica Nanoparticle-Based Drug Delivery System for Synergetic Therapy of Tumor', *International Journal of Nanomedicine* **11** (2015): 93–105.
[168] Professor Dr Ludwig Reimer, 'Elements of a Transmission Electron Microscope', in *Transmission Electron Microscopy*, Springer Series in Optical Sciences 36 (Springer Berlin Heidelberg, 1993), 86–135.
[169] David B. Williams and C. Barry Carter, *Transmission Electron Microscopy* (Boston, MA: Springer US, 2009), http://link.springer.com/10.1007/978-0-387-76501-3.
[170] Robert J. Keyse, *Introduction to Scanning Transmission Electron Microscopy* (BIOS Scientific Publishers, 1998).
[171]'JEOL USA JEM-1400Plus Transmission Electron Microscope', accessed 1 May 2016, http://www.jeolusa.com/PRODUCTS/Transmission-Electron-Microscopes-TEM/120-kV/JEM-1400Plus.
[172] 'Transmission Electron Microscope (TEM) | Instrument', *Encyclopedia Britannica*, accessed 1 May 2016, http://global.britannica.com/technology/transmission-electron-microscope.
[173] 'Scanning Electron Microscope (SEM) | Instrument', *Encyclopedia Britannica*, accessed 1 May 2016, http://global.britannica.com/technology/scanning-electron-microscope.
[174] K. D. Vernon-Parry, 'Scanning Electron Microscopy: An Introduction', *III-Vs Review* **13** (2000): 40–44.
[175] David C Joy, 'Scanning Electron Microscopy for Materials Characterization', *Current Opinion in Solid State and Materials Science* **2** (1997): 465–68.
[176] K. S. W. Sing, 'Reporting Physisorption Data for Gas/Solid Systems with Special Reference to the Determination of Surface Area and Porosity (Recommendations 1984)', *Pure and Applied Chemistry* **57** (2009): 603–619.
[177] Stephen Brunauer, P. H. Emmett, and Edward Teller, 'Adsorption of Gases in Multimolecular Layers', *Journal of the American Chemical Society* **60** (1938): 309–19.
[178] Jean Rouquerol, Françoise Rouquerol, Philip Llewellyn, Guillaume Maurin, and Kenneth S. W. Sing, *Adsorption by Powders and Porous Solids: Principles, Methodology and Applications* (Academic Press, 2013).
[179] Elliott P. Barrett, Leslie G. Joyner, and Paul P. Halenda, 'The Determination of Pore Volume and Area Distributions in Porous Substances. I. Computations from Nitrogen Isotherms', *Journal of the American Chemical Society* **73** (1951): 373–80.

[180] P. I. Ravikovitch, D. Wei, W. T. Chueh, G. L. Haller, and A. V. Neimark, 'Evaluation of Pore Structure Parameters of MCM-41 Catalyst Supports and Catalysts by Means of Nitrogen and Argon Adsorption', *The Journal of Physical Chemistry B* **101** (1997): 3671–79.
[181] John Landers, Gennady Yu. Gor, and Alexander V. Neimark, 'Density Functional Theory Methods for Characterization of Porous Materials', *Colloids and Surfaces A: Physicochemical and Engineering Aspects*, Characterization of Porous Materials: From Angstroms to Millimeters A Collection of Selected Papers Presented at the 6th International Workshop, CPM-6 April 30 – May 2nd, 2012, Delray Beach, FL, USA Co-sponsored by Quantachrome Instruments, **437** (2013): 3–32.
[182] A. W. Coats and J. P. Redfern, 'Thermogravimetric Analysis. A Review', *Analyst* **88** (1963): 906–24.
[183] T. Hatakeyama and F. X. Quinn, *Thermal Analysis: Fundamentals and Applications to Polymer Science* (Wiley, 1999).
[184] 'STA 449 F1 Jupiter® - NETZSCH Analyzing & Testing', 449, accessed 1 May 2016, https://www.netzsch-thermal-analysis.com/us/products-solutions/simultaneous-thermogravimetry-differential-scanning-calorimetry/sta-449-f1-jupiter/.
[185] Renliang Xu, *Particle Characterization: Light Scattering Methods* (Springer Science & Business Media, 2006).
[186] Wolfgang Schärtl, *Light Scattering from Polymer Solutions and Nanoparticle Dispersions* (Springer Science & Business Media, 2007).
[187] Marie Gaumet, Angelica Vargas, Robert Gurny, and Florence Delie, 'Nanoparticles for Drug Delivery: The Need for Precision in Reporting Particle Size Parameters', *European Journal of Pharmaceutics and Biopharmaceutics* **69** (2008): 1–9.
[188] Duncun J Shaw, *Introduction to Colloid and Surface Chemistry*, 3rd edition (Butterworth & Co (Publishers) Ltd., 1980), http://www.alibris.com/Introduction-to-Colloid-and-Surface-Chemistry-Duncan-J-Shaw/book/3309561.
[189] 'Zetasizer Nano ZS for Size, Zeta Potential, Protein Mobility and Microrheology', accessed 2 May 2016,http://www.malvern.com/en/products/product-range/zetasizer-range/zetasizer-nano-range/zetasizer-nano-zs/.
[190] Ralph Sherman Becker, *Theory and Interpretation of Fluorescence and Phosphorescence* (Wiley Interscience, 1969).
[191] 'Fluorescent Probes', accessed 2 May 2016, https://www.thermofisher.com/fi/en/home/life-science/protein-biology/protein-biology-learning-center/protein-biology-resource-library/pierce-protein-methods/fluorescent-probes.html.
[192] 'Virtual Labs', accessed 2 May 2016, http://ccnsb01-iiith.virtual-labs.ac.in/exp5/index.html#.
[193] Rosaleen J. Anderson, David J. Bendell, and Paul W. Groundwater, 'Ultraviolet–visible (UV-Vis) Spectroscopy', in *Organic Spectroscopic Analysis*, 2004, 7–23, http://pubs.rsc.org/en/content/chapter/bk9780854044764-00007/978-0-85404-476-4.
[194] Heinz-Helmut Perkampus, *UV-VIS Spectroscopy and Its Applications* (Berlin, Heidelberg: Springer Berlin Heidelberg, 1992), http://link.springer.com/10.1007/978-3-642-77477-5.
[195] Lloyd R. Snyder, Joseph J. Kirkland, and Joseph L. Glajch, *Practical HPLC Method Development* (John Wiley & Sons, 2012).
[196] Zeno Földes-Papp, Ulrike Demel, and Gernot P. Tilz, 'Laser Scanning Confocal Fluorescence Microscopy: An Overview', *International Immunopharmacology* **3** (2003): 1715–29.
[197] Guy Cox, 'Biological Confocal Microscopy', *Materials Today* **5** (2002): 34–41.
[198] 'ZEISS Microscopy Online Campus | Live-Cell Imaging | Microscopy Techniques', accessed 2 May 2016, http://zeiss-campus.magnet.fsu.edu/articles/livecellimaging/techniques.html.
[199] Howard M. Shapiro, *Practical Flow Cytometry* (John Wiley & Sons, 2005).
[200] Marion G. Macey, *Flow Cytometry: Principles and Applications* (Springer Science & Business Media, 2007).
[201] 'Flow Cytometry - Semrock', accessed 2 May 2016, https://www.semrock.com/flow-cytometry.aspx.
[202] Veronika Mamaeva, Jessica M. Rosenholm, Laurel Tabe Bate-Eya, Lotta Bergman, Emilia Peuhu, Alain Duchanoy, Lina E. Fortelius, Sebastian Landor, Diana M. Toivola, Mika Lindén, and Cecilia Sahlgren, 'Mesoporous Silica Nanoparticles as Drug Delivery Systems for Targeted Inhibition of Notch Signaling in Cancer', *Molecular Therapy: The Journal of the American Society of Gene Therapy* **19** (2011): 1538–46.

[203] M. X. Tang and F. C. Szoka, 'The Influence of Polymer Structure on the Interactions of Cationic Polymers with DNA and Morphology of the Resulting Complexes', *Gene Therapy* **4** (1997): 823–32.

[204] O. Boussif, F. Lezoualc'h, M. A. Zanta, M. D. Mergny, D. Scherman, B. Demeneix, and J. P. Behr, 'A Versatile Vector for Gene and Oligonucleotide Transfer into Cells in Culture and in Vivo: Polyethylenimine', *Proceedings of the National Academy of Sciences of the United States of America* **92** (1995): 7297–7301.

[205] Samuel K. Lai, Ying-Ying Wang, and Justin Hanes, 'Mucus-Penetrating Nanoparticles for Drug and Gene Delivery to Mucosal Tissues', *Advanced Drug Delivery Reviews* **61** (2009): 158–71.

[206] Jason W. Locasale and Lewis C. Cantley, 'Altered Metabolism in Cancer', *BMC Biology* **8** (2010): 88.

[207] V. Meunier, M. Bourrié, Y. Berger, and G. Fabre, 'The Human Intestinal Epithelial Cell Line Caco-2; Pharmacological and Pharmacokinetic Applications', *Cell Biology and Toxicology* **11** (n.d.): 187–94.

[208] Helene Kettiger, Didem Sen Karaman, Laura Schiesser, Jessica M. Rosenholm, and Jörg Huwyler, 'Comparative Safety Evaluation of Silica-Based Particles', *Toxicology in Vitro* **30** (2015): 355–63.

[209] Tina Gulin-Sarfraz, Jixi Zhang, Diti Desai, Jarmo Teuho, Jawad Sarfraz, Hua Jiang, Chunfu Zhang, Cecilia Sahlgren, Mika Lindén, Hongchen Gu, and Jessica M. Rosenholm, 'Combination of Magnetic Field and Surface Functionalization for Reaching Synergistic Effects in Cellular Labeling by Magnetic Core–shell Nanospheres', *Biomaterials Science* **2** (2014): 1750–60.

[210] Didem Şen Karaman, Diti Desai, Jixi Zhang, Sina Tadayon, Gözde Unal, Jarmo Teuho, Jawad Sarfraz, Jan-Henrik Smått, Hongchen Gu, Tuomas Näreoja, and Jessica M. Rosenholm, 'Modulation of the Structural Properties of Mesoporous Silica Nanoparticles to Enhance the T1-Weighted MR Imaging Capability' **4** (2016): 1720–32.

[211] Koen Raemdonck, Kevin Braeckmans, Jo Demeester, and Stefaan C. De Smedt, 'Merging the Best of Both Worlds: Hybrid Lipid-Enveloped Matrix Nanocomposites in Drug Delivery', *Chem. Soc. Rev.* **43** (2013): 444–72.

[212] Johanna Tuomela, Jouko Sandholm, Peeter Karihtala, Joanna Ilvesaro, Katri S. Vuopala, Joonas H. Kauppila, Saila Kauppila, Dongquan Chen, Christine Pressey, Pirkko Härkönen, Kevin W. Harris, David Graves, Päivi K. Auvinen, Ylermi Soini, Arja Jukkola-Vuorinen, and Katri S. Selander, 'Low TLR9 Expression Defines an Aggressive Subtype of Triple-Negative Breast Cancer', *Breast Cancer Research and Treatment* **135** (2012): 481–93.

ISBN 978-952-12-3469-9